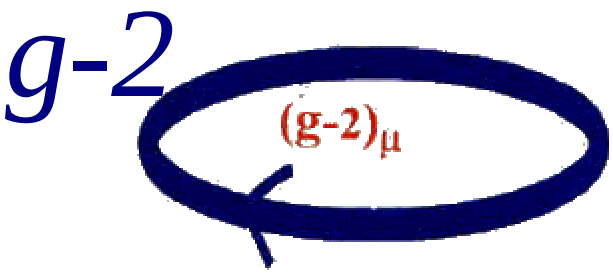

Brookhaven National Laboratory

Brookhaven Science Associates

Upton, New York 11973

Muon g-2 Note No. 391

Title: **1999 w_a Analysis Using the Ratio Method**

Author(s): **Long Duong**

Affiliation: **University of Minnesota**

Date: **April 11, 2001**

1999 ω_a Analysis Using the Ratio Method

Long Duong
University of Minnesota

January 23, 2001

Abstract

This note will present results of an ω_a analysis of the 1999 data using the ratio method. Data processed using both the g2off and G2Too analysis packages were studied. The final values of $R = (f_o - f_a)/f_o$ ($f_o = 229.1$ kHz) are $143.37 \pm 1.28 \pm 0.17$ ppm (g2off) and $143.03 \pm 1.28 \pm 0.19$ ppm (G2Too), where the first uncertainty is statistical and the second systematic specifically related to the fit procedure. R as given has an arbitrary offset. The data overlap between g2off and G2Too allows for a statistical fluctuation of about 0.27*1.28 = 0.35 ppm, and hence the two R values are statistically consistent.

Contents

1 Introduction

This note will detail the results of an ω_a analysis of the 1999 data using the ratio method, see [1] for a complete description of the formulation and implementation of the ratio method. For the current analysis, data processed using both the g2off and G2Too software packages were used. Event reconstruction from the raw WFD traces are described in [2] for the fortran/PAW-based g2off package and in [3] for the c++/ROOT-based G2Too package. The pulse reconstruction for G2Too to which this note refers is also known as G2Too (NEW). This pulse fitter uses constant errors in fitting the WFD ADC samples to the average pulse shape, and is essentially the same as the pulse fitter used in g2off. Because my focus was primarily the ratio method, no independent data selection study was conducted. Rather, I have used for the g2off data Cenap's selection [4], and for the G2Too data Gerco's selection [5].

Often the important principal elements are missed when accompanied by presentation of detailed results. To avoid this, I will explicitly state now that for the final fitting to extract the ω_a values as given in the abstract, the ratio method was applied to histogrammed data that had been treated with fill randomization [6], to wash out the effects of fast rotation, and pileup subtraction using shadow pulses [7]. The two physical effects of muon losses and coherent betatron oscillation (CBO) did not have to be included in the fit due to the unique nature of the ratio formulation, in contrast to the multiparamter fit. The other physical effects of AGS flashlets, double CBO, vertical waist, and energy calibration shifts within a fill will be given systematic errors, as well as the CBO and muon losses.

Finally, for ease of communication, the following color code will always be followed when plotting results, unless otherwise stated.

- RED: results for g2off data
- BLUE: results for G2Too (NEW) data
- BLACK: results for (g2off - G2Too) or for simulated data

2 A Review of The Ratio Method

Basically, the ratio method is a filter which takes a five-parameter like function $N(t)$

$$N(t) = N_o e^{\frac{-t}{\tau_\mu}}[1 - A * cos(\omega_a t + \phi)] + B(t) \tag{1}$$

with $B(t)$ small compared to N_o and transforms it into a ratio function $R(t)$ where

$$\begin{aligned} R(t) &= \frac{N\left(t+\frac{1}{2}\tau_a\right) + N\left(t-\frac{1}{2}\tau_a\right) - 2N(t)}{N\left(t+\frac{1}{2}\tau_a\right) + N\left(t-\frac{1}{2}\tau_a\right) + 2N(t)} \\ &= [1 - B_{den}(t)] * A * cos(\omega t + \phi) + \frac{1}{16}\left(\frac{\tau_a}{\tau_\mu}\right)^2 + B_{num}(t) \end{aligned} \tag{2}$$

in which the ratio background terms $B_{num}(t)$ and $B_{den}(t)$ are constructed from $B(t)$ by

$$B_{num}(t) = \frac{B\left(t+\frac{1}{2}\tau_a\right) + B\left(t-\frac{1}{2}\tau_a\right) - 2B(t)}{4N_o e^{\frac{-t}{\tau_\mu}}} \tag{3}$$

$$B_{den}(t) = \frac{B\left(t+\frac{1}{2}\tau_a\right) + B\left(t-\frac{1}{2}\tau_a\right) + 2B(t)}{4N_o e^{\frac{-t}{\tau_\mu}}} \tag{4}$$

It will be shown later in the results section that with fill randomization and pileup subtraction applied, the remaining data can be acceptably (meaning a good χ^2/ndf and small systematic fitting errors) parameterized by the function in Eq. 2 with $B_{num}(t) = 0$ and $B_{den}(t) = 0$. Therefore, all the final fitting results to be presented will use the function

$$R(t) = A * cos(\omega_a t + \phi) + \frac{1}{16}\left(\frac{\tau_a}{\tau_\mu}\right)^2 = A * cos(\omega_a t + \phi) + 0.00028736 \tag{5}$$

with the three parameters (A, ω_a, ϕ). A second function with one more parameter, K, to account for pileup, will also be used in studying the systematic uncertainty associated with pileup subtraction. In that case, the function $R_K(t)$ is

$$R_K(t) = [1 - Ke^{-\frac{t}{\tau_\mu}}] * A * cos(\omega_a + \phi) + 0.00028736 \tag{6}$$

where the pileup parameter K is defined to be

$$K \quad = \quad \epsilon_d \left(\frac{A - A_d}{A}\right) \tag{7}$$

In Eq. 7, ϵ_d is the fraction of pileup to singles pulses at injection, and A_d is the asymmetry of the pileup pulses. Throughout the rest of this note, $R(t)$ and $R_K(t)$ will always denote the functions as given in Eqs. 5 and 6, respectively. Furthermore, (A, ω_a, ϕ, K), will always be used to refer to the parameters as defined in Eqs. $5 - 7$. Note that the three parameters (A, ω_a, ϕ) have the usual physical meanings: A is the muon forward-backward decay asymmetry, ω_a is the anomalous spin precession frequency, and ϕ is the g-2 phase. For a final comment, do not confuse $R(t)$ which refers to the ratio function in Eq. 5 with the parameter $R = (\omega_o - \omega_a)/\omega_o$ ($\omega_o = 2\pi * 229100$ rad/s) used as an alternative expression for ω_a.

2.1 Systematic Uncertainty in the Ratio Fitting Method

In Ref. [1], the background term $B(t)$ in Eq. 1 was set to zero (so that $B_{num}(t) = 0$ and $B_{den}(t) = 0$ as well in Eq. 2), and the ratio fitting procedure itself was then quantitatively characterized using analytical techniques as well as using fits to 1600 sets of data simulated to have about the same statistical power as the 1999 data, i.e. ≈ 1.2 ppm uncertainty in ω_a. The pertinent results of that study are enumerated below.

1. The distribution of (χ^2/ndf) for the ratio fitting procedure is gaussian with mean (1.00069 ± 0.00047) and width $(0.96 \pm 0.01)(\sqrt{2/ndf})$, (Section 4.2, pg 6-7).

2. The distribution of values $\mathcal{R} = (\omega_{a(fit)} - \omega_{a(MC)})/(\omega_{a(MC)})$ is gaussian with mean -0.020 ± 0.030 ppm and width 1.14 ± 0.02 ppm, (Section 4.2, pg 6).

3. When comparing the fitted values of ω_a between the ratio and five-parameter like fits, the distribution of values $\mathcal{D} = \omega_a(\text{five-parameter}) - \omega_a(\text{ratio})$ is a Gaussian with mean zero and width $\approx 13\%$ of the statistical uncertainty, (Section 4.3, pg 7-8).

The results above were for a fit start time of 25 μs. The value of -0.02 ppm above is statistically consistent with zero. Therefore, for a 90% CL, a value of 0.05 ppm can be ascribed to the fitting error for the ratio method itself using the statistical uncertainty of 0.03 ppm. In the fitting routine the time assigned to the binned data was the time at the center of time bins of width 149.185 ns. Therefore, this uncertainty of 0.05 ppm includes the error for the ratio fitting procedure as well as binned data. This value of 0.05 ppm will be one of the entries in the systematic fitting uncertainties table, Section 4.7.

3 Endpoint Energy Calibration and Average Energy

3.1 Endpoint Energy Calibration

Figure 1 shows a plot illustrating the details of the endpoint energy calibration procedure for G2Too. First, the millifit area distribution with a time cut of 200 μs for about 80% of all the 1999 data was constructed. The maximum count N_{max} was then found, at area ≈ 170 in Figure 1. Next the area distribution in the area range corresponding to $(0.6 - 0.2)^* N_{max}$ was fitted to a straight line, and the point at which the straight line crosses the area axis is set to be the endpoint energy, 464.8 in Figure 1, which corresponds to 3.1 GeV. For G2Too data, a single endpoint value was used for each detector for all runs used in the analysis, whereas for g2off data, different run intervals may have different endpoint values [4],[10]. Figure 2 shows a comparison over all the 1999 data for the endpoint calibrations for g2off (as was done in [4]), versus G2Too data. The endpoint values for g2off is ≈ 3.09 GeV and for G2Too is ≈ 3.10 GeV, a 0.3% difference. However, keep in mind that this is does not transform directly into a data overlap since the two endpoint calibration schemes may differ by more, a few percents, for any particular run.

3.2 Average Energy

The average energy versus time in a fill were studied using two very different methods: a macroscopic method (similar to the one Alex uses), and a microscopic method via pileup construction using shadow pulses. The macroscopic method, [8] Section 4.4, uses the fact that changes of the average energy due to pileup vary with upper energy cuts. Therefore, taking ratios of the average energies for different upper energy cuts can give estimates for the pileup contribution to the average energy. By correcting for such contributions, the pileup-free average energy is extracted. In the microscopic pileup subtraction, energy (E) and number (N) histograms of the singles pulses ($S1, S2$) used to construct the pileup pulses (D) are combined to extract the pileup-free average energy by the formula

$$< E(t) >= \frac{E_{ALL}(t) - [E_D(t) - E_{S1}(t) - E_{S2}(t)]}{N_{ALL}(t) - [N_D(t) - N_{S1}(t) - N_{S2}(t)]} \tag{8}$$

Figures $3 - 5$ show plots of the average energy changes, normalized to values in the range $200 - 400$ μs, versus time in a fill for all 22 detectors used in the analysis. Note the excellent agreement between the two macroscopic and microscopic methods, giving confidence that the average energy changes as shown are accurate. With the exception of 1, all detectors have normalized energy changes for times > 30 μs that are within $\pm$ 0.1% of 1.0. For all the detectors except 4, g2off and G2Too data agree very well. For reference it should be noted that for normalized energy changes that are linear with magnitude 0.1% per 200 μs, the systematic error in ω_a is about 0.1 ppm. Therefore, with the exception of 1, the individual detectors have energy calibrations that are good to about 0.1 ppm in ω_a. Figure 6 shows the normalized average energy for the sum of all the detectors. In this case, the average energy changes are $< 0.03\%$, and hence summing the detectors together and then fitting will incur a smaller systematic error due to energy calibration changes within a fill, see Section 4.2.

4 Systematic Fitting Uncertainties

4.1 Fast Rotation Randomization

The systematic fitting uncertainty associated with the randomization procedure [6] can be estimated as follows. Begin with an illustrative example of the four t0 pulses shown in Figure 7. The t0 pulses shown have widths of 21.8 ns. Consider that the means of the four t0 pulses in Figure 7 are at

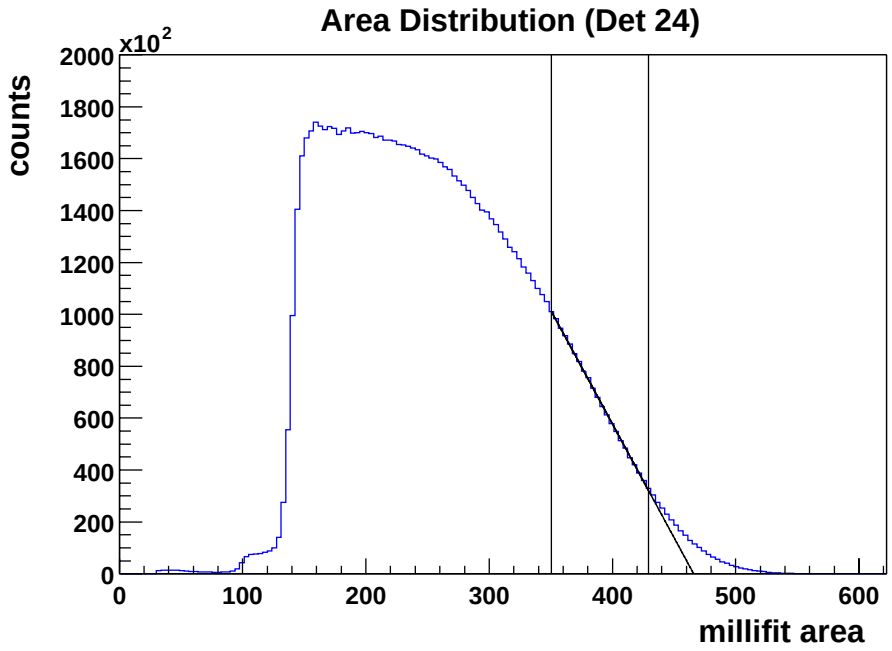

Figure 1: Endpoint energy calibration for detector 24 (blue line indicates G2Too data).

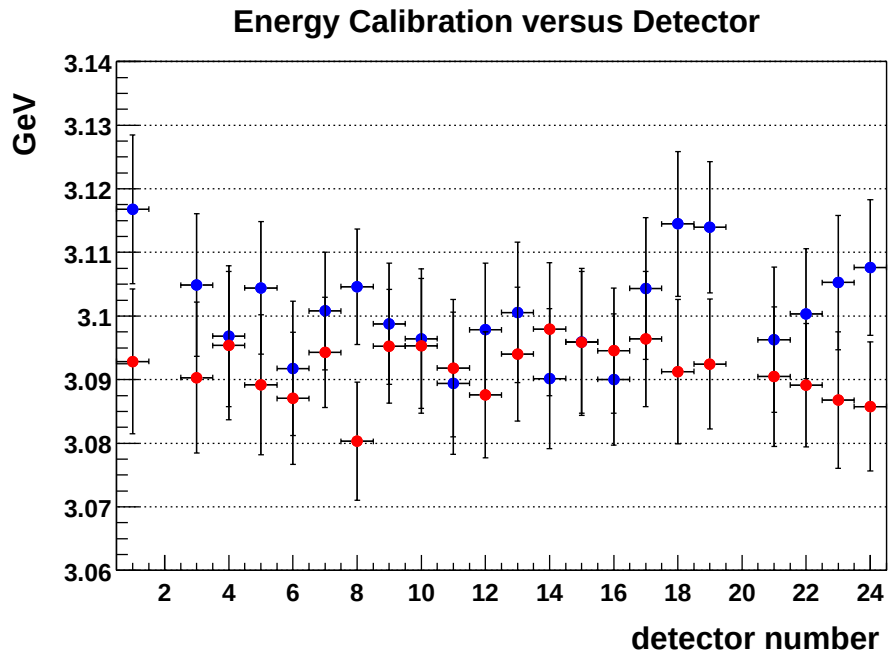

Figure 2: Endpoint energy calibration as a function of detector for both g2off (red) and G2Too (blue).

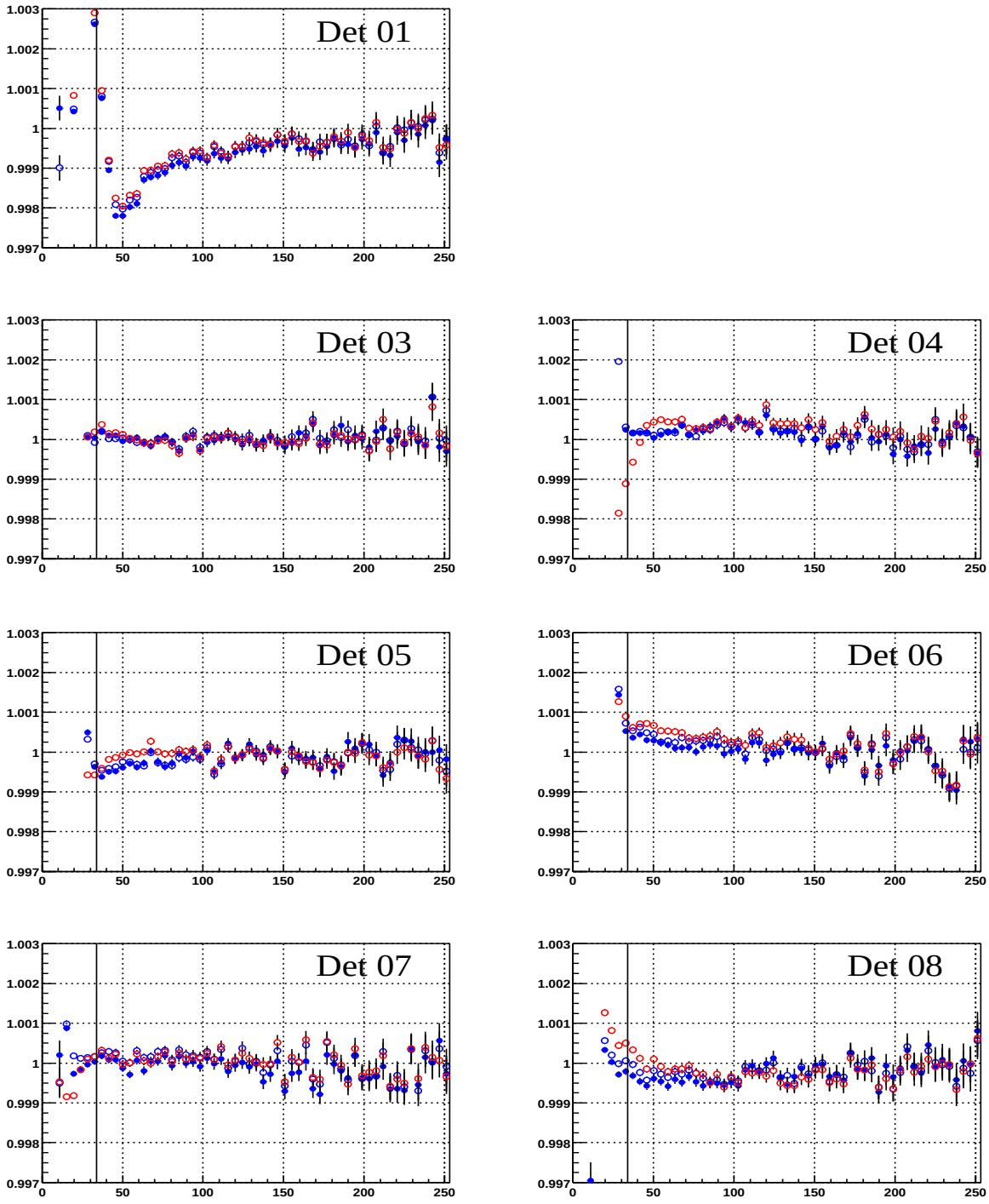

Figure 3: Average energy versus time (in μs), normalized to values in the range $200 - 400$ μs for detectors $1 - 8$. Macroscopic (open circles) and microscopic (closed circles) pileup subtraction are both used. The vertical line indicates the 34 μs mark.

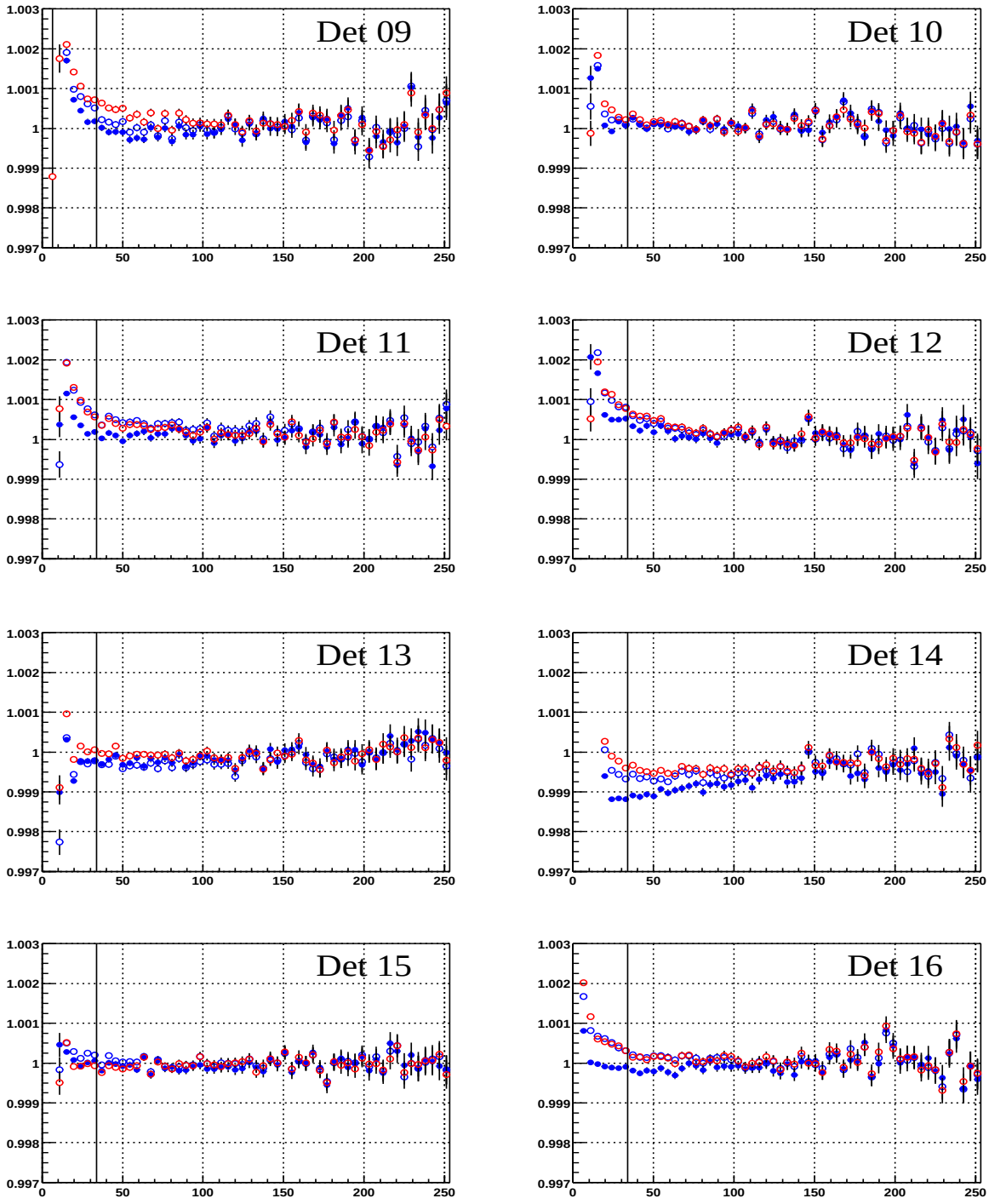

Figure 4: Average energy versus time (in μs), normalized to values in the range $200 - 400$ μs for detectors $9 - 16$. Macroscopic (open circles) and microscopic (closed circles) pileup subtraction are both used. The vertical line indicates the 34 μs mark.

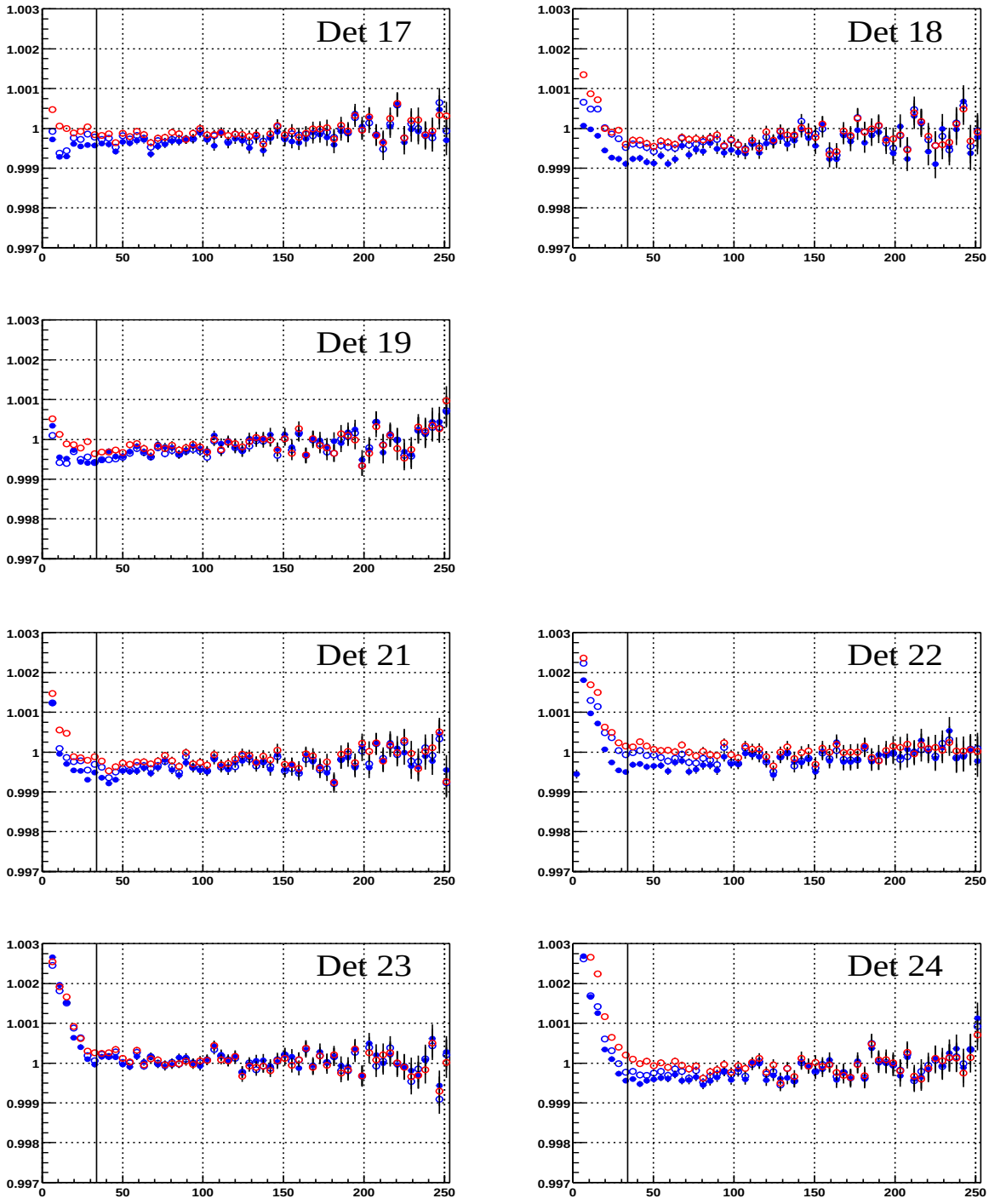

Figure 5: Average energy versus time (in μs), normalized to values in the range $200 - 400$ μs for detectors $17 - 24$. Macroscopic (open circles) and microscopic (closed circles) pileup subtraction are both used. The vertical line indicates the 34 μs mark.

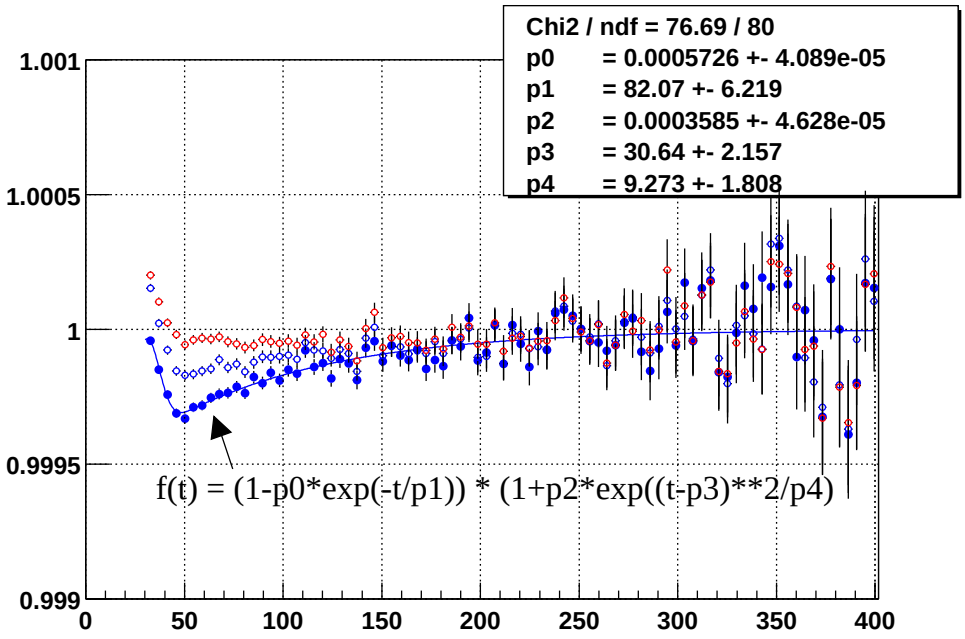

Figure 6: Average energy versus time (in μs), normalized to values in the range $200 - 400$ μs, and averaged over all detectors. Both macrocospic (open circles) and microscopic (closed circles) pileup subtraction are used. The fitted function f(t) will be used to estimate the systematic uncertainty due to energy calibration changes.

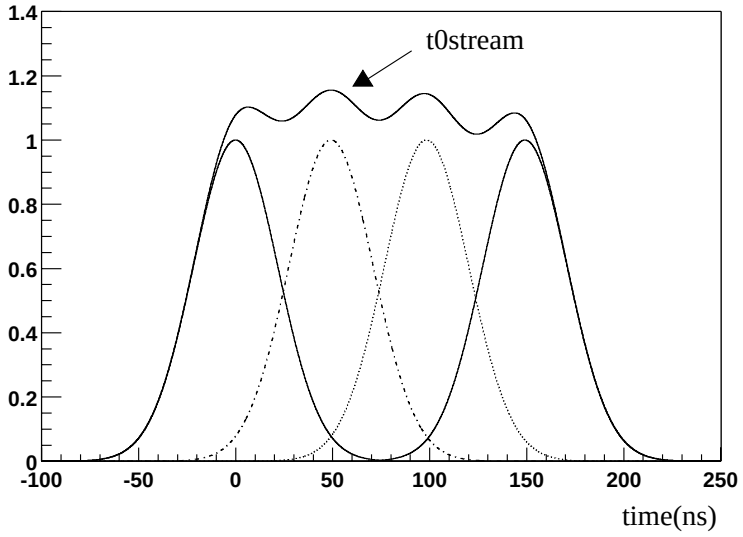

Figure 7: Illustration of the idea of the t0stream: the four individual t0 pulses are randomized so that the effective t0 pulse more closely approximates a constant across the fast rotation period of 150 ns.

the four values (0, 0.33, 0.66, 1.0) times the fast rotation period of 149.105 ns. The sum of these four "randomized" t0 pulses forms the "t0stream". From the detector's view point then, fill randomization makes the decay positrons look as though they originated from the t0stream. In the limit of many, many randomized t0 pulses, the effective t0 is then nearly a constant over the fast rotation period.

Figure 8 shows a plot of the calculated t0stream for the case of randomizing t0 pulses using a ranlux sequence with seed 4292730. This is one of the random number sequences used in the implementation of fill randomization for detector 1, g2off data. The t0 pulses used were gaussian in shape with widths 21.8 ns. To account for the varying beam intensities, the magnitudes of the individual t0 pulses were taken from a gaussian distribution with a width equalling $\approx 1/3$ the mean, mimicking the variation over the 1999 data run. Notice that the effective t0 structure is now roughly constant, having a fractional peak of magnitude $\approx 2/1028 = 0.002$.

Figure 9 shows a plot of simulated g-2 data with the fast rotation structure not randomized, and Figure 10 shows the ratio of the plot in Figure 9 divided by the normal five-parameter function to isolate the fast rotation factor $\mathcal{F}(t)$. The simulated function shown in Figure 10 was derived at as follows. Fast rotation peaks at early times, $5 - 35\ \mu s$ from injection, for detector 24 were fitted to gaussian functions, and the means and widths of these fits were extracted. The slope of the mean versus time after injection was consistent with a fast rotation period of 149.105 ns, and the widths were fitted to a quadratic function with the result

$$\sigma_{fr}(t) = 21.77 + 0.01585 * t + 0.0005868 * t^2 \tag{9}$$

where both the time t and the fast rotation width σ_{fr} are in ns. The plot in Figure 10 was then calculated as follows. Gaussian functions of widths as given by Eq. 9 with area 1 and means equalling integral values of the fast rotation period were added together. The resulting sum was normalized so that the value at 60 μs is 1, and the difference from 1 is plotted in Figure 10. The envelope of the oscillation was fitted to a third degree polynomial with the result

$$\mathcal{A}(t) = 3.183 - 1.828e^{-4} * t + 3.485e^{-9} * t^2 - 2.203e^{-14} * t^3 \tag{10}$$

Considering the idea of the t0stream, then the effect of fill randomization is the replacement $\mathcal{F}(t) \rightarrow 0.002 * \mathcal{F}(t)$. The histogrammed data then becomes $G(t)(1 + \mathcal{F}(t)) \rightarrow G(t)(1 + 0.002 * \mathcal{F}(t))$, where $G(t)$ is the usual five-parameter function, and the background term is $B(t) = 0.002 * G(t)\mathcal{F}(t)$.

In Ref. [1], it was shown that for the ratio method, the systematic error in fitting data of the form $(R(t) + \epsilon F(t))$, with $\epsilon \ll 1$, to only the function $R(t)$ can be well estimated by

$$\frac{\delta\omega_a}{\omega_a} \approx \left(\frac{\epsilon}{2\pi A_o}\right)\left(\frac{\tau_a}{\tau_\mu}\right)\left(\frac{cd - be}{ac - bb}\right) \tag{11}$$

where (a, b, c, d, e) are functions of the fitting time interval and of the background term $F(t)$. The background $B(t)$ in the normal g-2 histogrammed data will contribute to the background $\epsilon F(t)$ in the ratio method by

$$\epsilon F(t) = -B_{den}(t) * Acos(\omega_a t + \phi) + B_{num}(t) \tag{12}$$

where $B_{num}(t)$ and $B_{den}(t)$ are as defined in Eqs. 3 and 4, respectively. Figure 11 shows a plot of calculations using Eq. 11 for the case of the background term $B(t) = 0.002 * G(t)\mathcal{F}(t)$ for fast ratation peaks as seen by detector 1. Notice that the fitting error versus fit start time oscillates at the g-2 frequency, and that the errors are minimized at zero crossings of the g-2 signal. The preceding calculation gives that for fill randomization of one detector, the systematic fitting error is < 0.2 ppm for all start times $> 30\ \mu s$. For another simple check, the error formula was applied to detectors on opposite sides of the ring, see Figure 12. As expected, the fitting errors are 180 degrees out of phase.

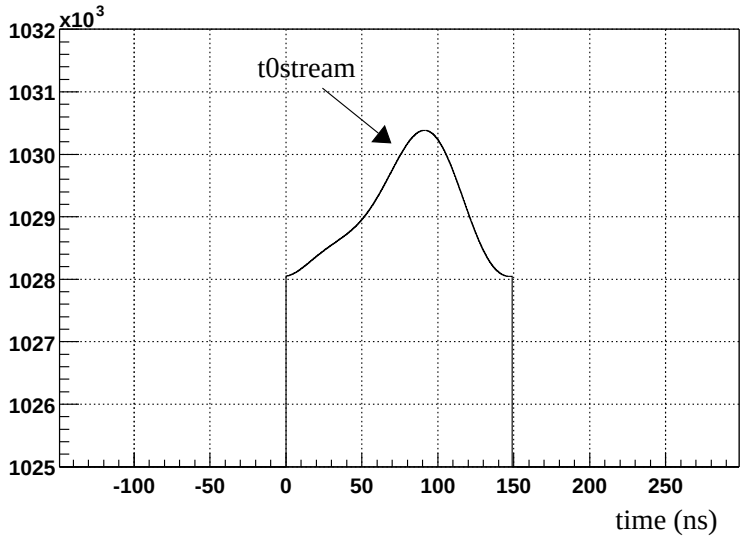

Figure 8: The t0stream for fill randomization over 806 runs. The ranlux sequence with seed 4292730 was used. This is one of the sequences used for fill randomization of detector 1, g2off data.

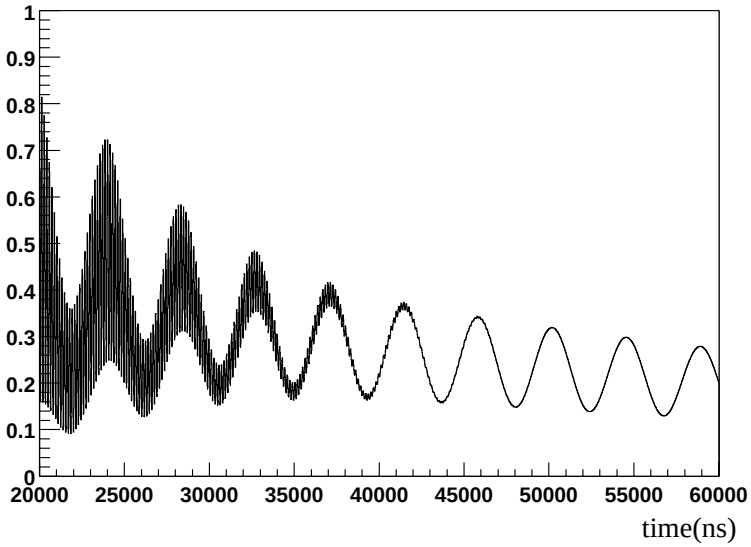

Figure 9: Simulated g-2 function with the fast rotation structure; the function is $N(t) = G(t) * (1 + \mathcal{F}(t))$ where $G(t)$ is the five-parameter function, $G(t) = N_o * exp\left(-\frac{t}{\tau_\mu}\right) * [1 - A * cos(\omega_a t + \phi)]$, and $\mathcal{F}(t)$ is the fast rotation factor.

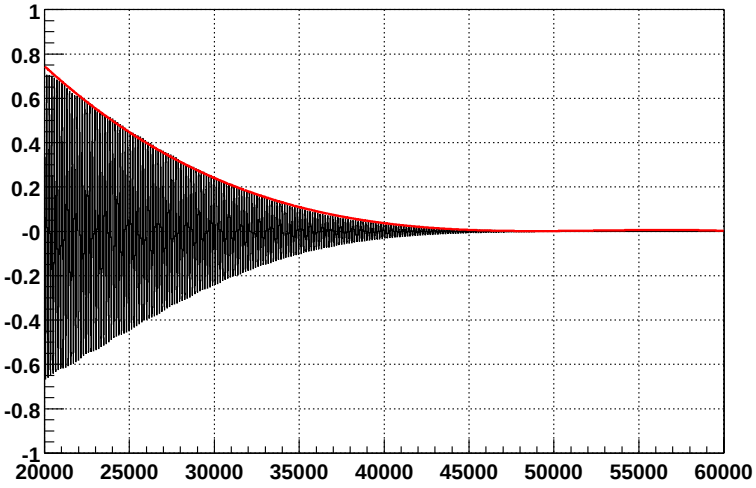

Figure 10: The fast rotation factor $\mathcal{F}(t)$. The envelope of the oscillation was fitted to a third degree polynomial (red line).

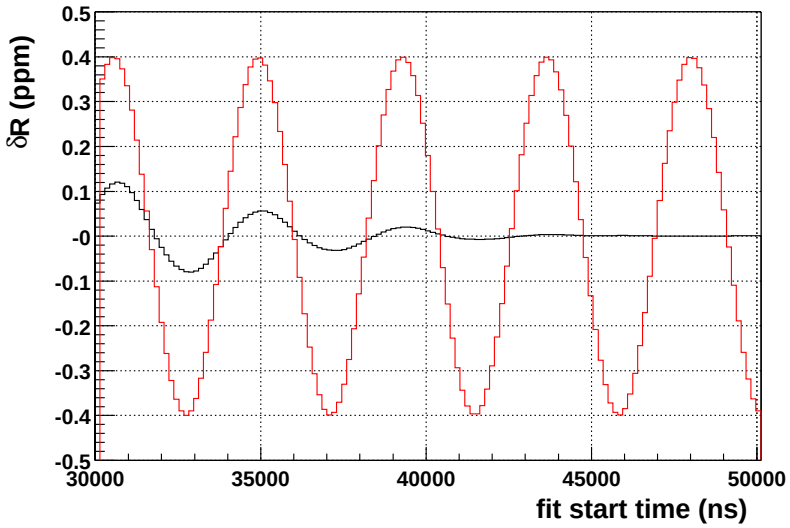

Figure 11: Systematic fitting error δR (ppm) for the case of fill randomization for one detector (black). The ratio function $R(t)$ formed using g2off data (red) is also plotted. Note that the fitting error versus start time oscillates at the g-2 frequency, and that the error is minimized at zero crossings of the g-2 function.

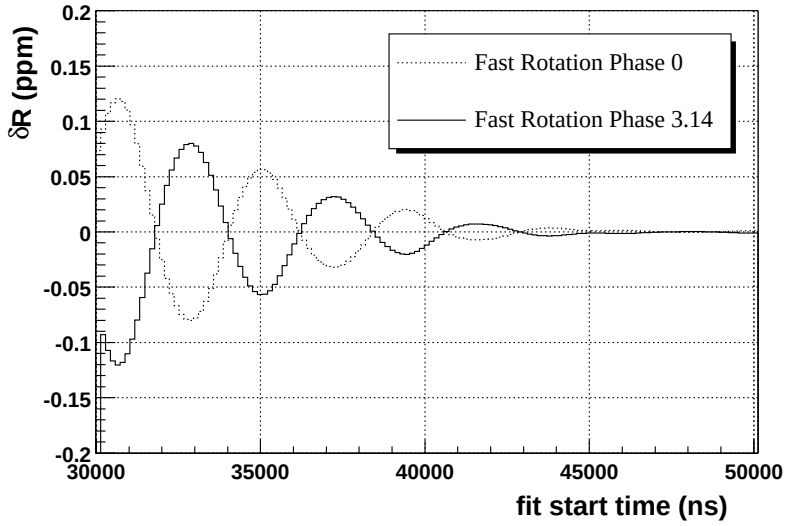

Figure 12: Systematic fitting error δR (ppm) for the case of fill randomization for detectors on opposite sides of the ring.

To estimate the effect of fill randomization error for 22 detectors, consider the following calculation. For simplicity, neglect the fast rotation envelope $\mathcal{A}(t)$ and consider only the sinusoidal component. Then for all 24 detectors with their g-2 phases aligned,

$$\mathcal{F}(t) = \frac{1}{24}\sum_{i=1}^{24}\left(1 + 0.002 * cos\left(\omega_{fr}t - \frac{i}{24}2\pi\right)\right) \tag{13}$$

Since we have only 22 detectors, the sum in Eq. 13 would retain detectors 14 and 8, diametrical opposites of 2 and 20, respectively,

$$\mathcal{F}(t) = 1 + \frac{1}{22} * 0.002 * \left(cos\left(\omega_{fr}t - \frac{14}{24}2\pi\right) + cos\left(\omega_{fr}t - \frac{8}{24}2\pi\right)\right) \tag{14}$$

The sum of the two cosine terms are at most 2 and hence adding the 22 detectors together yield another factor of ≈ 10 (2/22) in the reduction of the fast rotation structure. Therefore, for fitting the sum histogram of all 22 detectors together, the error is $< 0.2/10 = 0.02$ ppm.

Another check of the fill randomization procedure was the sensitivity of the fitted value of ω_a to the fast rotation period. Figure 13 shows plots of the differences in the fitted value of R for the cases of 147.2063 ns and 151.2063 ns compared to the case of 149.2063 ns. The effect is about 0.04 ppm over an uncertainty of 4 ns. We certainly know the fast rotation period to better than 0.4 ns, and hence this effect is negligible.

From the preceding analysis, it is then desirable for reducing the systematic fitting uncertainties due to fast rotation randomization that the sum of all detectors be used to extract the final value of ω_a, and that the g-2 phases of the detectors should be aligned. It is also known that the randomization procedure itself introduces a statistical fluctuation in the fitted value of ω_a at the level of about 10% of the statistics. For a goal of 1.3 ppm in ω_a, I will use six random sequences so that the uncertainty due to statitiscal fluctuation is $0.13/\sqrt{6} = 0.05$ ppm. Combining the fitting error with the statistical fluctuation gives that for fill randomization, the systematic fitting uncertainty is 0.06 ppm for the detectors summed and the phases aligned. Note also that choosing zero crossings of the g-2 signal will make this error nearly zero.

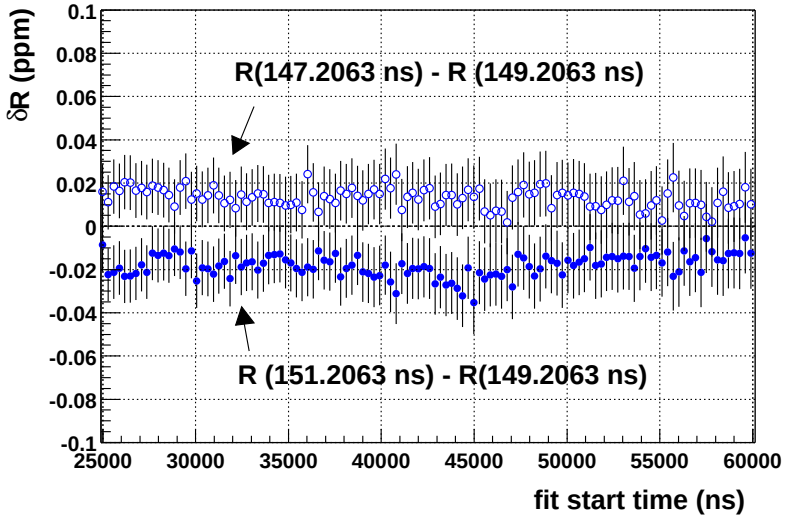

Figure 13: Systematic fitting error due to uncertainty in the knowledge of the fast rotation period. Notice that over a range of 4 ns $(147-151)$ in the accuracy of the fast rotation period, the variation in R is only 0.04 ppm.

4.2 Energy Calibration Shifts (EC)

With an eye toward fitting for the final value of ω_a from the summed histogram of all the detectors, the function $f(t)$ as fitted from the normalized average energy in Figure 6 will be used to estimate the effect on R of EC shifts within the fill. The function $f(t)$ is repeated here for reference with all times in μs.

$$f(t) = \left(1 - 0.00057 * exp\left(-\frac{t}{82}\right)\right) * \left(1 + 0.00036 * exp\left(-\left(\frac{t-31}{9.3}\right)^2\right)\right) \tag{15}$$

To estimate the error in R due to EC changes, a time changing software threshhold was applied using $f(t)$. Pulses with energy $E(t)$ were replaced by $E(t) * f(t)$ with the two amplitudes 0.00057 and 0.00036 multiplied by 20. The factor of 20 is used so that the software inflated EC changes would be larger than that seen in data by a factor of 10; the extra factor of 2 is needed to go from the average energy (as in Figure 6) to an energy threshhold.

Figures 14 and 15 show plots of the errors in R due to software EC changes having only the exponential component of $f(t)$ and both the exponential and gaussian components of $f(t)$, respectively. Notice that there is a phase pulling error at twice g-2 frequency about the zero line of magnitude < 0.5 ppm for all start times > 30 μs. Note also in Figure 14 that the g-2 zero crossing at 34 μs actually falls at the peak of the phase pulling error. Using the average energy changes as seen in Figure 6, then for both the g2off and G2Too data, the maximal error in R due to EC shifts in a fill is $0.5/10 = 0.05$ ppm.

Not all the detectors in the analysis experience the same average energy changes, and hence the question arises as to what the effect is when only one or two detectors see large EC changes, and the rest do not. Figure 16 shows a plot similar to that in Figure 15, but in this case only detectors 10 and 15 had software inflated EC changes at 110 times the level seen in data. The EC averaged over all 22 detectors is as before, 10 times the level seen in data. Note that the phase pulling error is as before, e.g. 0.3 ppm in amplitude at 40 μs. The systematic shift of 0.2 ppm is

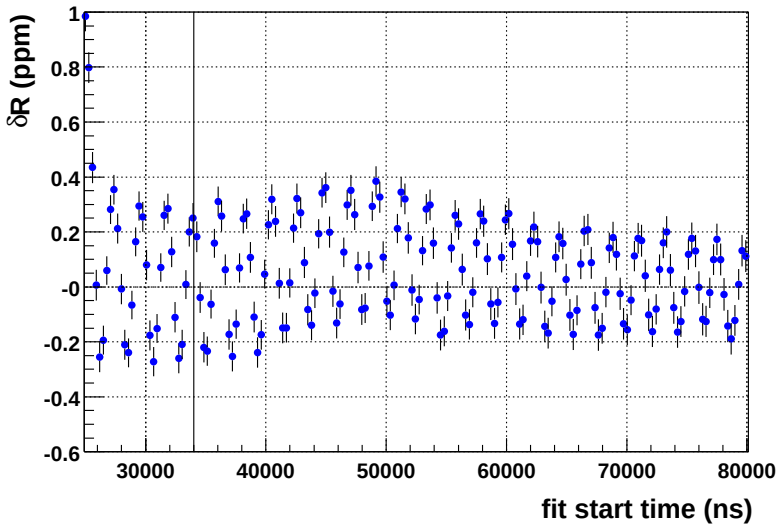

Figure 14: The error δR (ppm) due to a time changing energy threshhold implemented in software at 10 times the level seen in the data. Only the exponential part of $f(t)$ in Eq. 15 is used. The vertical line indicates the 34 μs mark, and is a zero crossing of the g-2 function. Note that the errors shown due to energy calibration changes are actually maximal at zero crossings of the g-2 function.

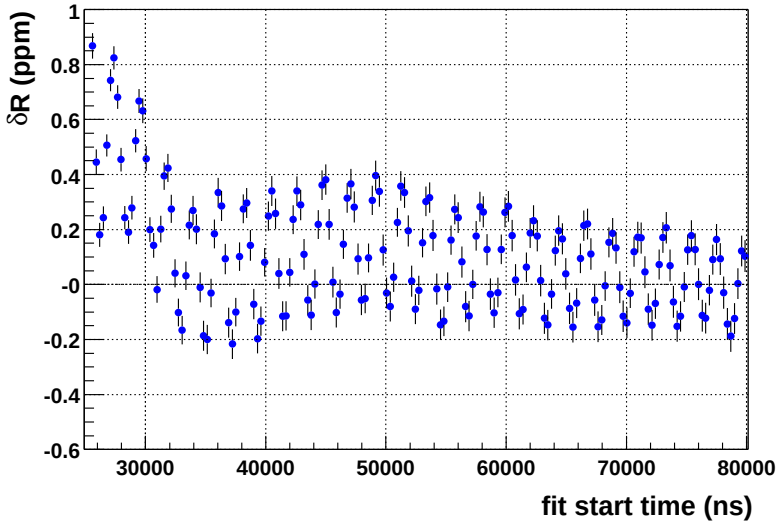

Figure 15: The error δR (ppm) due to a time changing energy threshhold implemented in software at 10 times the level seen in the data. Both the gaussian and exponential parts of $f(t)$ in Eq. 15 are used.

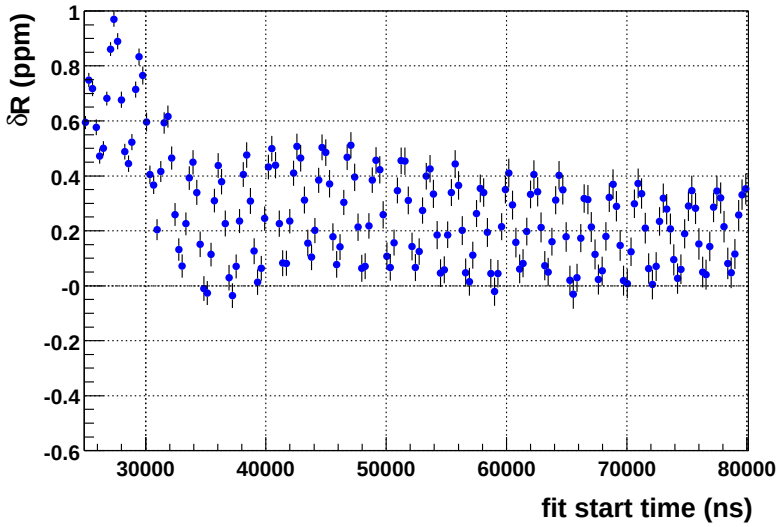

Figure 16: The error δR (ppm) due to a time changing energy threshhold implemented in software at 10 times the level seen in the data. Both the gaussian and exponential parts of $f(t)$ in Eq. 15 are used. However, only two detectors (10 and 15) were affected at the level 110 times seen in the data so that EC changes averaged over 22 detectors is at 10 times the level seen in data.

due to statistical fluctuations. In particular, the level of 110 times the exponential component in $f(t)$ is equal to an 8.7% change in the energy threshhold at 30 μs, which is roughly 17% difference in the positron count. Summing over the 22 detectors yield a data overlap of (20 + 2*0.83)/22 = 0.98. Assuming for simplicity that the extra counts have the same asymmetry as the rest, then the Kawall correlated statistics is 14% of the statistical power in R, 0.14*1.3 = 0.18 ppm.

4.3 Muon Losses

In Ref. [1], it was shown that besides using Eq. 11, the fitting errors δR in the ratio method can also be well estimated by fitting to data simulated without any statistical fluctuation. This method will be used in this section to estimate the systematic error due to neglecting the muon losses term in the ratio fitting procedure. With muon losses, the normal five-parameter function $G(t)$ is modified to $G(t) * MUL(t)$ where

$$MUL(t) = 1 + A_m * e^{-\frac{t}{\tau_m}} \tag{16}$$

Figure 25 shows a plot of the errors due to the extra term $MUL(t)$. The input muon losses parameters used were $A_m = 0.025$ and $\tau_m = 27$ μs [4]. The 0.01 ppm phase pulling error at later start times, > 80 μs, is due to neglecting second order terms in the ratio fitting method. The errors due to the muon losses term cancel the 0.01 ppm errors in the ratio method in the time range $45 - 65 \mu s$. For earlier start times, the error due to the muon losses adds to the width of the 0.01 ppm peaks in the ratio fitting error. Clearly, this effect is negligible, at about 0.01 ppm.

4.4 AGS Flashlet

The same method used in the last section will again be used in this section to estimate systematic fitting errors due to the AGS flashlets contamination. Simulated data with a flashlet/positron level of 126 ppm, Figure 18, was generated using the time distribution (with t in μs) [9]

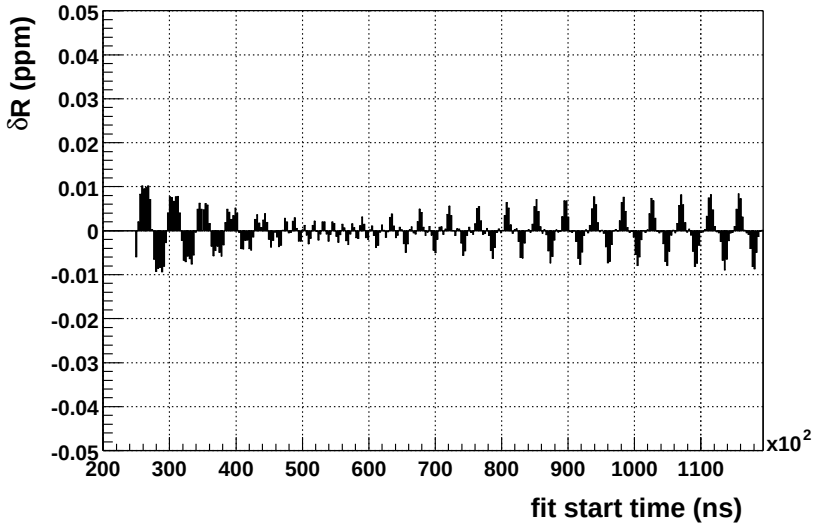

Figure 17: Systematic fitting errors δR due to neglecting the muon losses term in the ratio fit. The input muon losses function is $(1 + A_m * e^{-\frac{t}{\tau_m}})$ where $A_m = 0.025$ and $\tau_m = 27\ \mu s$.

$$FLA(t) = \left(\frac{11.409 - 0.0016947 * t - 0.00053516 * t^2}{398.982294} \right) * MIC(t) \tag{17}$$

where $MIC(t)$ is the microstructure per AGS cycle having four peaks of varying amplitudes separated by 1/6 of an AGS period, and is given by by the following function

$$\begin{aligned} MIC(t) \;=\; & 0.17 \sum_{i=1}^{i<=51} \delta(t - 2.694 * i) + 0.21 \sum_{i=1}^{i<=51} \delta(t - 0.449 - 2.694 * i) + \\ & 0.28 \sum_{i=1}^{i<=51} \delta(t - 0.898 - 2.694 * i) + 0.34 \sum_{i=1}^{i<=51} \delta(t - 1.347 - 2.694 * i) \end{aligned} \tag{18}$$

In the presence of the AGS flashlets, the observed time spectrum becomes $G(t) \rightarrow (G(t) + FLA(t))$, where $G(t)$ is the five-parameter function. Figure 19 shows the error in R due to the presence of the extra term $FLA(t)$. Since the integral of the ratio of flashlet/positron is increasing from injection, the error in R is growing as a function of fit start times and is not maximal until about 80 μs, reaching a value of 0.12 ppm. Figure 20 shows the same plot as in Figure 19 for the time range $20 - 65\ \mu s$. Since the final value of R will be quoted for fit start time around 35 μs, a systematic error of 0.06 ppm per 126 ppm flashlet/positron contamination can be quoted. Since our knowledge of $FLA(t)$ is not exact, a final conservative value of 0.10 ppm will be assigned.

4.5 Coherent Betatron Oscillation (CBO)

The same method used in the previous two sections will again be used in this section to estimate the systematic fitting uncertainty due to neglecting the CBO term in the g-2 time spectrum. The CBO can be parameterized approximately by

$$CBO(t) = 1 - A_c * e^{-\left(\frac{t}{\tau_c}\right)^2} cos(\omega_c t + \phi_c) \tag{19}$$

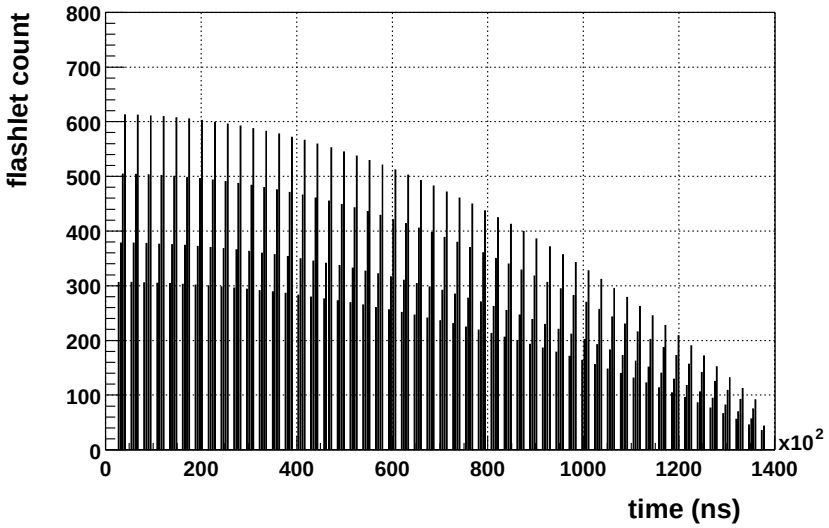

Figure 18: Simulated time distribution of the AGS flashlets for one of the four ratio subhistograms. Integrated over all times, the flashlet contamination is 126 ppm of the total $\left(\frac{1}{4}\right) 2 \times 10^9$ positrons.

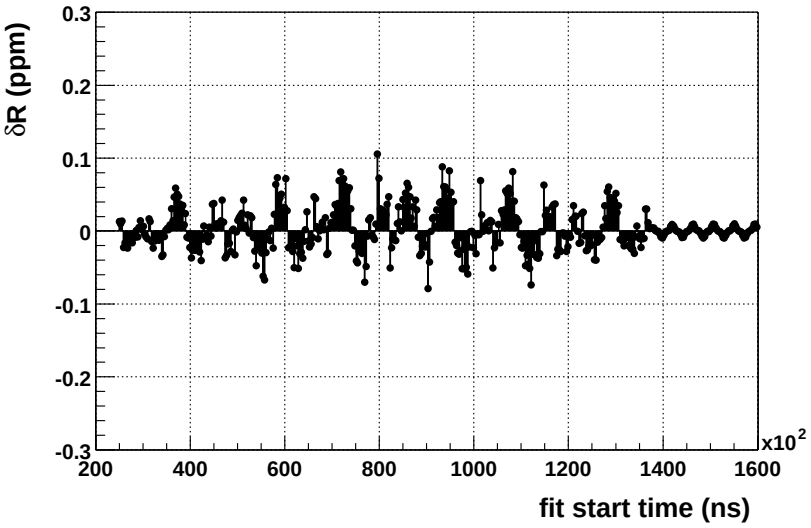

Figure 19: Systematic fitting error δR versus fit start time due to AGS flashlets. The ratio of flashlet to positron counts over all time is 126 ppm, and the AGS flashlets are parameterized by a parabolic envelop with four subpeaks per AGS period of 2.694 μs, or frequency of 371 kHz.

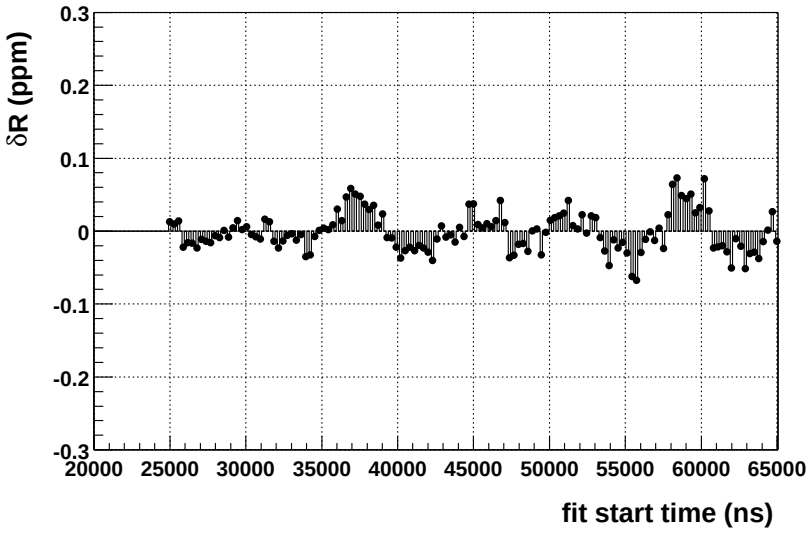

Figure 20: Systematic fitting error δR versus fit start time due to AGS flashlets. The ratio of flashlet to positron counts over all time is 126 ppm, and the AGS flashlets are parameterized by a parabolic envelope with four subpeaks per AGS period of 2.694 μs.

I did not myself study the CBO parameters. Rather, I will use values as extracted by Alex [10], $A_c \approx 0.0028$, $\tau_c \approx 132$ μs, $\omega_c \approx 470$ kHz, $(\phi_c - \phi) \approx 1.0$ rad, and study the ratio fit sensitivity to changing those parameters. Note that the CBO parameterization here is $(1 - A_c)$ instead of $(1 + A_c)$ in [10]. This is because I use $(1 - A)$ instead of $(1 + A)$ for the positron time spectrum, and hence the minus sign is used in Eq. 19 to keep the phase shift value of 1.0 rad.

Figure 21 shows the fitting error due to neglecting the CBO parametization. For all times $>$ 30 μs, the magnitudes of the fitting error is < 0.03 ppm. Note that the simulated CBO magnitude is more than 3 times larger than that seen in the data, 0.01 compared to 0.0028. Figure 22 shows the effect on the fitting error for the three cases of $(\phi_c - \phi) = 0.0,\ 1.0,\ 1.57$ radians. Note the complicated time structure of the oscillations in the fitting errors. The relative CBO phase shift to g-2 essentially shifts the phase of the fitting error by the same amount. However, the magnitudes are not affected. Figure 23 shows the effect on the fitting error for the three cases of $\tau_c = 112,\ 132,\ 152$ μs; the fit error is not sensitive to the CBO time constant. Figure 24 shows the effect on the fitting error for the three cases of $\omega_c = 460,\ 470,\ 480$ kHz. Note that 460 kHz is close to twice g-2, 458.2 kHz. The error in that case is zero from the nature of the ratio formulation shifting things around by 1/2 g-2 period. However, the CBO amplitude at 480 kHz is about 0.09 ppm, and hence the fitting error magnitude has a growing dependence on $(\omega_c - 2 * \omega_a)$.

As intuitively expected, the ratio method is a frequency filter and hence is only sensitive to the CBO frequency. The CBO frequency is known to about $\pm$ 2 kHz, and so assuming a linear interpolation between 470 and 480 kHz gives a value of 0.042 ppm as an estimate of the fitting error given the uncertainty in the knowledge of ω_c. For the CBO signal seen in data, the value of 0.014 ppm will then be used (for detectors summed). Like the muon losses error, this effect is negligible.

Figure 25 shows the difference in the value of R when the detectors are fitted individually and then averaged versus when the detectors are summed and then fitted. There is an oscillation of magnitude 0.1 ppm and periodicity ≈ 80 μs, which is near the difference $(\omega_c - 2*\omega_a)$ $(470 - 2*229.1 = 11.8$ kHz $\rightarrow$ 4365.4*229.1/11.8 $= 84.7$ $\mu s)$. The oscillation looks too regular and is too close to the expected beat frequency to be interpreted as a statistical fluctuation. Therefore, this will be added

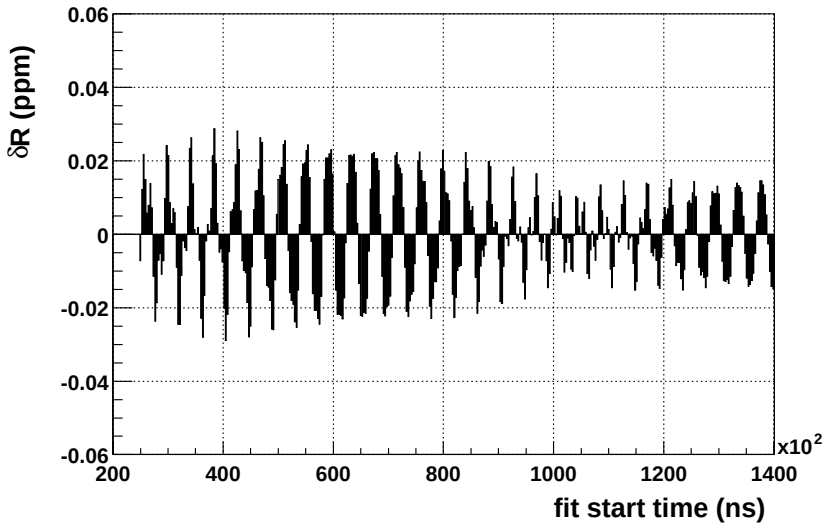

Figure 21: Systematic fitting error δR due to neglecting the CBO term in the ratio fit. The input CBO function is $(1 - A_c * exp(-(t/\tau_c)^2) * cos(\omega_c t + \phi_c))$, where $A_c = 0.01$, $\tau_c = 132\ \mu s$, $\omega_c = 470$ kHz, and $(\phi_c - \phi) = 1.0$ rad. This CBO amplitude is about three times that seen in the data when all detectors are summed.

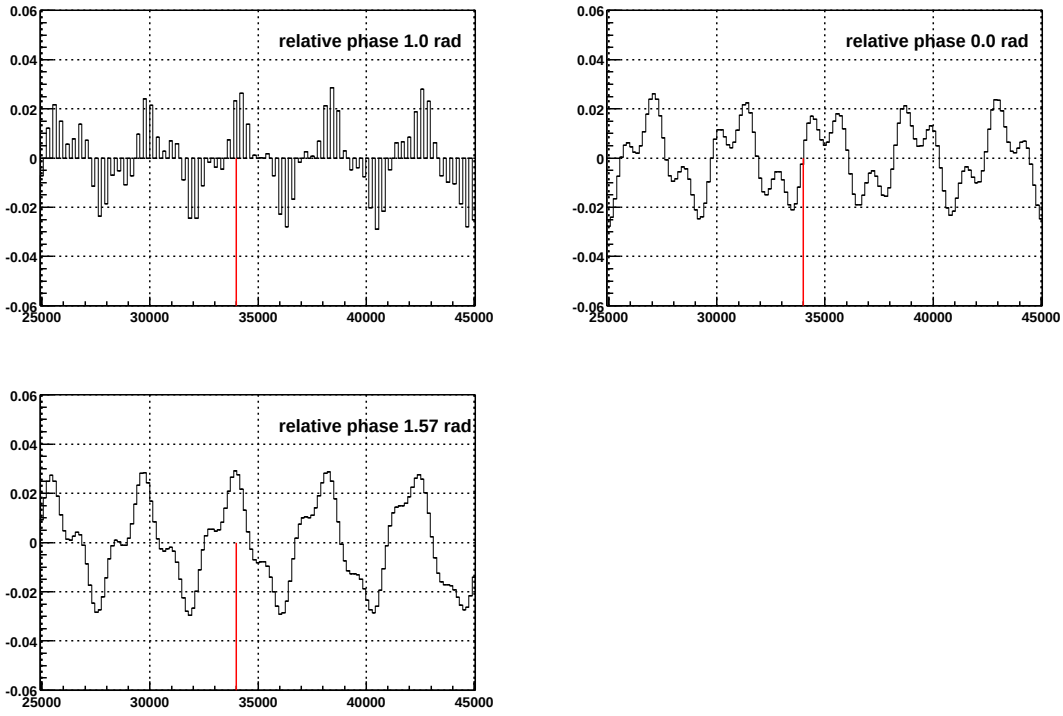

Figure 22: The effect on δR of changing the CBO phase for the three cases $(\phi_c - \phi) = 0$, 1.0 and 1.57 radians. As in Figure 21, the axes are δR (ppm) versus fit start time (ns). The red line is at 34 μs and is at a zero crossing of the g-2 function.

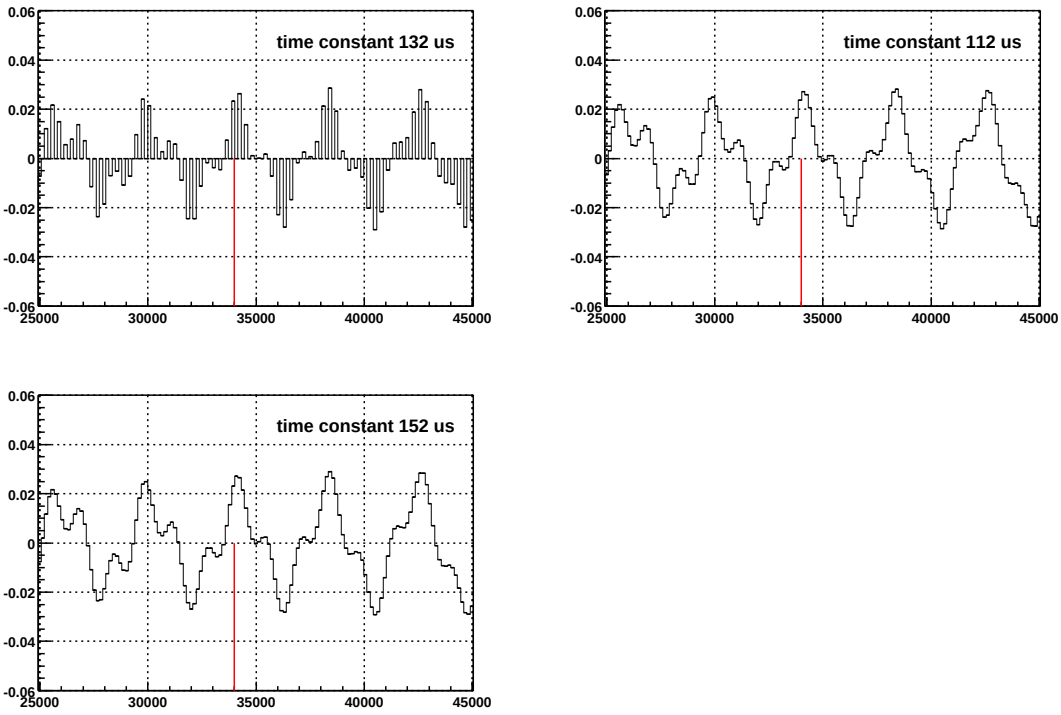

Figure 23: The effect on δR of changing τ_c for the three cases of 112, 132, 152 μs. As in Figure 21, the axes are δR (ppm) versus fit start time (ns). The red line is at 34 μs and is at a zero crossing of the g-2 function.

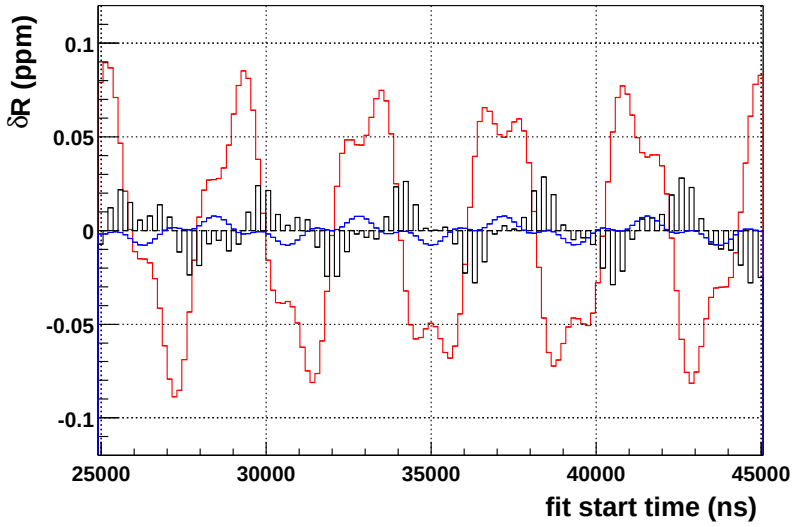

Figure 24: The effect on δR of changing ω_c for the three cases of 460 (blue line), 470 (black line) and 480 (red line) kHz.

to the systematic error due to the CBO. It is known that in the sum of the detectors, the CBO signal is reduced by about 1/3 compared to the individual ones. Therefore, an error of 0.05 ppm will be assigned to this effect. The final systematic uncertainty for the CBO is then 0.05 ppm.

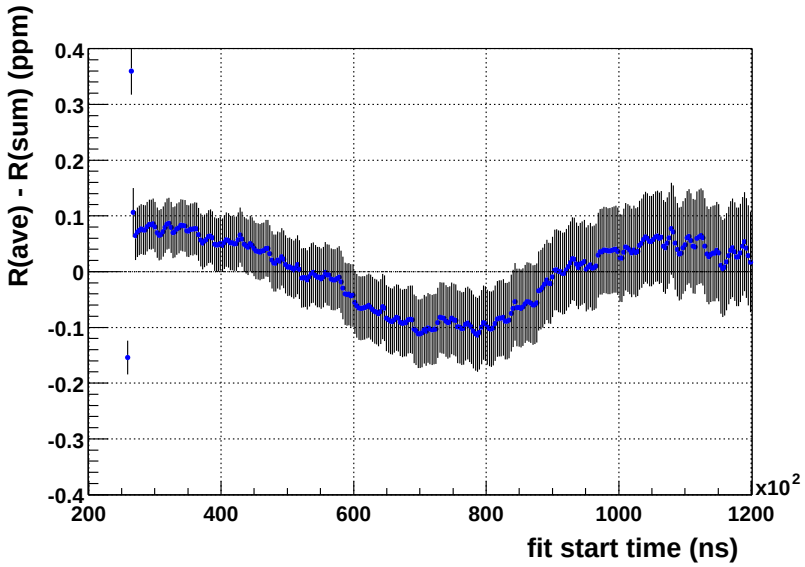

Figure 25: The difference vs fit start time of R(averaged over all detectors) - R(sum of all detectors). The error bars plotted are Kawall errors.

4.6 Software Pileup Subtraction (PUS)

Consider first the systematic fitting error in the ratio method due to neglecting the pileup term completely. In this case, the background $B(t)$ is

$$B(t) = \epsilon_d N_o e^{-\frac{2t}{\tau_\mu}}[1 - A_d * cos(\omega_a t + \phi_d)] \tag{20}$$

where N_o is the singles normalization constant, ϵ_d is the fraction of pileup to singles at time 0, A_d is the pileup asymmetry, and ϕ_d is the pileup phase. Figure 26 shows a plot of the fitting errors as calculated using Eq. 11 for the case of $\epsilon_d = 0.008$, $A_d = 0.1$, $\phi_d = -0.1$, $A = 0.4$ (these input values were chosen to be close to what Cenap [4] finds). The values shown in Figure 26 are the expected fitting errors in R if in the data we have pileup with parameters as given, and the ratio fit was implemented using the function $R(t)$. To compare this to the case of real data, the following was done. Values of R from fits to data without PUS were subtracted from values of R from fits to data with PUS, and the results are plotted in Figures 27 and 28, g2off and G2Too data, respectively. Note that the error oscillates at twice the g-2 frequency about an offset that decreases with fit start time with a time constant of 64 μs. The magnitudes of the error oscillations should scale with the g2off/G2Too pulse resolution times of 2.9/5.0. From Figure 27, the magnitude at 30 μs is 0.2 ppm; from Figure 28, the magnitude at 30 μs is 0.3 ppm.

Figure 29 shows plots of the difference $dR = R$(no PUS and fitted to $R_K(t)$) $- R$(PUS). The function $R_K(t)$ has one additional parameter that can account for the pileup fraction and asymmetry but neglects the phase differences between the pileup and singles pulses. In this case the phase error oscillations are gone, but the offset is still there. As in the case of the error oscillations, this error is expected to scale with the pulse resolution time 2.9/5.0 as well. Figure 29 does not show this. This is probably due to a statistical fluctuation which is suggested by the "kink" at 80 μs.

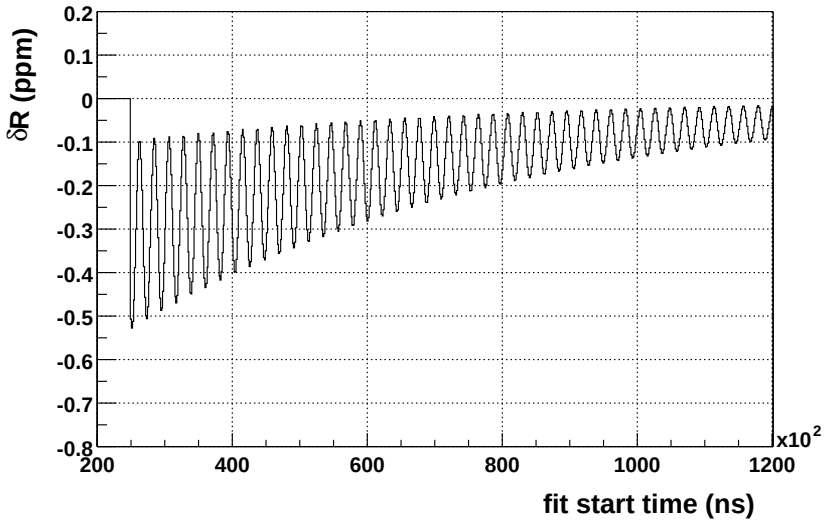

Figure 26: Calculated fitting error δR using Eq. 11 for the cae of the neglecting the background term $B(t) = \epsilon_d N_o * exp(-\frac{2t}{\tau_\mu})[1 - A_d * cos(\omega_a t + \phi_d)]$ where $\epsilon_d = 0.008$, $A_d = 0.1$, and $\phi_d - \phi = -0.1$.

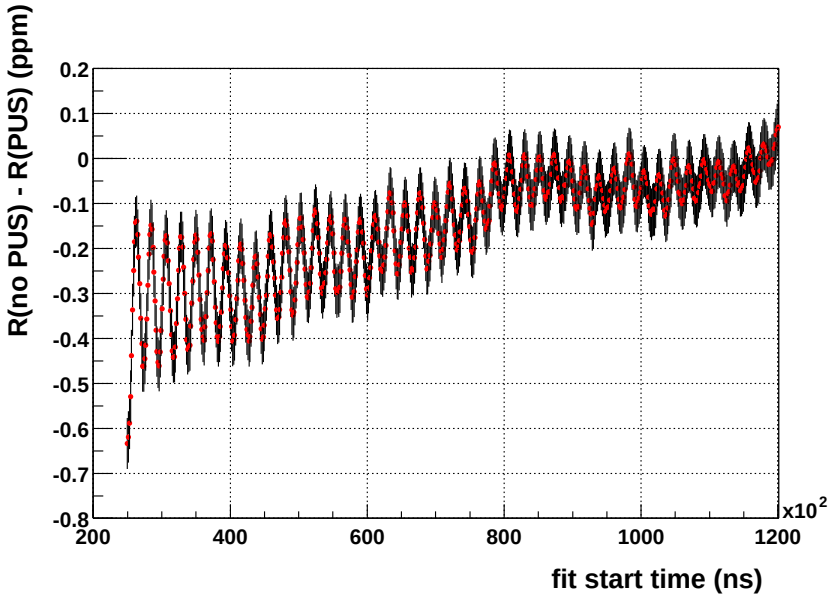

Figure 27: R (without PUS) $-$ R (with PUS) (g2off data). This is the fit error in the ratio method due to completely neglecting the pileup pulses. Note that besides the 0.2 ppm oscillation of twice g-2 frequency, there is also a systematic offset of magnitude ≈ 0.3 ppm at 30 μs which decreases with roughly a 64 μs time constant.

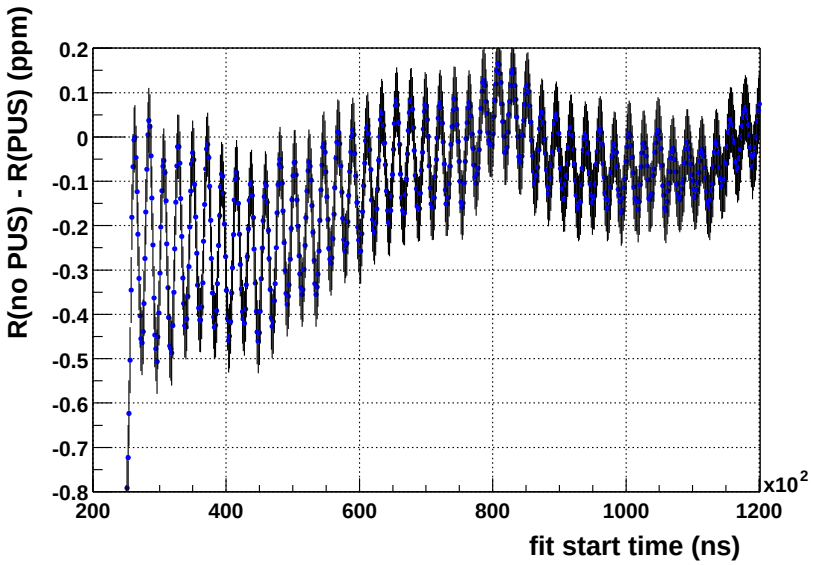

Figure 28: R (without PUS) $-$ R (with PUS) (G2Too data). This is the fit error in the ratio method due to completely neglecting the pileup pulses. Note that besides the 0.3 ppm oscillation of twice g-2 frequency, there is also a systematic offset of magnitude $\approx$ 0.3 ppm at 30 μs which decreases with roughly a 64 μs time constant.

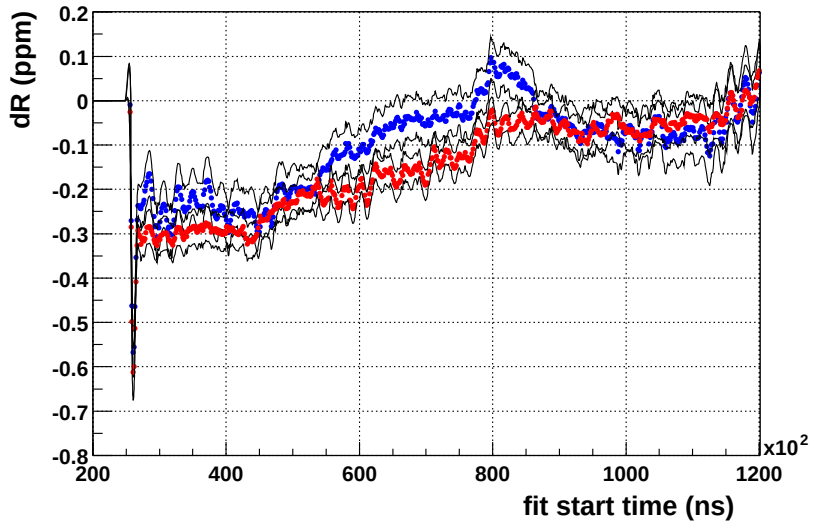

Figure 29: The quantity $dR = R$ (no PUS fitted using $R_K(t)$) $-$ R (PUS). This is the fit error in the ratio method due to neglecting the phase difference between the pileup and singles pulses.

This method of software PUS using shadow pulses is complete to about 90% [4]. Therefore, for estimates of the error due to PUS, a factor of 0.1 times the values as given in Figures $27-29$ can be used. For g2off data at times $> 30\ \mu s$, the error offset is 0.4 ppm (this value is extrapolated from 0.3 ppm at 40 μs), plus the oscillation magnitude of 0.2 ppm gives 0.6 ppm. Scaling by 5/3 gives 1.0 ppm for G2Too. Therefore, the final estimates for the systematic uncertainty due to PUS is 0.06 ppm (g2off) and 0.1 ppm (G2Too).

4.7 Summary of Systematic Uncertainties

Table 1 below summarizes the results of the systematic fiting uncertainties relating to the ratio fitting procedure as discussed in Sections $4.1-4.6$. The correlations between the various effects as studied are small. For example, the energy calibration is affected by the fast rotation, but in both the macroscopic and microscopic methods, the effects of the fast rotation are subtracted out to a large extent. For another example, the PUS is affected by the energy calibration. However, this is small since pileup only accounts about 1% of the pulses and so an error of 0.1% in the average energy affects the total data at the level of 0.01*0.001. The AGS flashlets of course don't care about any other thing. The next possible correlation among the various systematic errors is in their correlations to the g-2 phase. For example, the fitting error due to EC shifts are known exactly to oscillate at twice g-2 and is at its maximum at 34 μs. Column 3 in Table 1 lists the sign, if known, of the fitting error at the start time of 34 μs. The STAT status of the fast rotation is due to the statistical fluctuation from the 6 random sequences. The STAT status of the fitting method error was already explained in Section 2.1; the actual error due to neglecting higher order terms in the fitting method itself was shown to be at only 0.01 ppm [1]. Considering the two STAT errors and the nearly equal magnitudes of + and - errors give reason to add the systematic errors in quadrature giving final values of **0.17 ppm** (g2off) and **0.19 ppm** (G2Too). The uncertainty estimates for the double CBO and vertical waist will be considered in Section 5.5 on fit residuals.

Table 1: The division of systematic fitting uncertainties for the ratio method. The values are applicable for all start times $> 30\ \mu s$ (except the AGS flashlet which is limited to start times $< 50\ \mu s$ as well). The SIGN of the error at 34 μs is denoted if it is known in the last column. The STAT in the last column denotes that the uncertainty itself is dominated by statistics.

EFFECT	δR (ppm)	SIGN
Fitting/binned data	0.05	STAT
Fast rotation randomization (six random sequences)	0.06	STAT
Energy calibration shifts	0.05	+
Muon losses	0.01 (negligible)	
AGS flashlets (126 ppm)	0.10	UNKNOWN
CBO	0.05	+
Double CBO	0.01 (negligible)	
Vertical Waist	0.02	UNKNOWN
Pileup subtraction	0.06 (g2off) 0.10 (G2Too)	-
TOTAL (added in quadrature)	**0.17** (g2off) **0.19** (G2Too)	

5 Fit Results

In this section fit results using the ratio method for both g2off and G2Too will be presented. In Section 4 it was shown that the systematic uncertainies can be made smaller by summing the 22 detectors together. Therefore, this section will focus mainly on fit results for the detectors summed (fit results versus start time for the individual detectors are attached at the end of the report). For all the results to be presented, both fill randomization, with fast rotation periods of 149.1202 ns (g2off) and 149.2063 ns (G2Too), and pileup subtraction were applied to the data. Hence fitting with the ratio method requires only the three parameters (A, ω_a, ϕ) or (A, R, ϕ). In all time histograms, bins of width 149.185 ns were used, and all fits had a stop time of 500 μs. This earlier stop time was needed to ensure gaussian statitics for all time bins included in the fit since to implement the ratio method, the positron data had to be divided into four subsets. Apart from section 5.4, all results are for the case of a 2.0 GeV lower energy cut and no upper energy cut. Finally, results of fits to simulated data will also be presented as a reference in helping judge the "goodness of fit".

5.1 Detector Variations

In this section fit results for the individual detectors for mostly the start time of 34 μs will be presented. In all results, the average over the six random sequences were taken.

The g-2 phases of all the detectors were aligned as follows. For about 80% of the runs, the data for each detector were fitted, and the values of ϕ at 40 μs were used as the phase offsets for the final histogramming of 100% of the 1999 data. Figure 30 shows plots of the fitted values of ϕ versus detectors at 40 and 34 μs. The detectors are aligned to $\pm$ 2 mrad which is $\pm$ 1.4 ns. This alignment is 1.4/150 = 1% of the fast rotation period and is good enough for the purposes of minimizing the fast rotation systematic error.

Figure 31 shows the fitted values of R at 34 μs for both the g2off and G2Too data as well as the differences versus detector. For g2off, the R values averaged over all detectors is 143.44 ± 1.27 ppm with $\chi^2/ndf = 1.25 \pm 0.31$, and for G2Too 143.11 ± 1.28 ppm with $\chi^2/ndf = 1.06 \pm 0.31$. Notice in Figure 31 (bottom) that assuming Fred's data overlap estimate of $0.327^*\sigma_R$ holds for all the 1999 data, then the differences seen between the g2off and G2Too data are consistent with statistical fluctations, $dR = 0.32 \pm 0.42$ ppm with $\chi^2/ndf = 1.15 \pm 0.31$.

Figure 32 shows the χ^2/ndf for fits to the individual detectors. For both data sets, the χ^2/ndf averaged over the detectors are 1.006 ± 0.005. However, the G2Too spread is better, having a fit χ^2/ndf to a constant of 0.87 ± 0.31, whereas for g2off data, the same value is only 0.29 ± 0.31. This value of 0.29 is $(1 - 0.29)/0.31 = 2.3$ sigmas from one, only a 2.8% probability! Figure 33 shows the fitted asymmetries versus detectors; the agreement between g2off and G2Too data is good.

5.2 Start Time Variations

In this section the results of fits for the sum of all the detectors averaged over the six random sequences will be presented. For organizational clarity the more detailed question of "goodness of fit" will be addressed in the next section.

Figure 34 shows a plot of the values of R versus start time for fits to the sum of all the detectors, and Figure 35 shows the other fit parameters, A and ϕ, as well as the fit χ^2/ndf. Note in Figure 34 that the R values of 143.37 and 143.03 are to be compared to the corresponding values of 143.44 and 143.11 in Figure 31. This difference was already discussed in Section 4.5 (CBO). The difference of 0.0004 in the asymmetries between g2off and G2Too is probably due to the different endpoint values of 3.09 and 3.10 GeV. The same physical point called 3.09 would result in slightly higher asymmetry positrons when the same software cut of 2.0 GeV is used. For both g2off and G2Too,

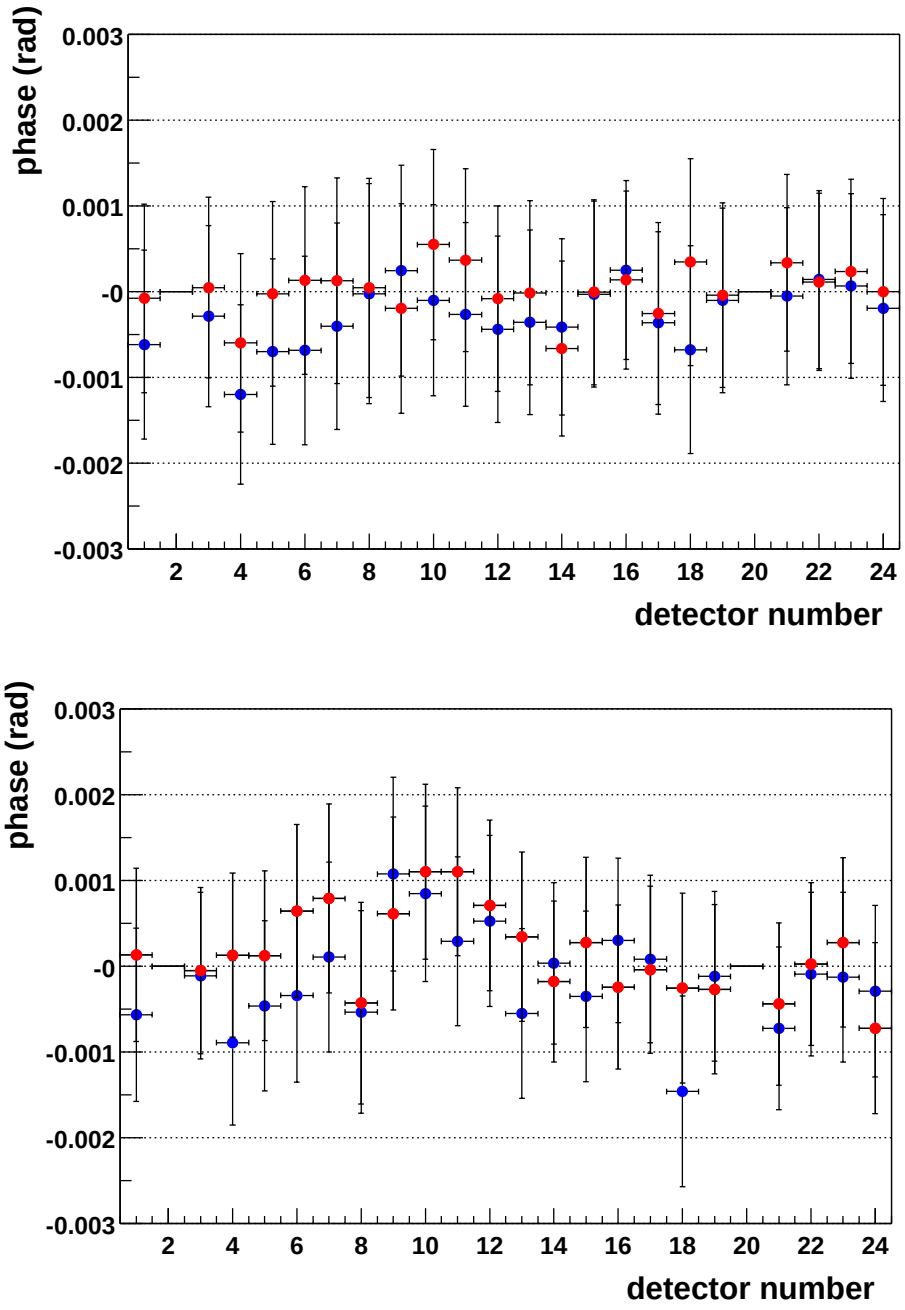

Figure 30: Φ versus detectors at 40 μs fit start time (top) and at 34 μs fit start time (bottom). The initial alignment of the g-2 phases were done at 40 μs using about 80% of all the 1999 data, and hence the alignment is better at 40 μs then at 34 μs.

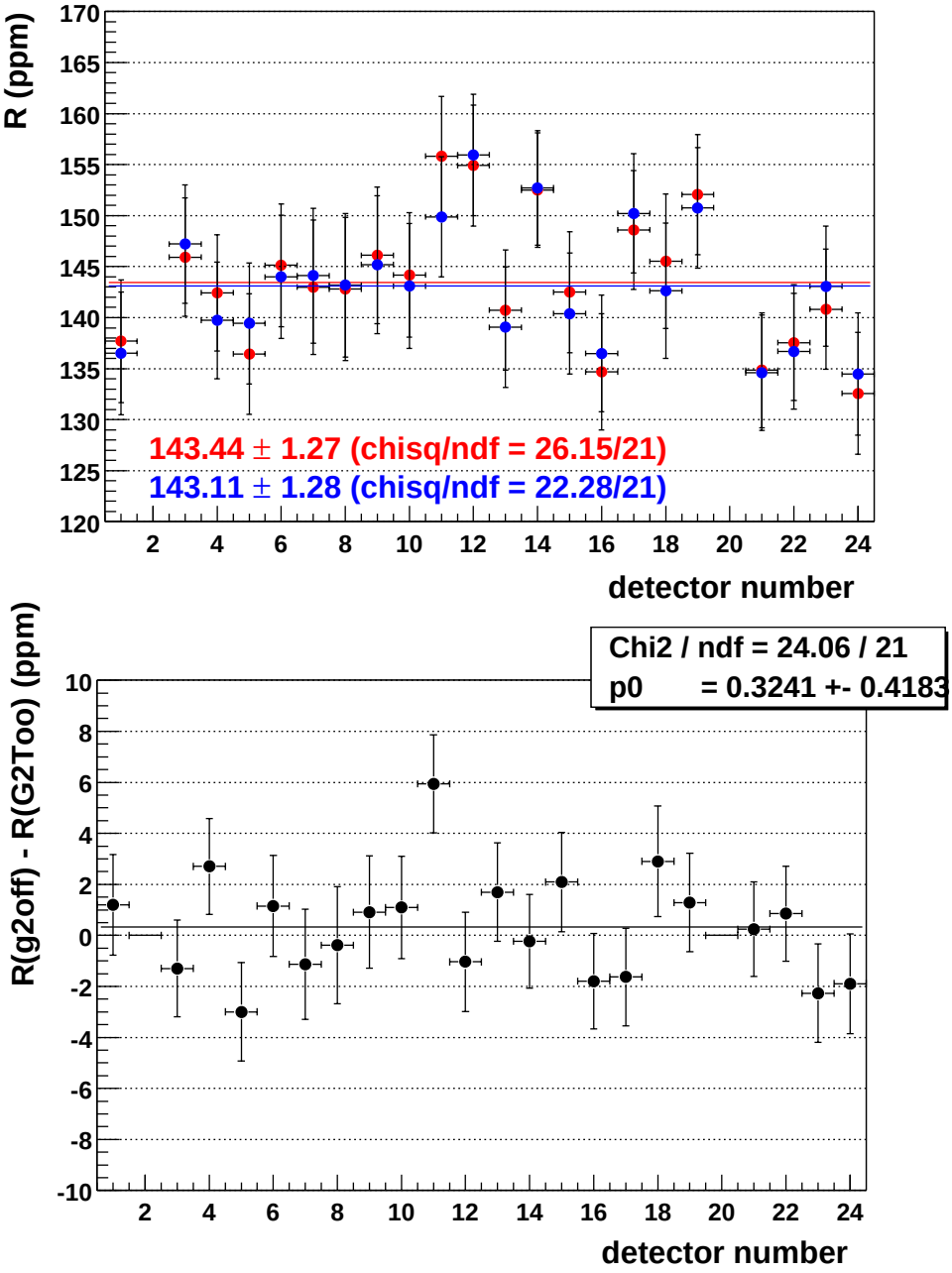

Figure 31: R versus detector at 34 μs fit start time (top). The differences between the g2off and G2Too R values are shown in the bottom plot. The error bars plotted with the differences in the bottom plot are the statistics of the fits from the top plot multiplied by 0.327. This value is Fred Gray's estimate for the allowed data overlap variation between g2off and G2Too using run 4330.

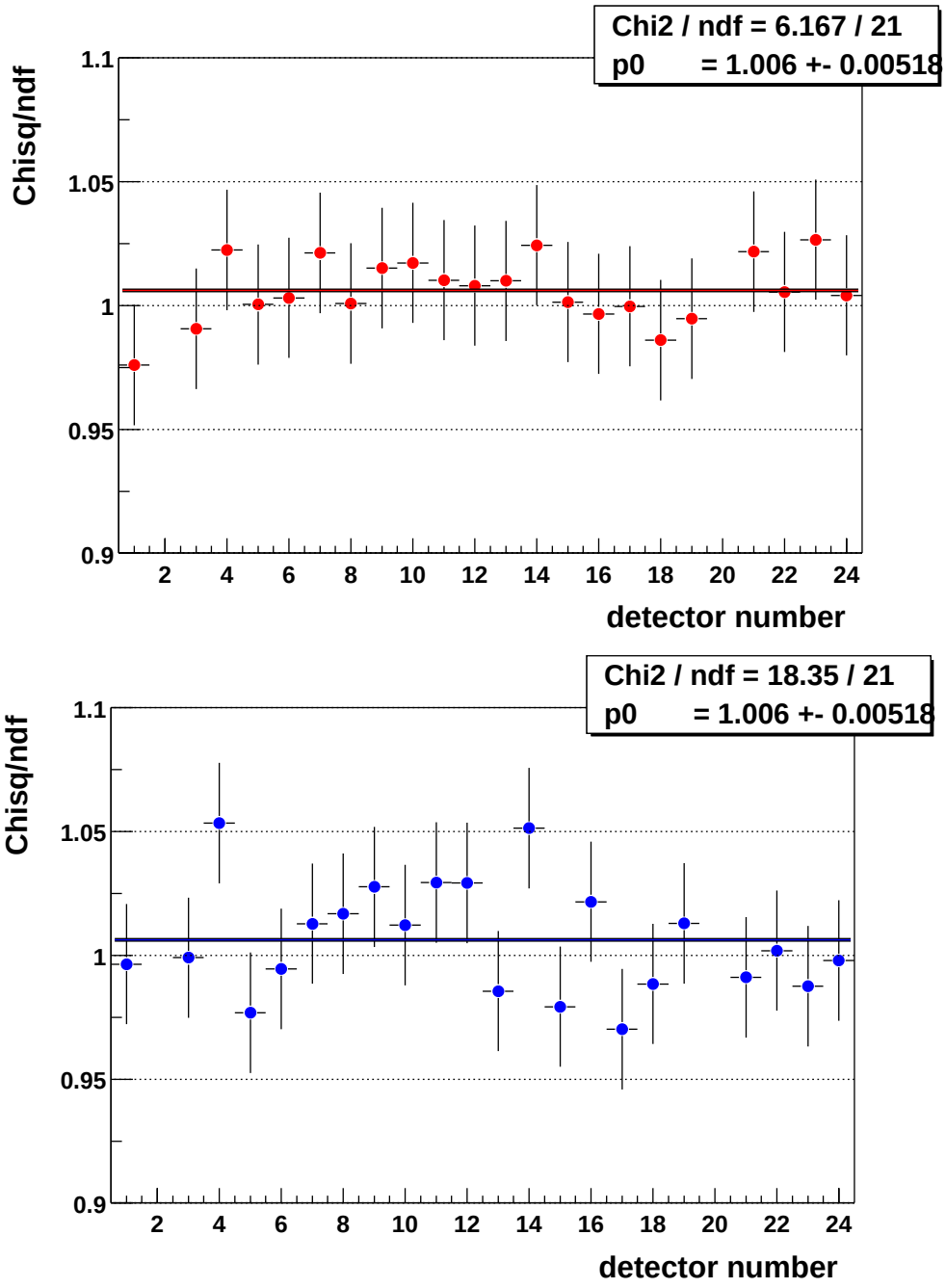

Figure 32: χ^2/ndf versus detector at the fit start time of 34 μs. Note that both g2off and G2Too distributions have means 1.006 ± 0.005. The error bars plotted with the χ^2/ndf values were calculated using $\sqrt{2/ndf}$ which is $\sqrt{2/(3352-228+1-3)} = 0.024$ for the start time 34 μs (bin 228) and stop time 500 μs (bin 3352).

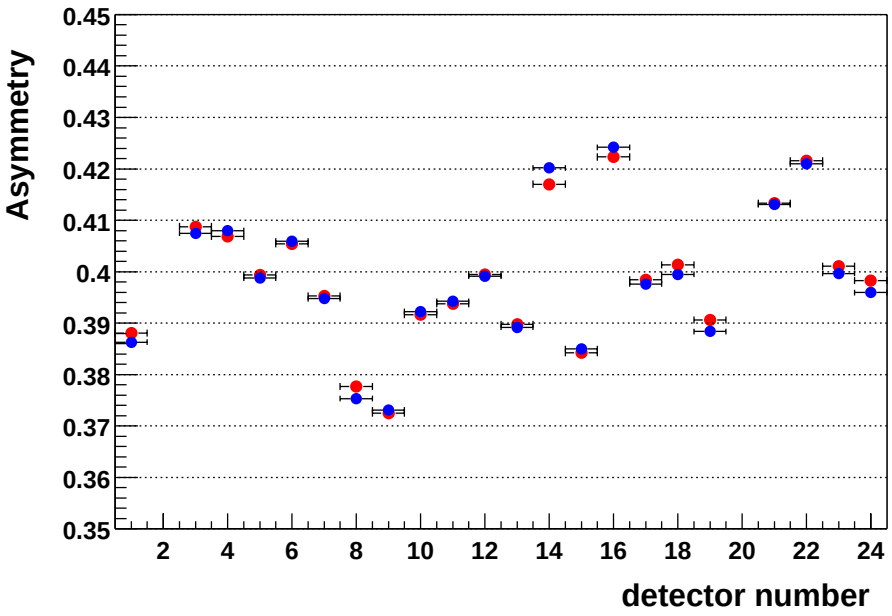

Figure 33: Asymmetry versus detector at the fit start time of 34 μs.

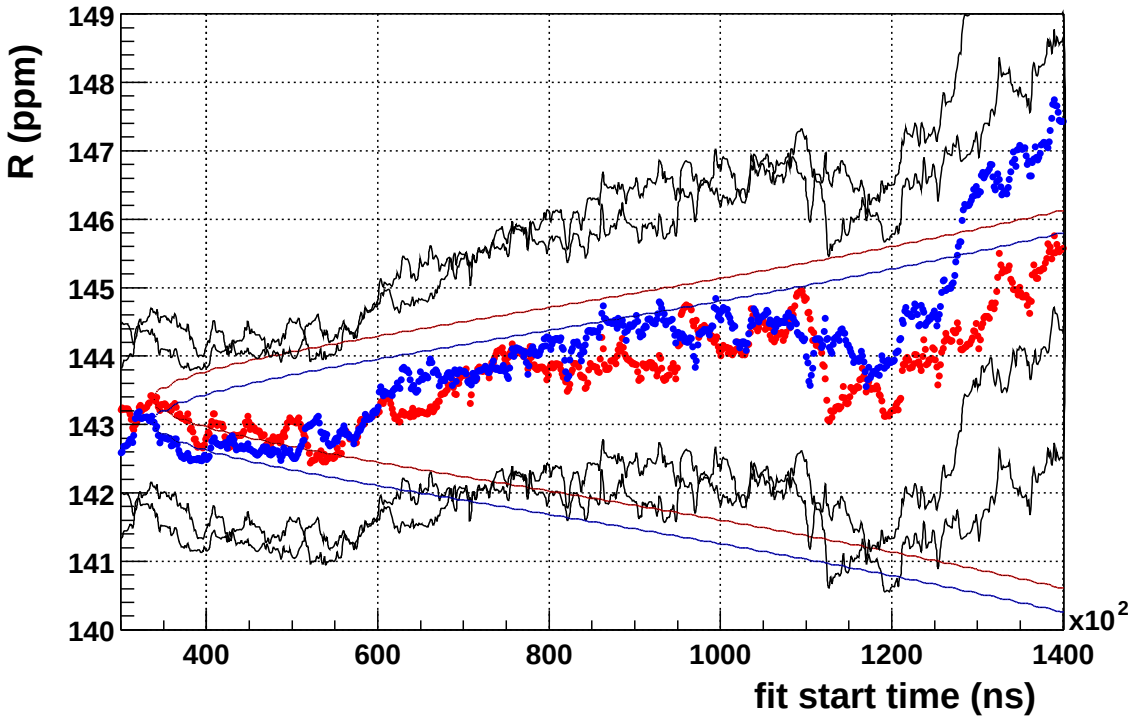

Figure 34: R versus fit start time. The correlated statistics bands were calculated in the usual way $\sigma_{cor} = \sqrt{\sigma_R(t)^2 - \sigma_R(33.94\ \mu s)^2}$. The R values at 33.94 μs are 143.37 ± 1.28 ppm (g2off) and 143.03 ± 1.28 ppm (G2Too).

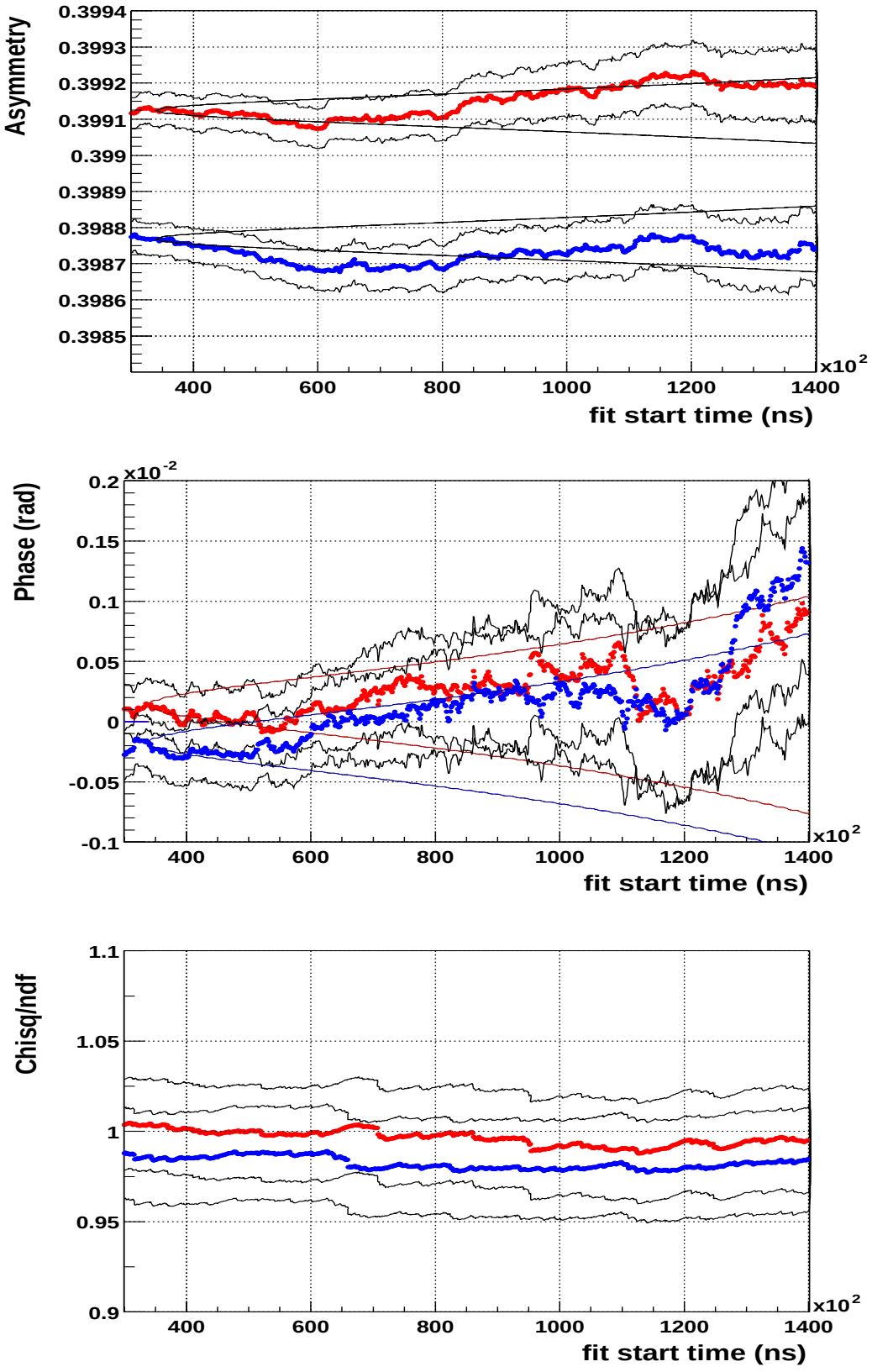

Figure 35: A, ϕ, and χ^2/ndf versus start time for fits to the sum of all detectors. The R values are given in Figure 34. The χ^2/ndf at 34 μs are 1.004 ± 0.025 (g2off) and 0.986 ± 0.025 (G2Too).

the fit χ^2/ndf's are consistent with one and are not seen to change with start time beginning at 30 μs.

5.3 Goodness of Fit and Correlated Statistics

In this section the issue of "goodness of fit" for results presented in the previous two sections will be addressed. In particular, the behavior of χ^2/ndf and fit parameters versus start time, and the behavior of the correlated (or Kawall) statistics will be studied. To aid in understanding the behavior of fit results versus start time for the ratio method, 60 sets of data were simulated and fitted. The data had time bins of width 149.185 ns, the input parameters were $\tau_\mu = 64.4$ μs, $A = 0.36$, $\tau_a = 4.366$ μs, $\phi = 0$, and the total number of positrons was 2×10^9 per set. These parameters give a fit statistical power of 1.24 ppm for the time range of $34 - 500$ μs. The fits were implemented beginning at time bin 168 (25 μs), skipping every two bins until bin 1100 (160 μs).

Note in Figure 35 that the χ^2/ndf for the g2off data have seemingly sudden jumps at 70 and 95 μs. However, Figure 36 shows that this behavior is not unexpected even for fitting perfectly simulated data, see the χ^2/ndf for data set 4 at 75 μs. Furthermore, note that for data sets 5 and 6, the fit χ^2/ndf actually moves by quite a bit versus start time. However, a "flat" χ^2/ndf is the typical case. Therefore, the fit χ^2/ndf seen in Figure 35 are acceptable. For comparison the fit χ^2/ndf for the case of no pileup subtraction for g2off data is plotted in Figure 37.

Figure 38 shows plots for the fitted R values corresponding to the χ^2/ndf in Figure 36. Note that for data sets 1, 2, 3 and 8, the values of R versus start time actually move outside the correlated statistics (CS) bands for ≈ 20 μs after the point at 34 μs. The R values then return back inside the CS bands and may also venture outside the CS bands at later times, sets 2, 6 and 7. Therefore, comparing the R values in Figure 34 to those in Figure 38 shows that R values for both g2off and G2Too behave acceptably versus start time.

Besides the χ^2/ndf and R versus start time checks, a more quantitative check of the fit parameters versus start time can be conducted, namely checking the distribution of values $\mathcal{D}_P$ that can be called the "correlated differences"

$$\mathcal{D}_P = \frac{P(t_2) - P(t_1)}{CS_P} = \frac{P(t_2) - P(t_1)}{\sqrt{\sigma_P(t_2)^2 - \sigma_P(t_1)^2}} \tag{21}$$

where the subscript P represents any of the fit parameters and CS_P is the "correlated" or Kawall statistics. In the present situation, $t_2 > t_1$, and therefore the fitted value of P for the start time t_2 will have come from data that is a complete subset of the data giving the fitted value of P at start time t_1. We've always assumed this distribution to be a gaussian centered at zero with a width of one. However, recent and ongoing analytical studies by Ernst Sichterman, Mario Deile and Sergei Redin have shown that for the multiparameter fit, the distribution $\mathcal{D}_P$ is non-gaussian for times t_1 and t_2 that are successive in time bins, i.e. $(t_2 - t_1) = 149.185$ ns for time bins of width 149.185 ns. I expect that the ratio method should behave in the same manner. I myself have not had time to analytically examine what the exact distribution of $\mathcal{D}_P$ is for the ratio method for $(t_2 - t_1) = 149.185$ ns. However, I have found in the fits to the 60 sets of simulated data that for times $(t_2 - t_1) = 2 * 149.184$ ns, the distributions $\mathcal{D}_P$ happen to be gaussian centered at zero with widths very close to 1, see Figure 39. Therefore, this result can be used as a means to check the "goodness of fit" versus start time for the fits thus far presented. To be absolutely clear, the distributions in Figure 39 can be written in the following way

$$\mathcal{D}_P = \sum_{i=228\ (even\ i)}^{1100-2} \frac{P(t_{i+2}) - P(t_i)}{\sqrt{\sigma_P(t_{i+2})^2 - \sigma_P(t_i)^2}} \tag{22}$$

where i is the bin number at which the fit was started, and $t_i = (i-1) * 149.185 + 74.5925$ ns.

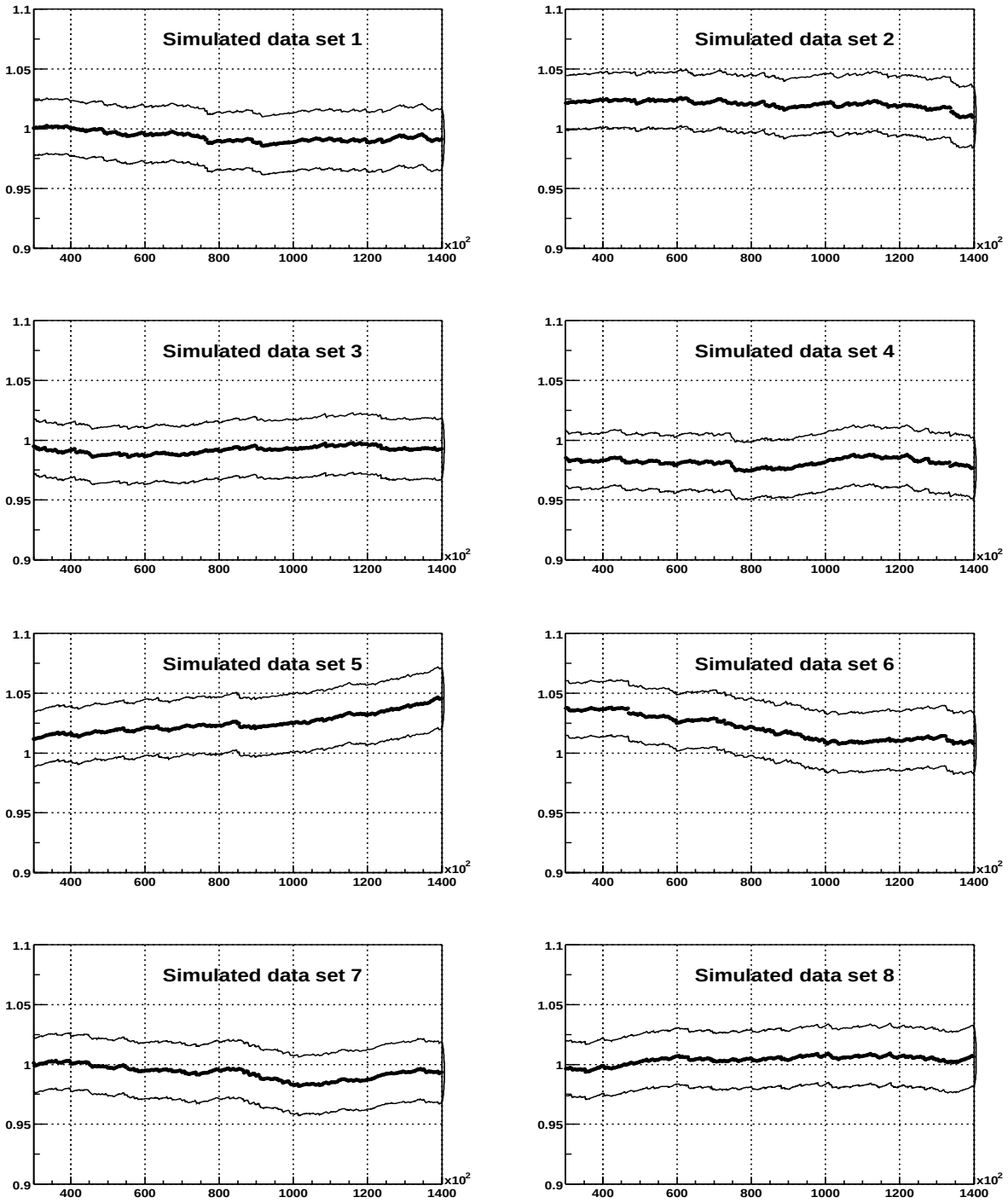

Figure 36: χ^2/ndf for fits to eight sets of data simulated to have a statistical power of 1.24 ppm at 34 μs start time (the fit stop time was 500 μs). The time axes are in ns.

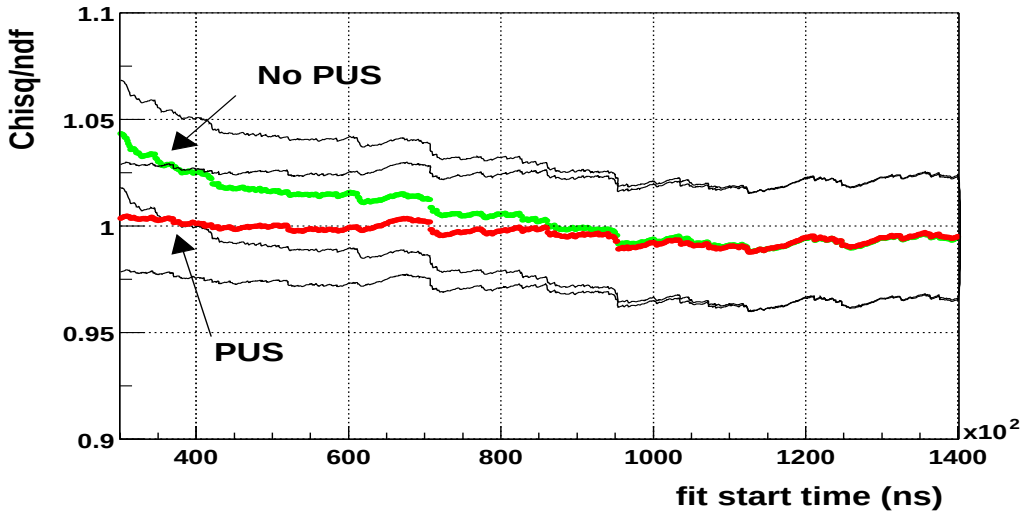

Figure 37: χ^2/ndf for the cases of PUS (red) versus no PUS (green) for g2off data.

One comment should be made regarding fill randomization. For the previous checks "by eye" of the behavior of χ^2/ndf and R versus start time, it is okay to average over the six random sequences. However, for the more rigorous quantitative check using the correlated differences, the same would not apply since the averaging procedure over the six random sequences would add correlations due to the shifting around of the same positrons six times. Therefore, only one random sequence should be used at a time when constructing the correlated differences.

To check whether the distributions $\mathcal{D}_P$ constructed from fits to real data are gaussian or not, it is not exactly correct to require these distributions to be gaussian functions with means zero and widths equalling one. Figure 40 shows what happens. The following was done. Each of the 60 distributions $\mathcal{D}_P$ constructed from fits to simulated data were individually fitted to a gaussian function, and the fitted means and widths were used to fill a histogram. For the same distributions, the mean and rms values were also calculated. Keep in mind that the original distribution from which the 60 sets was drawn is gaussian, and hence the calculated means and rms correctly describe the properties of $\mathcal{D}_P$. Notice in Figure 40 that the fitted means remain clustered around zero, but the fitted widths have moved to about 0.97. This is probably due to the missing tails when the distributions are statistics limited. Therefore, one way to test the goodness of the distributions $\mathcal{D}_P$ would be to fit them to a gaussian function and require that the mean be zero and the widths be about 0.97. I have chosen to do something different. Since I have the properties of the distributions $\mathcal{D}_P$ themselves from simulated data (as in Figure 40), I will directly compare the same properties from real data to those as a measure of goodness of fits to the real data. Figures 41, 42, 43 show the comparisons for the ratio fit parameters A, R, ϕ, respectively. The six random sequences are entered as six entries. Fits to both g2off and G2Too data are consistent with the expected distributions as seen from fits to simulated data. Since the simulated data was in the form of a five-parameter function $G(t)$ transformed into the ratio three-parameter function $R(t)$, this test shows that the fits to data are not different from the form $R(t)$ for both g2off and G2Too. As a final check the distribution $\mathcal{D}_R$ is calculated using Eq. 22 but this time beginning at bin 229 instead of 228. The result is shown in Figure 44. The mean and width properties are similar to those of the distributions for using Eq. 22 starting at bin 228.

A natural question arises as to the sensitivity of the above test. Figures 45 and 46 show the comparison of the distribution parameters $\mathcal{D}_A$ and $\mathcal{D}_R$ for g2off data with pileup subtraction and

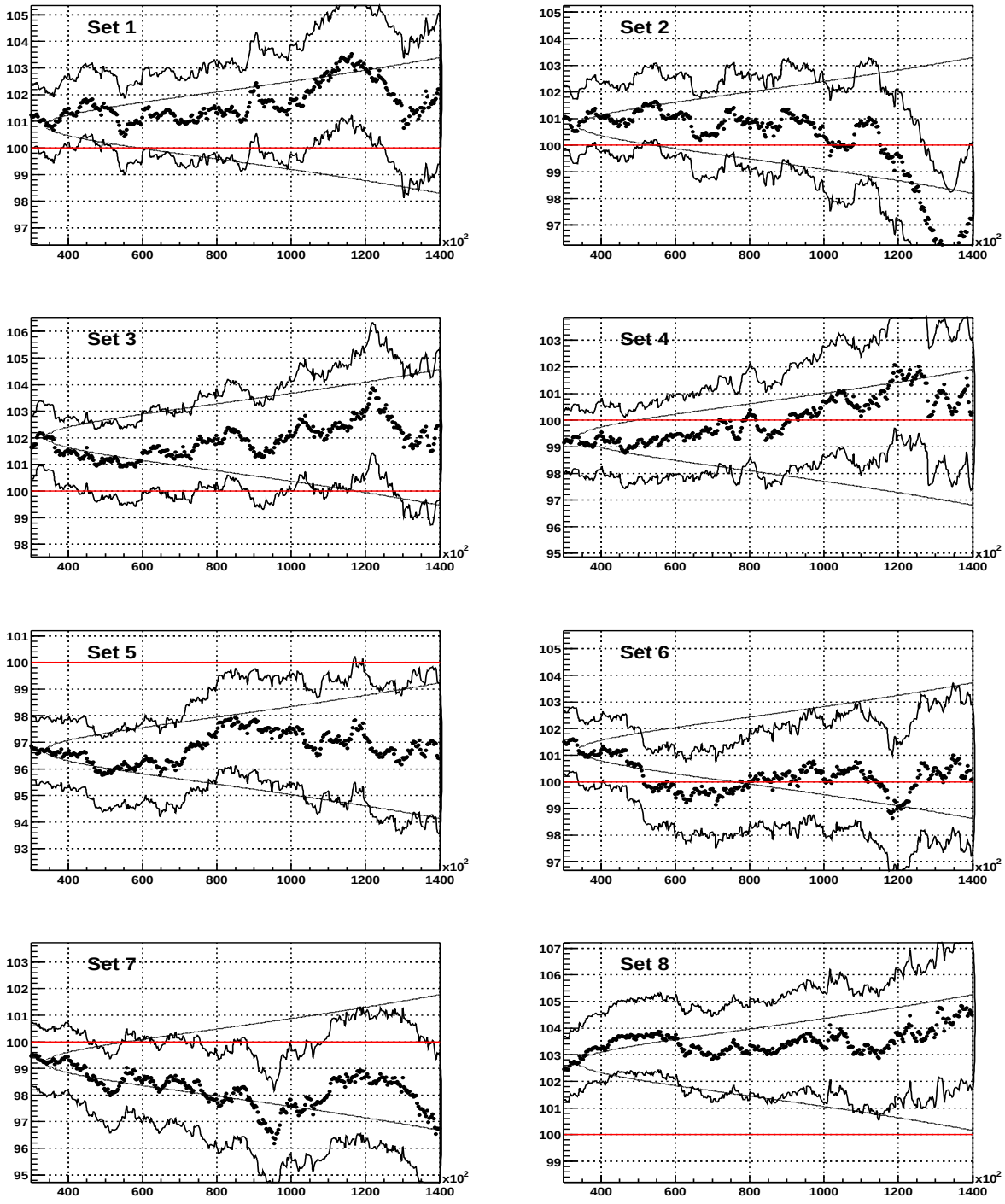

Figure 38: R values for eight sets of data simulated to have a statistical power of 1.24 ppm at 34 μs start time (the fit stop time was 500 μs). The time axes are in ns. The input ω_a value is 100 ppm in the plots (red line). The correlated statistical bands are calculated in the usual way $\sigma_{cor} = \sqrt{\sigma_R(t)^2 - \sigma_R(33.94\ \mu s)^2}$

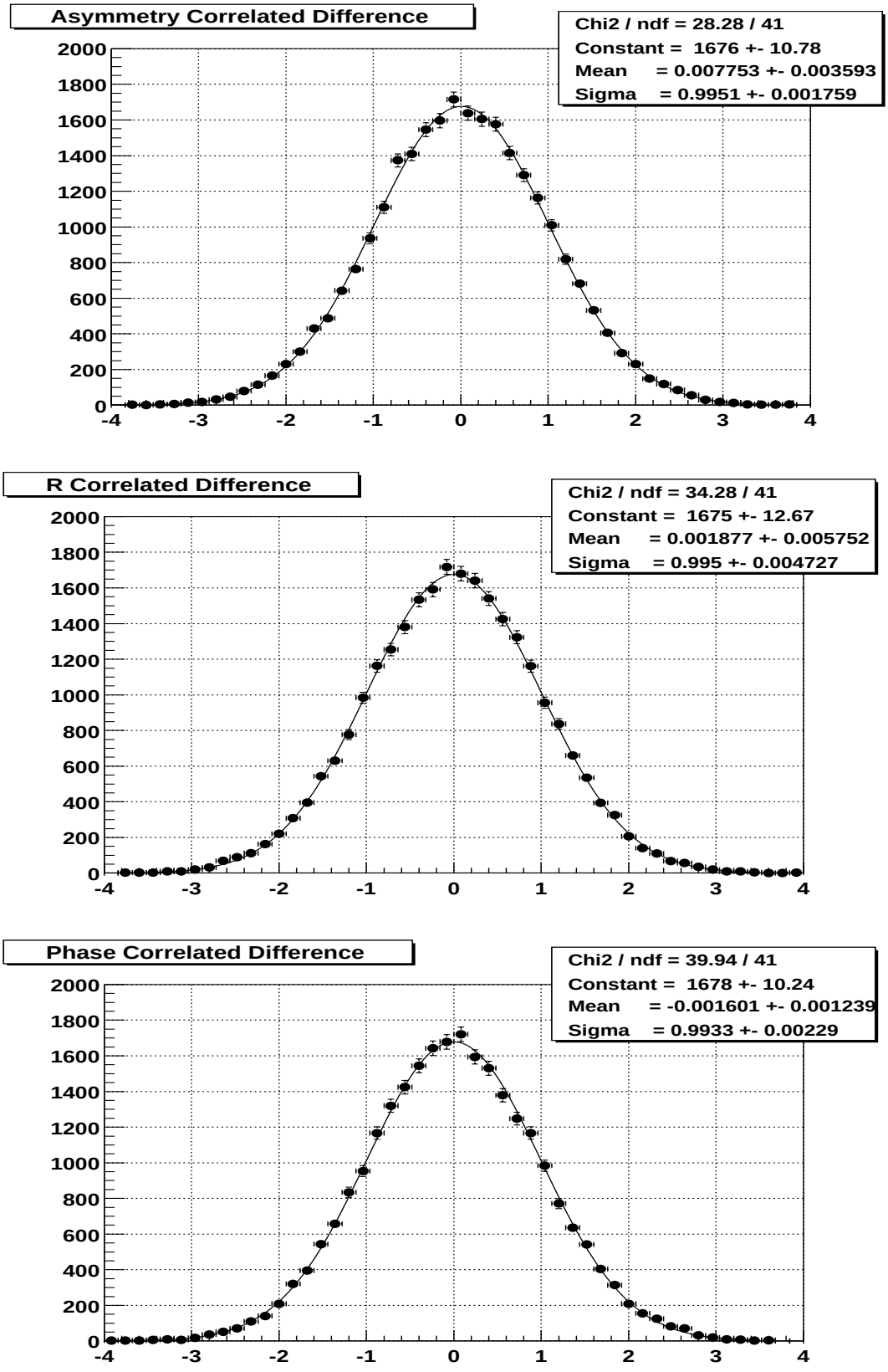

Figure 39: Distributions of values $\mathcal{D}_P = (P(t_2) - P(t_1))/\sqrt{\sigma_P(t_2)^2 - \sigma_P(t_1)^2}$ for the ratio fit parameters $P = (A, R, \phi)$ in the case of fitting to 60 sets of simulated data. The correlated differences $\mathcal{D}_P$ between start times separated by 2*149.185 ns were calculated for the start time range $34 - 160$ μs.

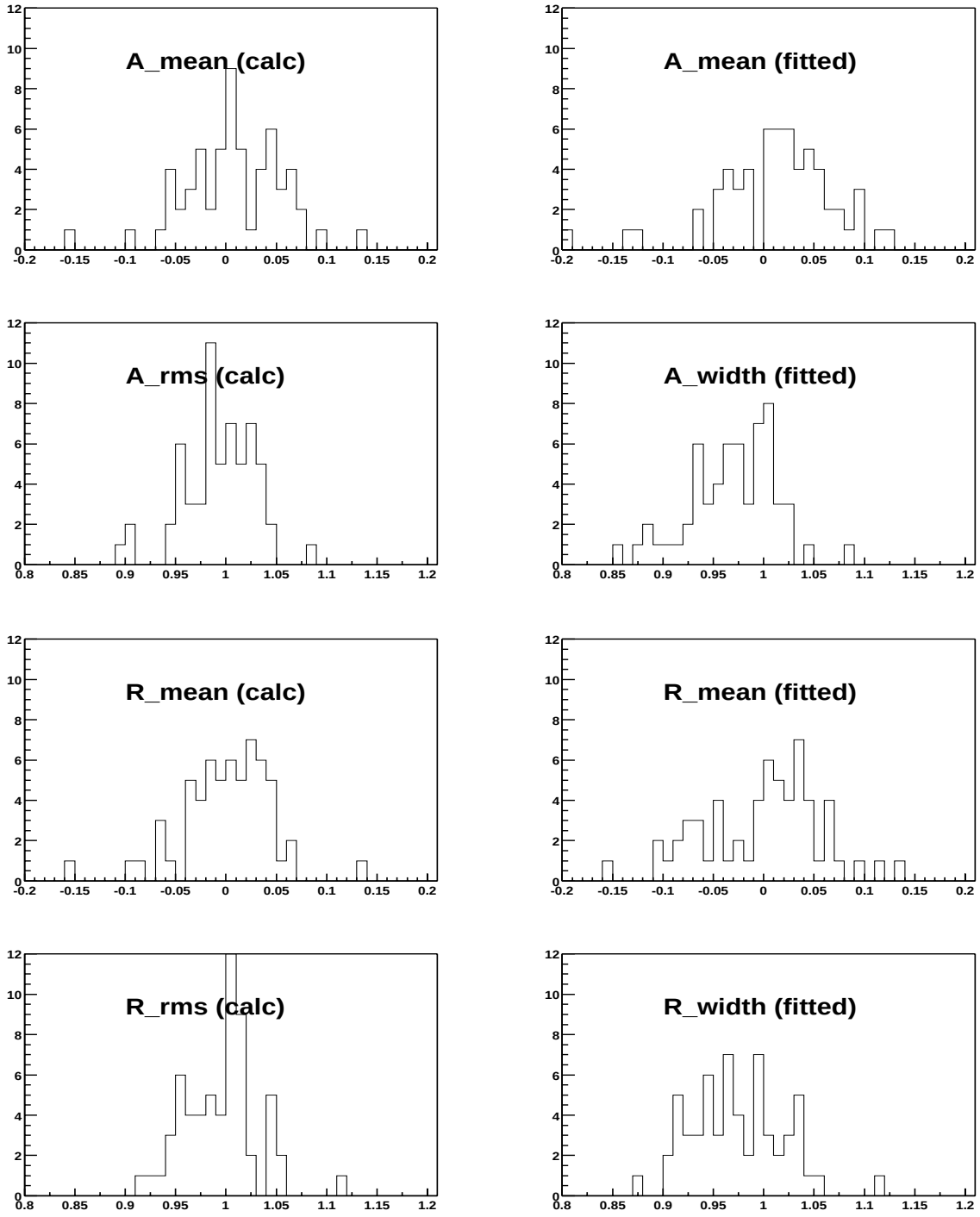

Figure 40: Properties of the distributions $\mathcal{D}_A$ and $\mathcal{D}_R$ for the 60 sets of simulated data. In the left column, the mean and rms values are calculated and plotted. In the right column, the mean and width values as returned by fitting to a gaussian function are plotted. The abscissa are either the mean or width of the correlated differences distributions $\mathcal{D}_A$ or $\mathcal{D}_R$. Notice that if a fit to a gaussian function is used, then the returned means are expected to be distributed about 0, but the returned widths are expected to be distributed about roughly 0.97 and not 1.

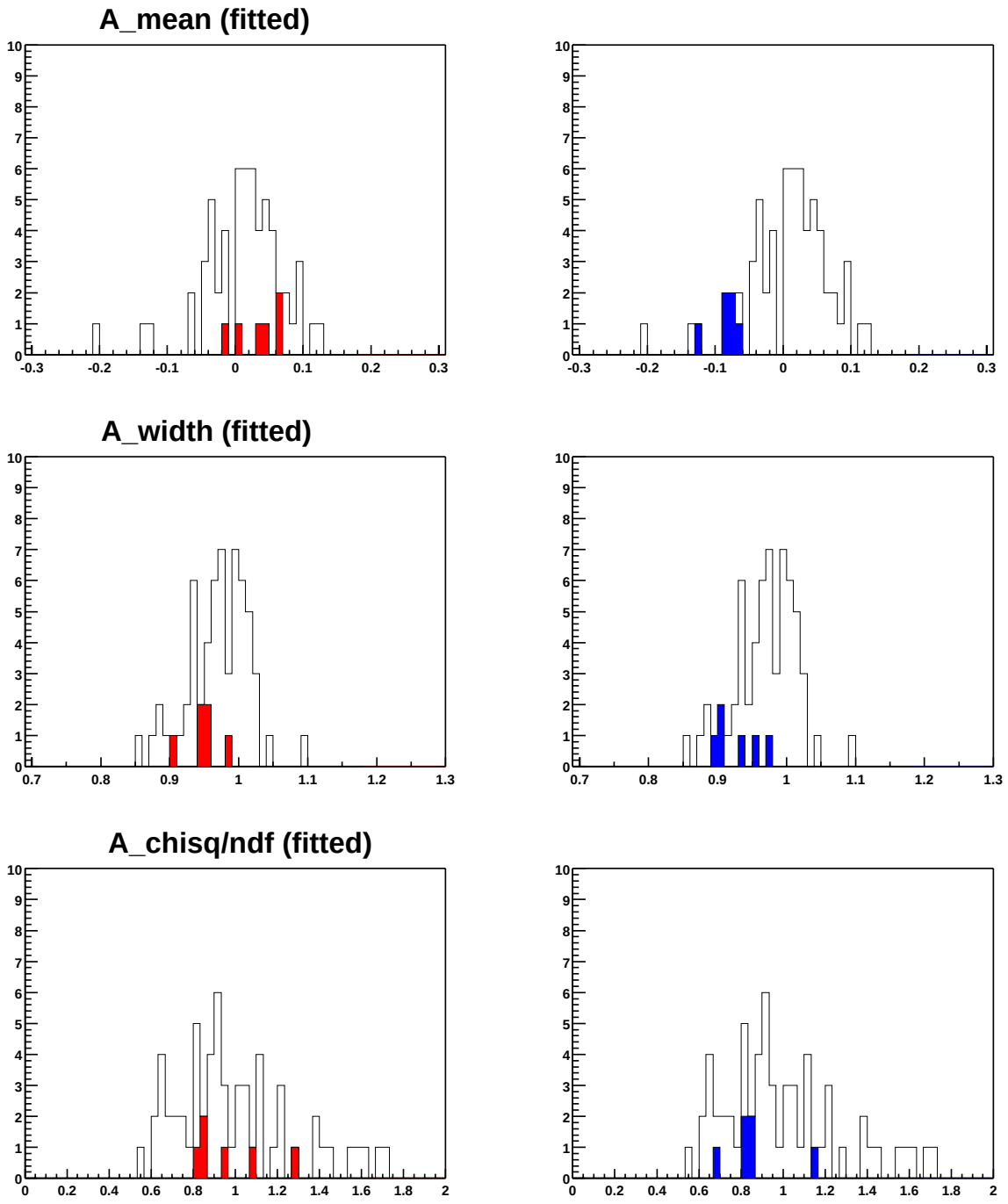

Figure 41: Properties of the distribution $\mathcal{D}_A$ for the ratio fit asymmetry parameter constructed from fits to data compared to the same properties constructed from fits to 60 sets of simulated data. As usual, the red is g2off and blue is G2Too. The six random sequences are shown as individual entries.

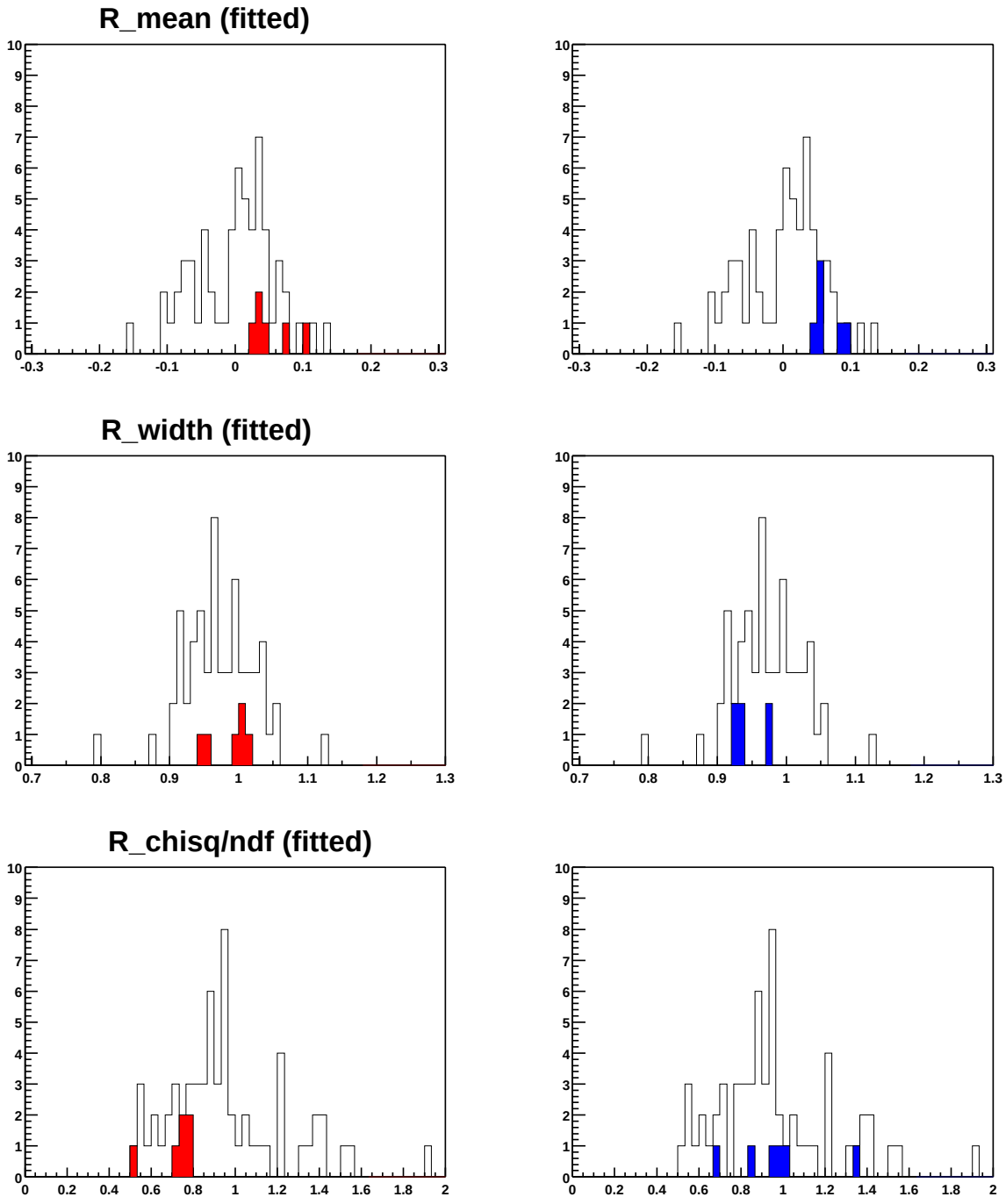

Figure 42: Properties of the distribution $\mathcal{D}_R$ for the ratio fit R parameter constructed from fits to data compared to the same properties constructed from fits to 60 sets of simulated data. As usual, the red is g2off and blue is G2Too. The six random sequences are shown as individual entries.

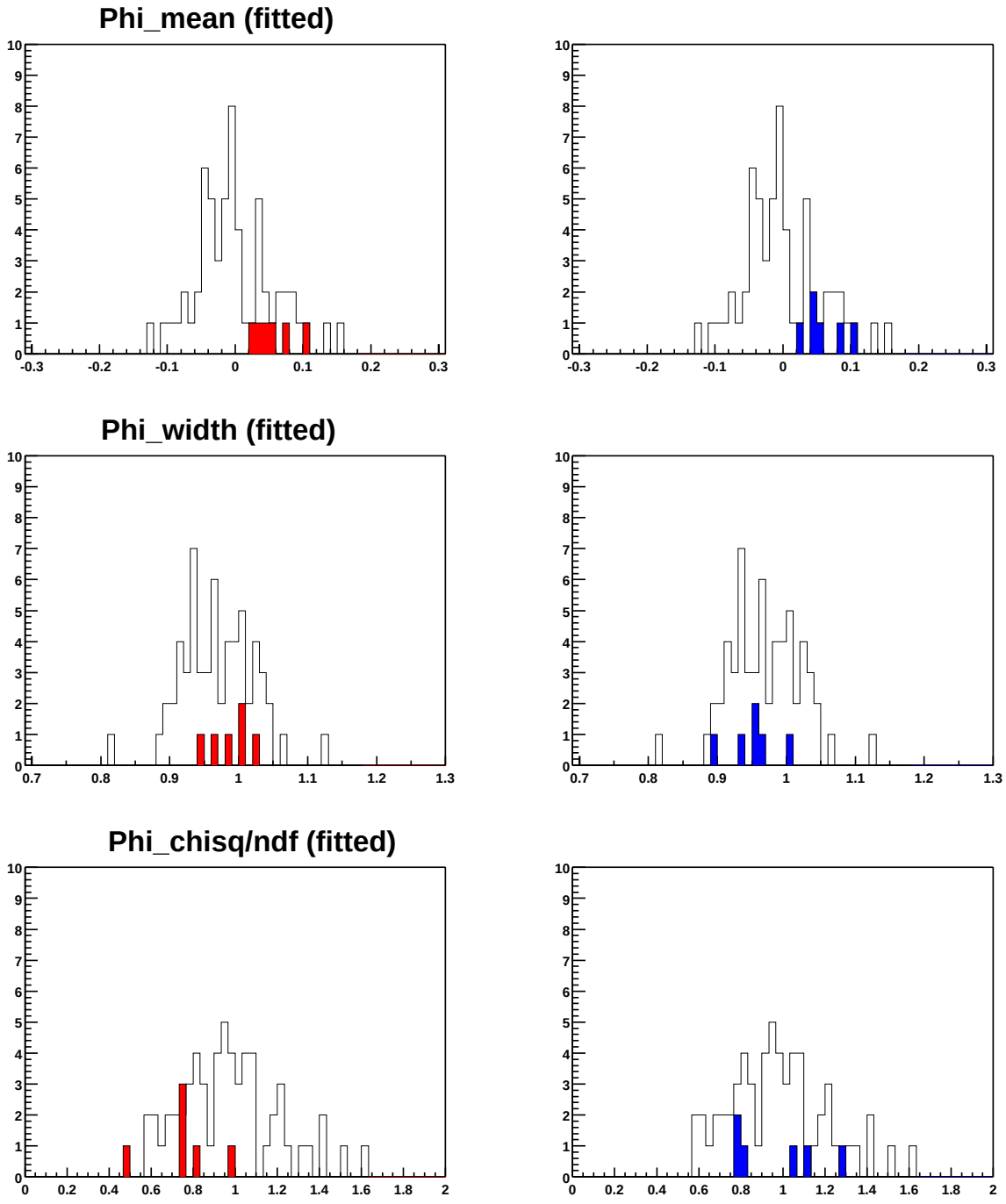

Figure 43: Properties of the distribution $\mathcal{D}_\phi$ for the ratio fit ϕ parameter constructed from fits to data compared to the same properties constructed from fits to 60 sets of simulated data. As usual, the red is g2off and blue is G2Too. The six random sequences are shown as individual entries.

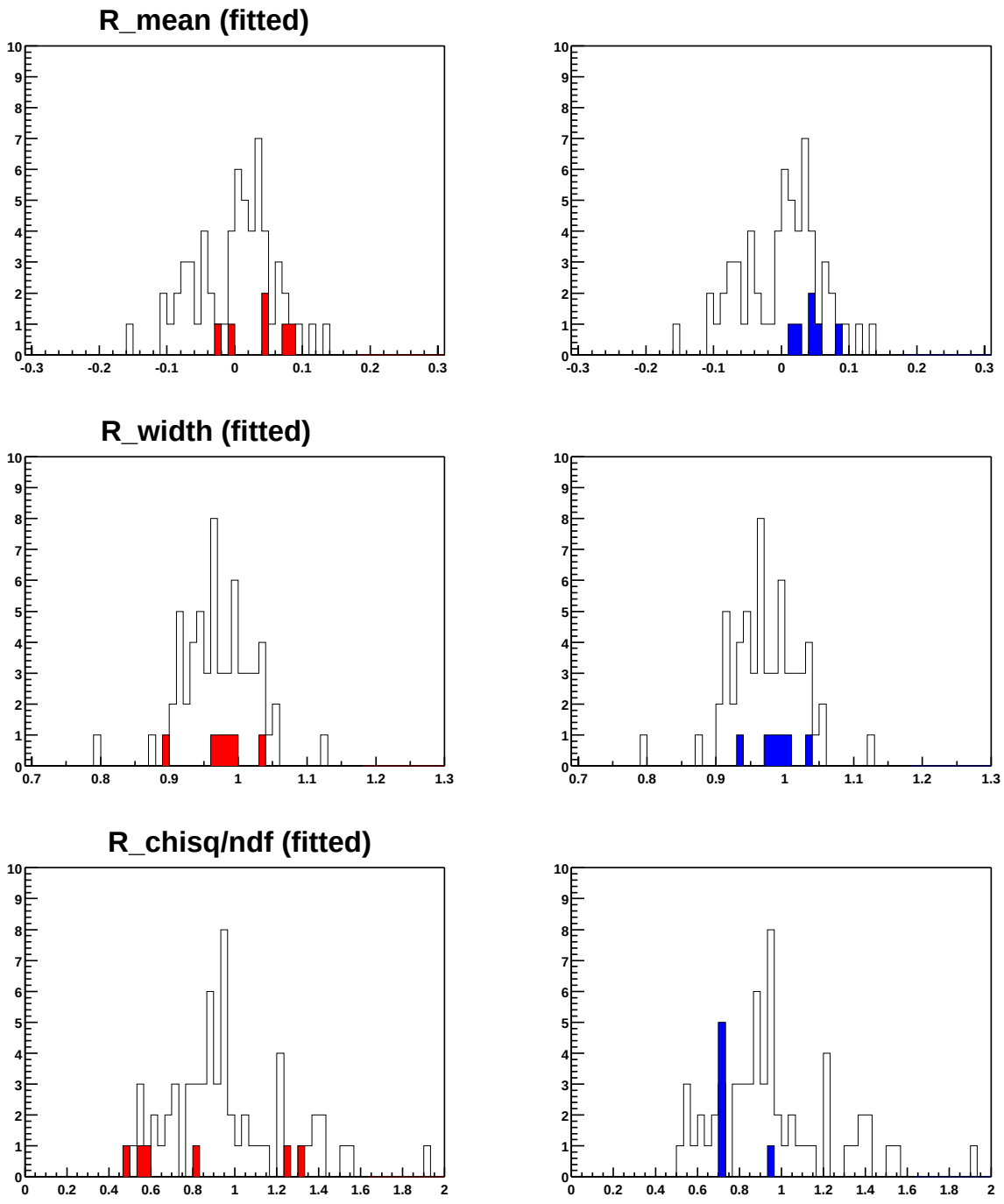

Figure 44: Properties of the distribution $\mathcal{D}_R$ for the ratio fit R parameter constructed from fits to data compared to the same properties constructed from fits to 60 sets of simulated data. As usual, the red is g2off and blue is G2Too. The six random sequences are shown as individual entries. The distribution $\mathcal{D}_R$ whose properties are shown here are different from the ones shown in Figure 42 in that the sum in Eq. 22 was started at bin 229 instead of at 228.

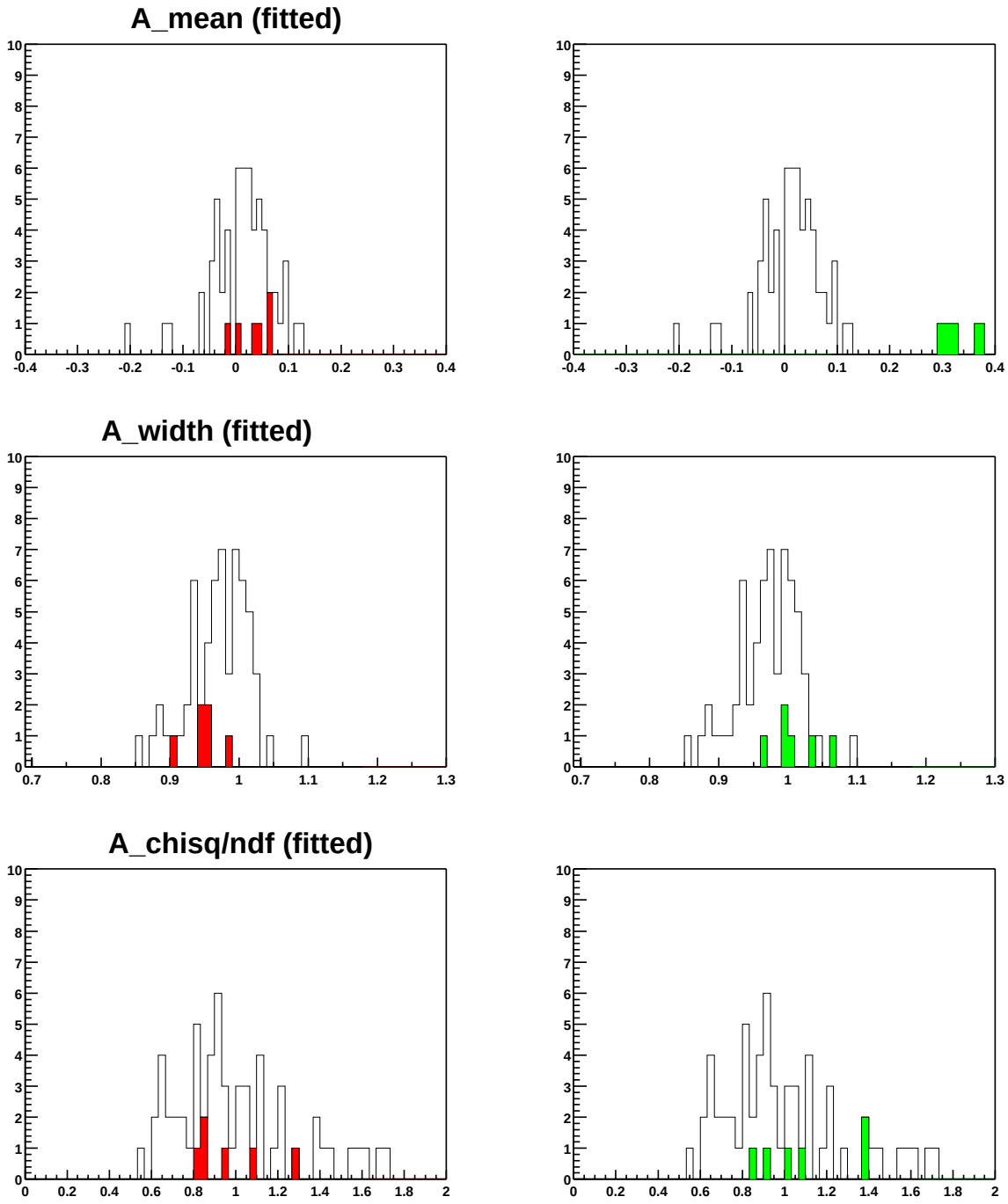

Figure 45: Properties of the distribution $\mathcal{D}_A$ for the ratio fit asymmetry parameter constructed from fits to data compared to the same properties constructed from fits to 60 sets of simulated data. The red is g2off with pileup subtraction, and the green is also g2off but with no pileup subtraction. Both data sets were fitted to the three- parameter ratio function $R(t)$. The six random sequences are shown as individual entries.

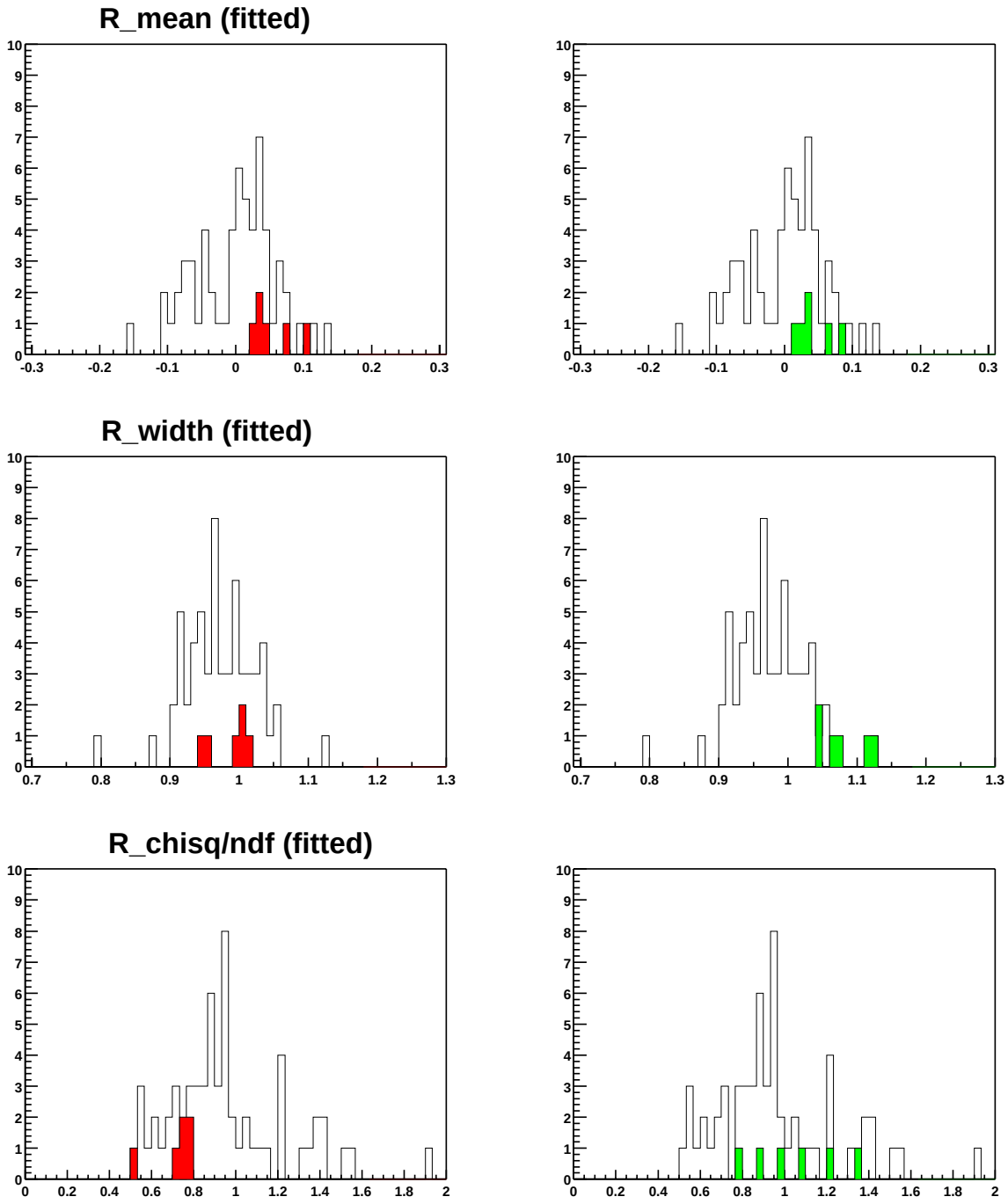

Figure 46: Properties of the distribution $\mathcal{D}_R$ for the ratio fit asymmetry parameter constructed from fits to data compared to the same properties constructed from fits to 60 sets of simulated data. The red is g2off with pileup subtraction, and the green is also g2off but with no pileup subtraction. Both data sets were fitted to the three- parameter ratio function $R(t)$. The six random sequences are shown as individual entries.

without pileup subtraction. Without pileup subtraction there is an 0.2 ppm oscillation in the fitted value of R as well as a systematic offset of about -0.3 ppm, Figure 27. Figure 46 shows that the 0.2 ppm oscillation shows up as a width in $\mathcal{D}_R$ that is on the edges of the distribution, about 1.1, but no discernable effect on the mean is seen due to the 0.3 ppm offset. The telltale sign in this case is however the large asymmetry mean of 0.3, more than 3 sigmas off from the expected distribution (this would probably have also been the case for G2Too (OLD) millifit pulse reconstruction). So the χ^2/ndf test, Figure 37, and this test would disprove that the data without pileup subtraction can be fitted in the ratio formulation to the three-parameter function $R(t)$. This is already known, but I think it is nice to see that the necessary tests which we do have would have shown this to be the case.

To summarize, the χ^2/ndf and fit parameters versus start times were checked both "by eye" and by the more quantitative correlated differences distributions. The fit results are not inconsistent with the expected functional $R(t)$.

5.4 Energy Variations

In this short section the fit results versus energy threshhold will be presented. Only G2Too data for one random sequence was studied.

Figure 47 shows fit results at 34 μs start time versus the lower energy threshold for the energy range of $2.0 - 2.6$ GeV, stepping by 0.05 GeV. As is seen in Figure 47 (top), the changes in R with energy threshold is not inconsistent with the expected fluctuations as given by the correlated statistics bands. The R value in Figure 47 at 2.0 GeV cut is 142.71 ± 1.28 ppm. The statistical deviation from this value to the value as given in Figure 34 is $0.15{*}\sigma_R = 0.19$ ppm (the 15% is due to both the fill randomization sequence and the randomization sequence used to fill the four ratio subhistograms), a 1.7 sigma deviation. A and ϕ are expected to vary with energy, and hence no statistical check is made. Figures 48 and 49 show the same plots as in Figure 47, but for the cases of start times 40 and 45 μs, respectively. The dependence of the R value on energy threshold is again not inconsistent with statistical fluctuations.

5.5 Fit Residuals and the Double CBO/Vertical Waist

In this section, the fit residuals will be studied for the case of summing the 22 detectors together. The focus, as in Section 5.3, is to consider the "goodnes of fit", in this case using the tool of the Fourier transform.

In the case of histogram counts, the data N_i can be directly Fourier transformed for frequency content. In that case,the variance in a time bin i is $\sigma_i^2 = N_i$, the number of positrons in that bin. Taking this as a guide, then the ratio histograms, being just a pure cosine, should be weighed by σ_R^2 to obtain the frequency content where

$$\sigma_R^2 = \frac{1 - R^2(i)}{u(i) + v(i)} \approx \frac{1 - R^2(i)}{4N_o e^{-\frac{t}{\tau_\mu}}} \tag{23}$$

See [1] for more details on the functions $u(i)$ and $v(i)$. For the present situation, it's enough to note that this weighing accounts for the more numerous positrons at earlier times as well as the differential positron counts from the g-2 oscillation, $R^2 \sim A^2 cos^2$.

Figure 50 shows the differences between taking the Fourier transform of R_i alone versus R_i/σ_R^2. The Fourier transform for the data N_i is also included for comparison. Notice that at the g-2 frequency, the frequency amplitude due to the muon decay exponential is reduced by a factor of 3 for the ratio time histogram, hence the reduced sensitivity of the ratio method to backgrounds that affect the 64.4 μs exponential such as energy calibration changes (see for example Alex's fits for detector 1 showing that without energy scale correction, the fitted value of R has a phase pulling error of magnitude about 5 ppm where as for the ratio fits attached at the end of the note, the

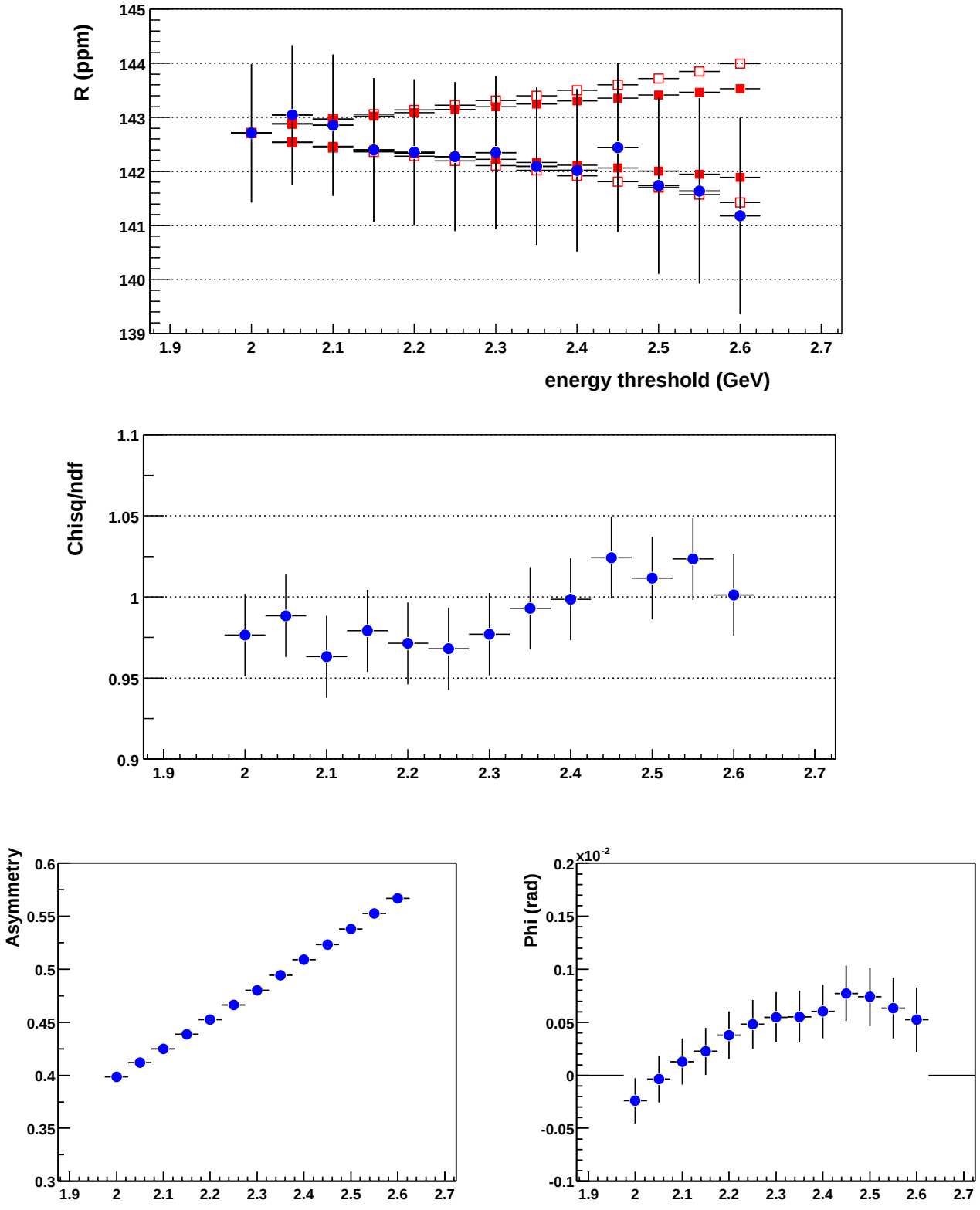

Figure 47: Fit parameters versus energy threshold for one random sequence for G2Too data at start time 34 μs. The open red squares were calculated using $\sigma^2_{cor} = (\sigma^2_2 - \sigma^2_1)$, and the closed red squares were calculated using $\sigma^2_{cor} = (\sigma^2_2 - \sigma^2_1) * \left(2\frac{A_1}{A_2} cos(\phi_1 - \phi_2) - 1\right)$ (suggested by Sergei Redin [11]). σ_1 is the statistical uncertainty in R at energy threshold 2.0 GeV and σ_2 the corresponding value for the varying energy thresholds $2.0 - 2.6$ GeV, (A_1 ϕ_1), (A_2 ϕ_2) the corresponding fit paramters.

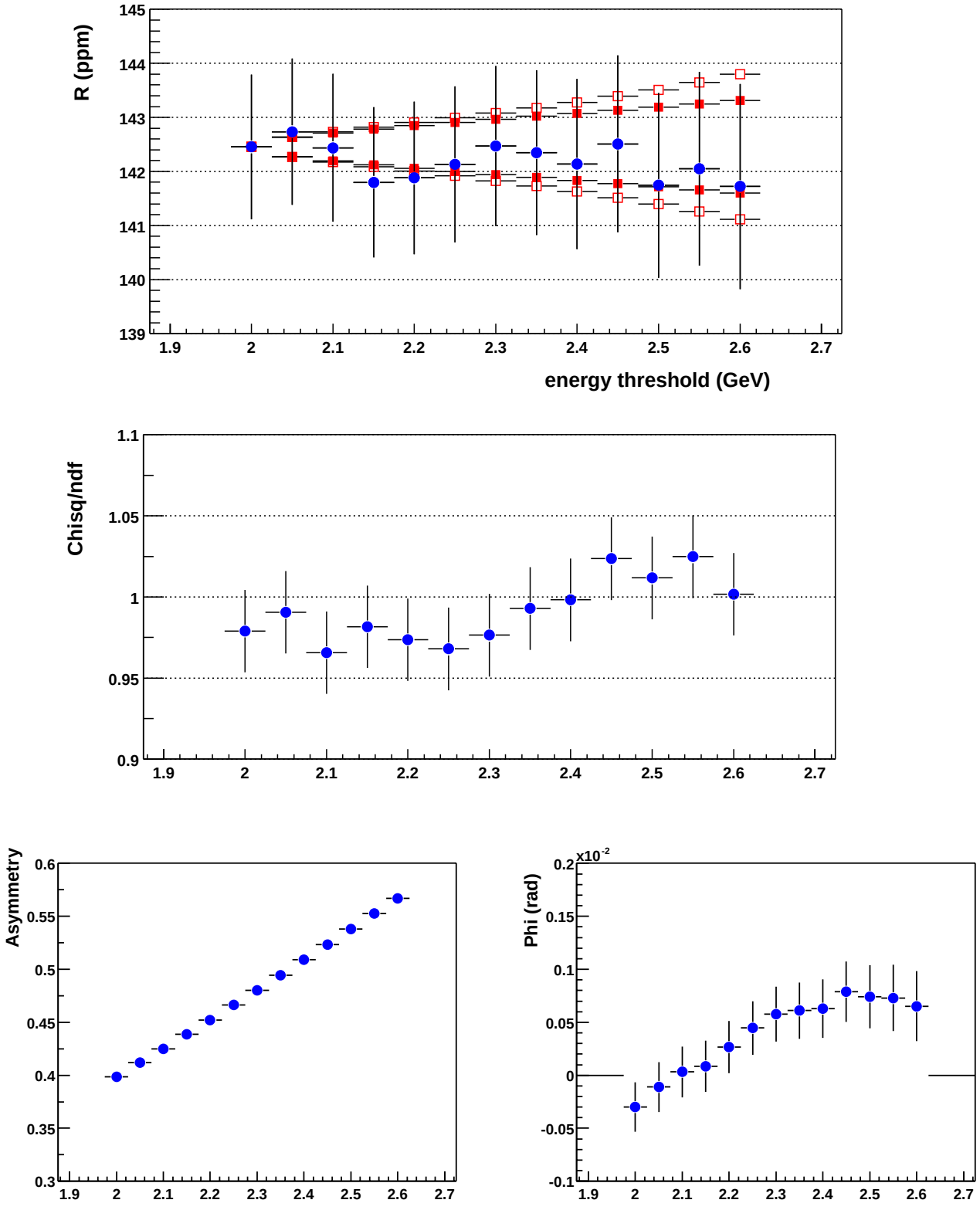

Figure 48: Fit parameters versus energy threshold for one random sequence for G2Too data at start time 40 μs. The open red squares were calculated using $\sigma^2_{cor} = (\sigma^2_2 - \sigma^2_1)$, and the closed red squares were calculated using $\sigma^2_{cor} = (\sigma^2_2 - \sigma^2_1) * \left(2\frac{A_1}{A_2}cos(\phi_1 - \phi_2) - 1\right)$ (suggested by Sergei Redin [11]). σ_1 is the statistical uncertainty in R at energy threshold 2.0 GeV and σ_2 the corresponding value for the varying energy thresholds $2.0 - 2.6$ GeV, (A_1 ϕ_1), (A_2 ϕ_2) the corresponding fit paramters.

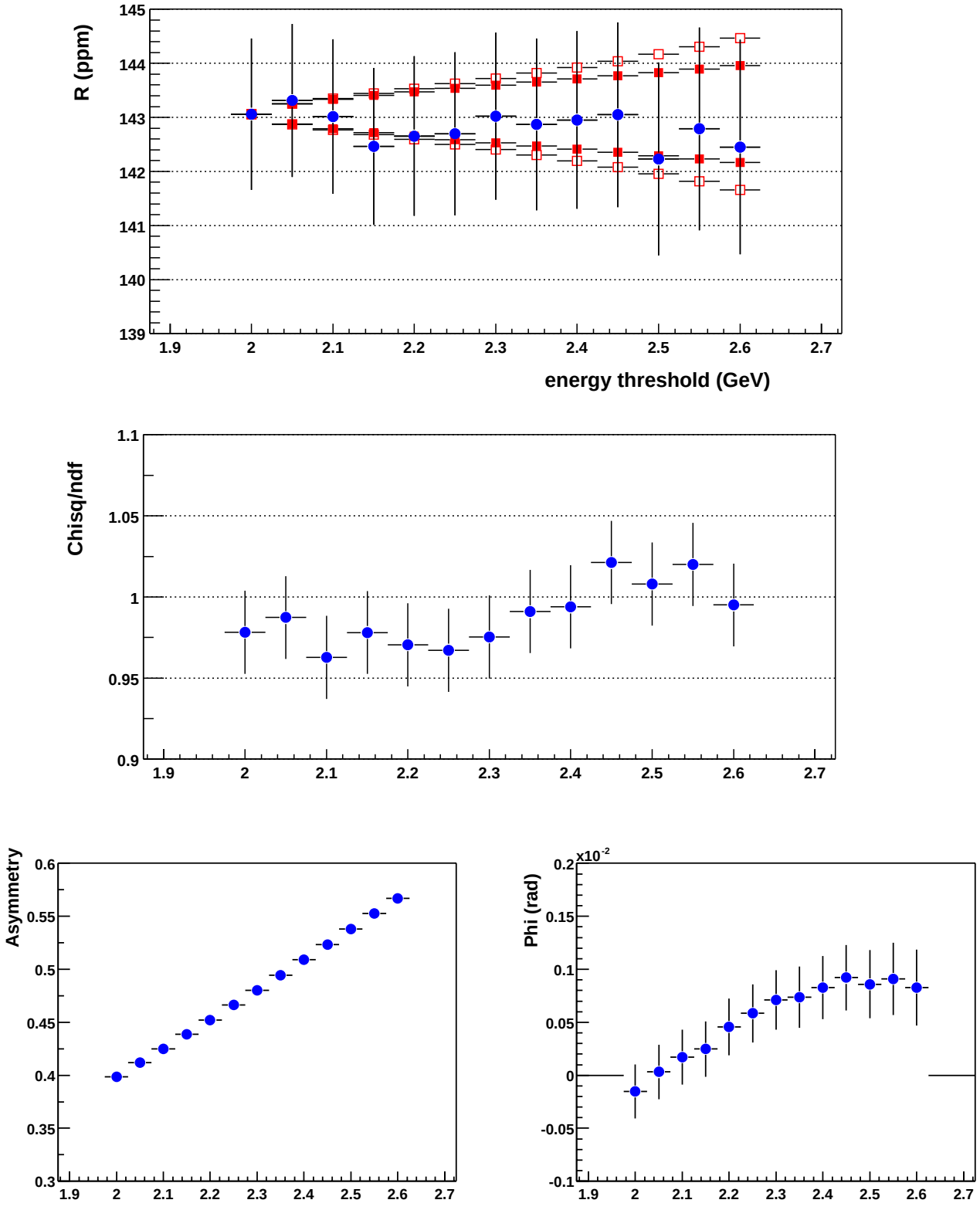

Figure 49: Fit parameters versus energy threshold for one random sequence for G2Too data at start time 45 μs. The open red squares were calculated using $\sigma^2_{cor} = (\sigma^2_2 - \sigma^2_1)$, and the closed red squares were calculated using $\sigma^2_{cor} = (\sigma^2_2 - \sigma^2_1) * \left(2\frac{A_1}{A_2}cos(\phi_1 - \phi_2) - 1\right)$ (suggested by Sergei Redin [11]). σ_1 is the statistical uncertainty in R at energy threshold 2.0 GeV and σ_2 the corresponding value for the varying energy thresholds $2.0 - 2.6$ GeV, (A_1 ϕ_1), (A_2 ϕ_2) the corresponding fit paramters.

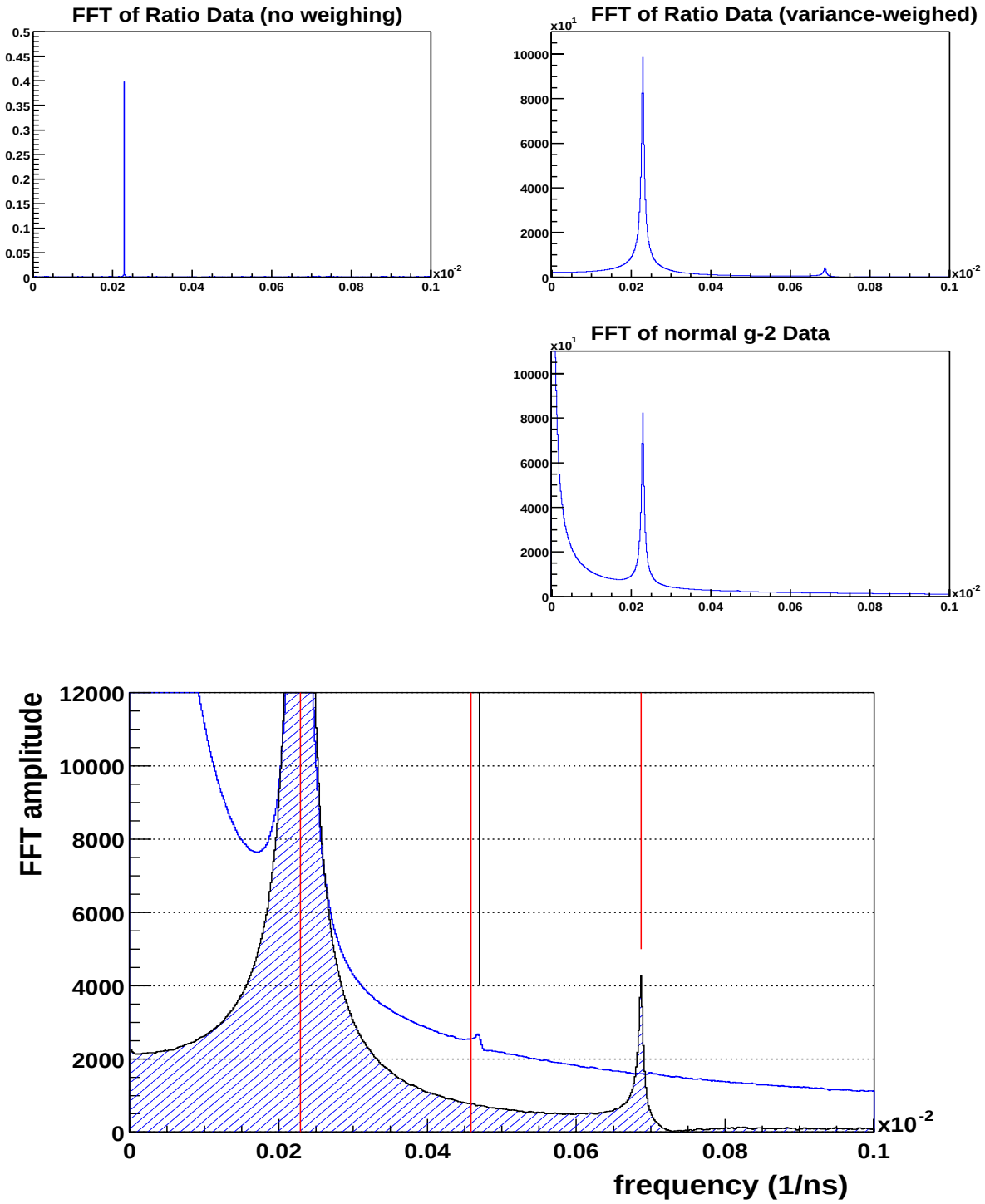

Figure 50: Fourier transform signals of the normal time histograms and of the ratio time histograms, G2Too data. The three smaller plots on top show that with the variance weighing effected, the FFT signal of the ratio time histogram produces a similar amplitude signal as the FFT of the normal time histogram. The lower plot shows the FFT signals of the normal and variance-weighed ratio time histograms for the amplitude range $0 - 12000$. The red lines are at the three frequencies $f_a = 229.1$ kHz, $2 * f_a$ and $3 * f_a$; the black line is at the CBO frequency $f_c = 470$ kHz. The shaded region is the FFT signal of the ratio time histogram, the unshaded region of the normal time histogram.

phase pulling error is only about 1 ppm). Note also that due to the 1/2 g-2 period shifting, there is a peak in the ratio FFT signal at three times g-2 frequency, and that the CBO signal is not seen at all in the ratio FFT signal.

In the case of the fit residuals, the quantity $\chi = (R_i - R(i))/\sigma_R$ itself is the more appropriate quantity to Fourier transform since were're interested in the frequency components that are above those accompanying the statistical fluctuations themselves. Figure 51 shows the FFT of χ for fit residuals to simulated data, g2off data, and G2Too data. Figure 52 shows the same plots as in Figure 51, but now zoomed into the region around the g-2 frequency. No apparent peaks are seen above the noise fluctuations.

For curiosity sake, consider the following question: if no frequency peaks are seen above the noise level, then what is the order of magnitude of the error that the fits can incur if the background is CBO-like, i.e. relating to beam dynamics. To answer this question and understand better the errors associated with the ratio method, the following was done. The CBO function

$$CBO(t) = 1 - A_c * e^{-(\frac{t}{\tau_c})^2} * cos(\omega_c t + \phi_c) \tag{24}$$

was used to simulate data which was then fitted, and the maximum error in the fitted value of R in the start time range $25 - 45$ μs was found as a function of the CBO frequency ω_c in the range $0 - 3$ MHz. This method of estimating the fitting error due to the CBO background is exactly the same as that used in Section 4.5. The input CBO parameters were $A_c = 0.008$, $\tau_c = 132$ μs, and $\phi_c - \phi = 1.0$. Figure 53 shows the magnitude of the fit error as a function of ω_c. This CBO magnitude is about $0.008/0.4 = 20000$ ppm of the g-2 signal. Notice that for even multiples of the g-2 frequency, the errors are zero, and for odd multiples, the errors are maximal, with those maximal values decreasing for increasing ω_c. For the vertical waist frequency of 1.7 MHz, the error is 0.5 ppm from Figure 53. From Figure 51, the background fluctuations are about 0.06 on that scale. For the same σ_R weighing in the FFT of the the ratio time signal (R_i/σ_R), the value of the g-2 peak is more than 120, which gives $0.06/120 = 500$ ppm. Taking the ratio of $500/20000$ then gives a value of 0.013 ppm for this frequency component if it had the functional form of the CBO. After the last g-2 collaboration meeting, Jan $11 - 12$, I also checked what the error would be for the case of a shorter $\tau_c \approx 10$ μs. In that case, the error was slightly larger but still less than 0.02 ppm. Hence the error for the vertical waist is set at 0.02 ppm in the systematic uncertainties table in Section 4.7. In the same manner, the systematic error for the double CBO is set at 0.01 ppm. Figure 54 shows the FFT signal for the normal g-2 time histgram for G2Too when all the detectors are summed. Notice that the vertical waist signal there is very small.

5.6 Statistical Properties of Fits to Individual Detectors

I had originally intended to not present detailed results for fits to the individual detectors because the final results were extracted from the sum histogram. It was enough to check that the fitted values of R across the detectors were not statistically inconsistent. However, in light of the "contiguous detector effect", I will add this following subsection detailing some statistical checks of fits to the individual detectors.

Figure 55 shows the "contiguous detector effect". Detectors which are grouped in contiguous halves of the g-2 ring, such as $1 - 12$, see movements in R which are seemingly large compared to the correlated statistics bands. Breaking the g-2 ring up into odd-even detectors for example do not show this effect. The question is then are we seeing an effect which is not statistical in nature?

Figure 56 shows plots of the properties of the distributions $\mathcal{D}_R$ and $\mathcal{D}_A$ for the 22 individual detectors, g2off data for one random sequence. The fitted means, widths, and fit χ^2/ndf was evaluated using exactly the same algorithm as outlined in Section 5.3. Figure 57 shows the same plots as in Figure 6 for G2Too data. Figures 56 and 57 show no discernible differences in the statistical properties of detectors $1 - 12$ compared to detectors $13 - 24$. Figures 56 and 57 also show

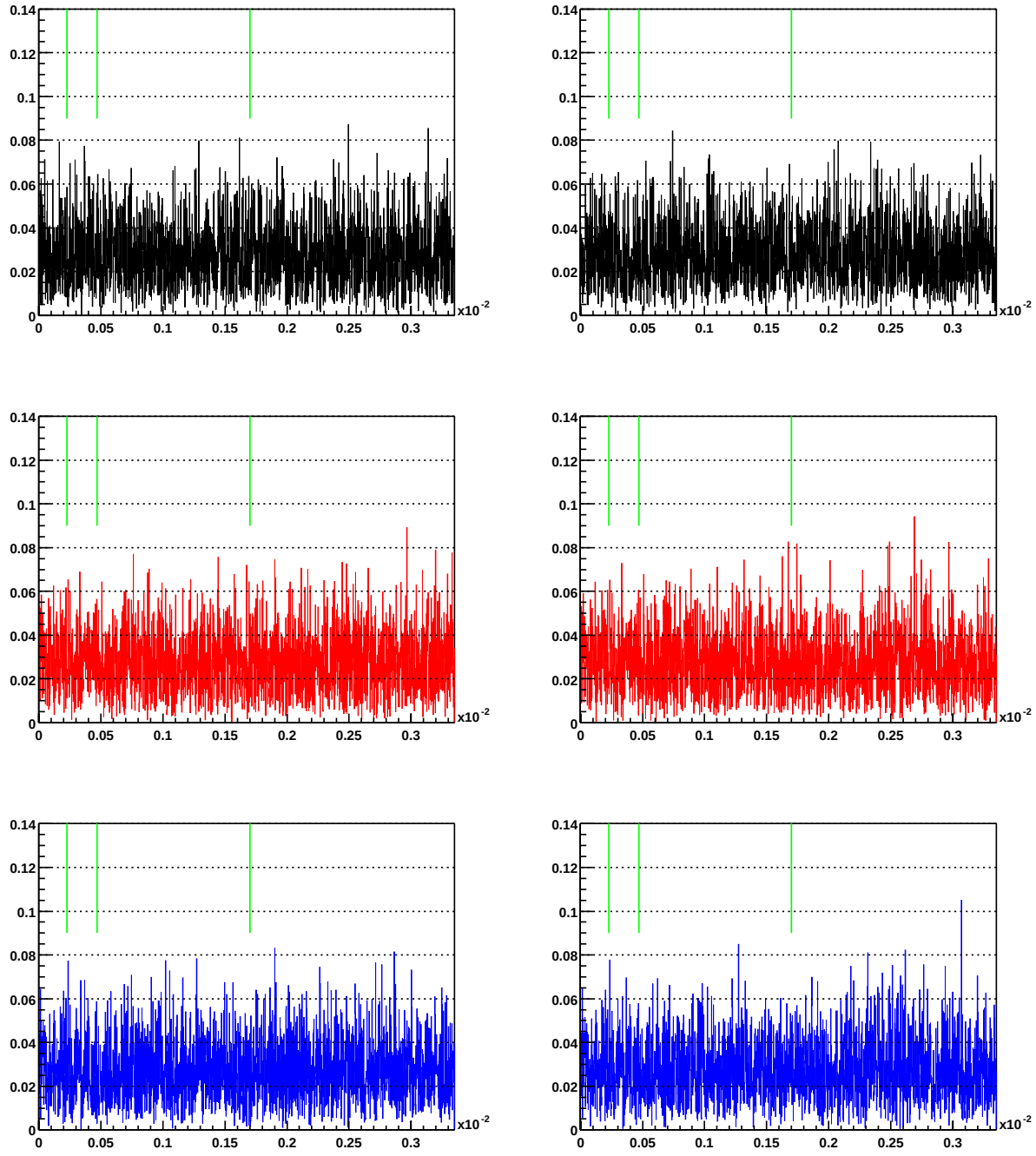

Figure 51: The FFT of $\chi = (R_i - R(i))/\sigma_R$ for fits to two of the 60 sets of simulated data (top), two random number sequences of the g2off data (middle) and two random number sequences of the G2Too data (bottom). The three green lines are the g-2 frequency at 229.1 kHz, the CBO frequency at 470 kHz, and the vertical waist frequency at 1700 kHz. The vertical axis is the FFT amplitude, and the horizontal axis is frequency in (1/ns). No apparent frequency peaks are seen above the noise level in the fit residuals for both g2off and G2Too data.

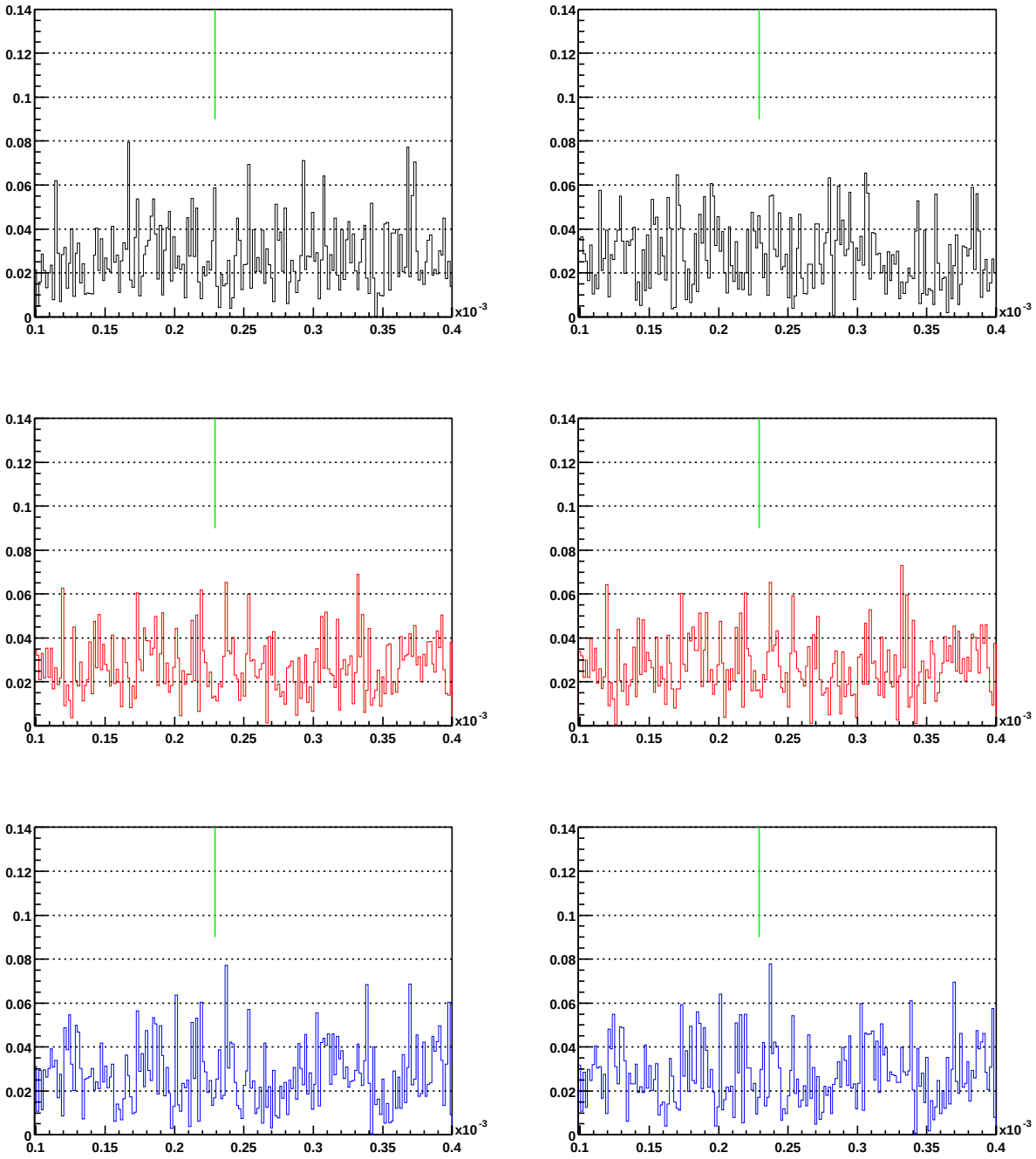

Figure 52: A zoomed in view around the region of the g-2 frequency of the FFT of $\chi = (R_i - R(i))/\sigma_R$ for fits to two of the 60 sets of simulated data (top), two random number sequences of the g2off data (middle) and two random number sequences of the G2Too data (bottom). The green line is at the g-2 frequency of 229.1 kHz. The vertical axis is the FFT amplitude and, the horizontal axis is frequency in (1/ns).

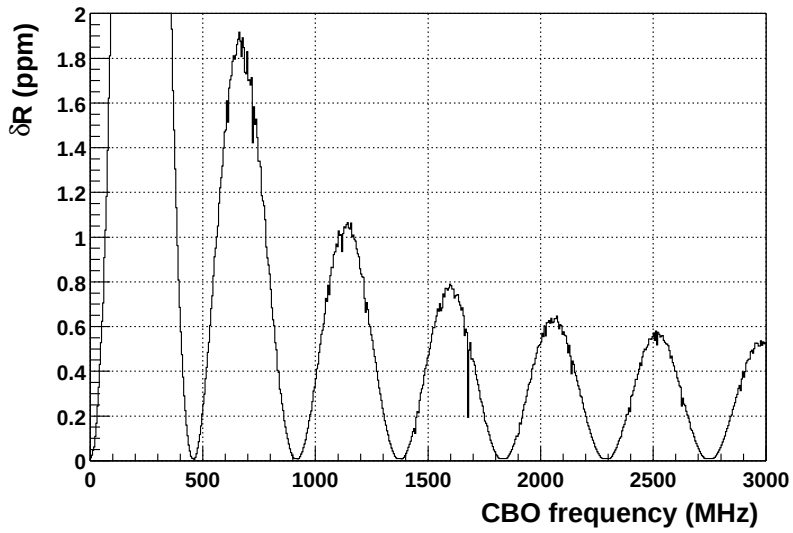

Figure 53: The error δR in the fitted value of R as a function of a CBO-like background $(1 - A_c * exp(-(t/\tau_c)^2) * cos(\omega_c t + \phi_c))$, with $A_c = 0.008$, $\tau_c = 132\ \mu s$, $\phi_c - \phi = 1.0$. The peak value at 229.1 kHz is 80.

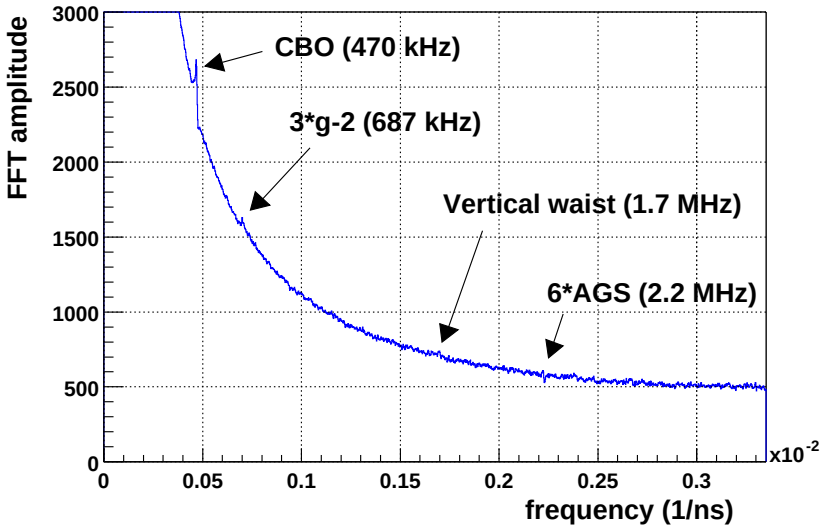

Figure 54: The frequency content of the normal g-2 time histogram for G2Too for all detectors summed. Notice that the CBO signal is about 200 above the exponential background where as the vertical waist at 1.7 MHz is hardly noticeable.

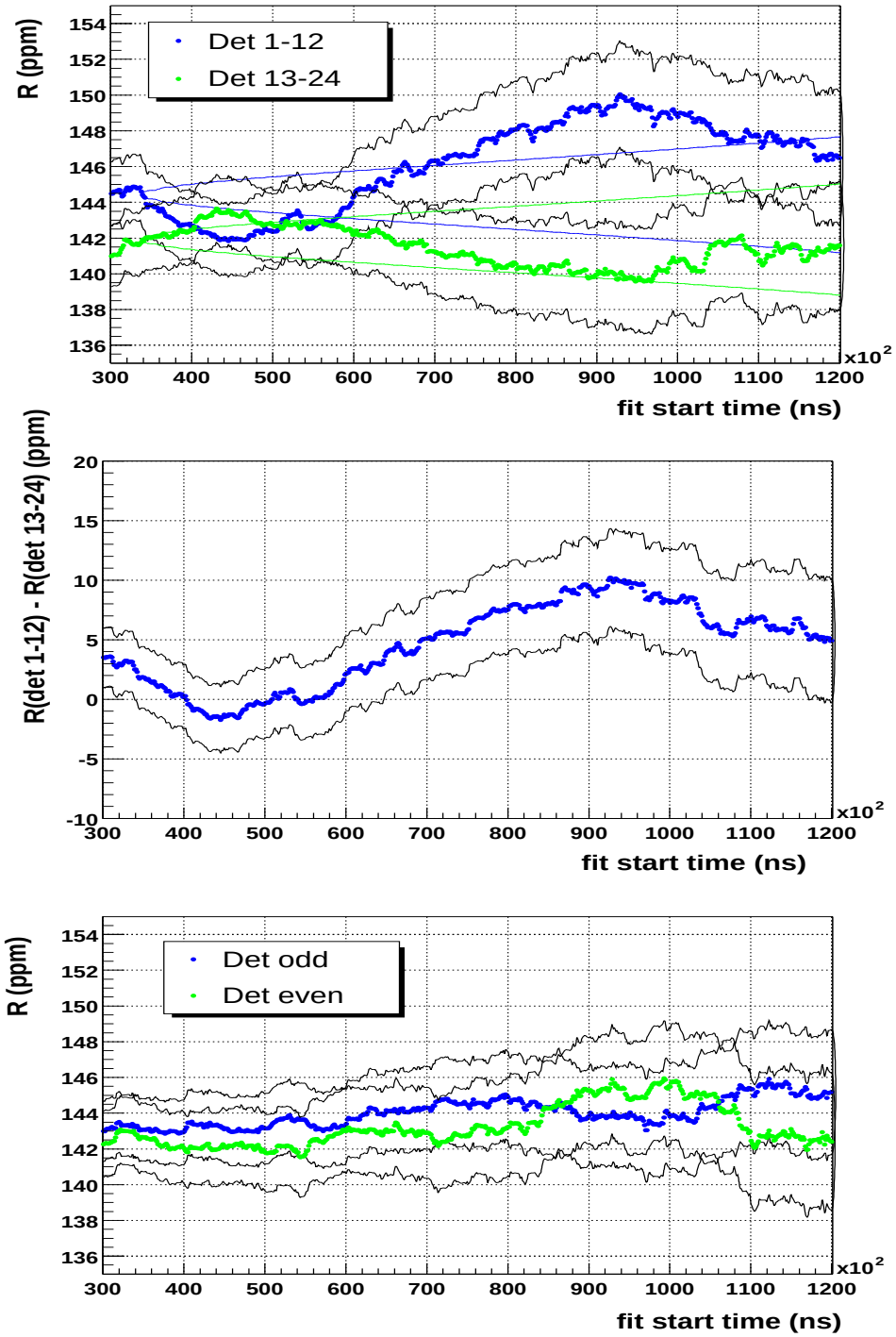

Figure 55: R averaged over the two groups of detectors $1-12$ and $13-24$ (top), and R averaged over the two groups (odd) and (even) (bottom). The middle plot shows the differences between the two R values in the top plot. Notice that there is quite a bit of movement in the R values versus start time for the group of detectors $1-12$. This is G2Too data averaged over the six random sequences.

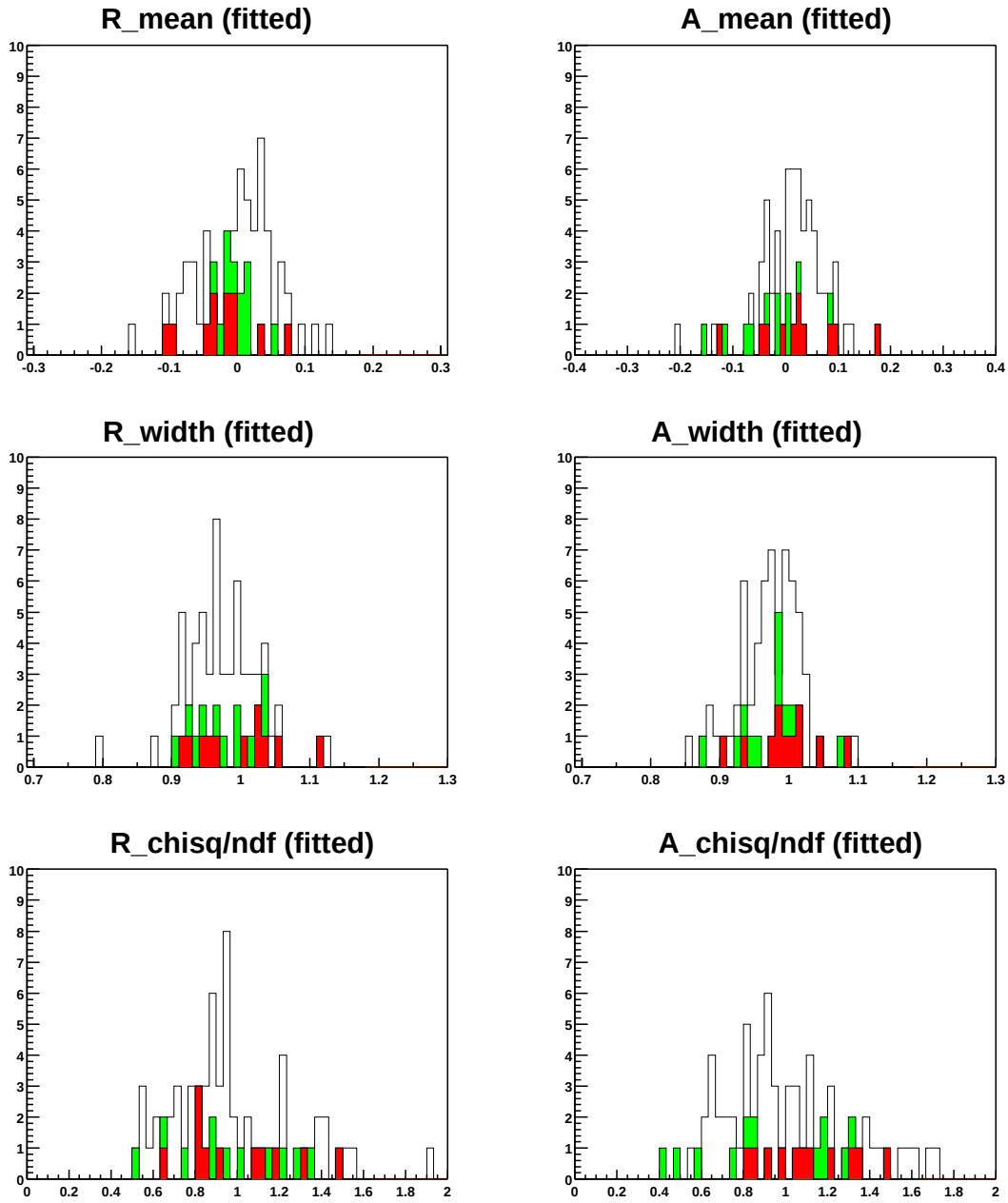

Figure 56: Properties of the correlated differences distributions $\mathcal{D}_R$ and $\mathcal{D}_A$ for fits to the individual detectors for g2off data, one random sequence. The green entries are for detectors $1-12$ and the red entries are for detectors $13-24$. The black lines are the properties of the 60 sets of simulated data.

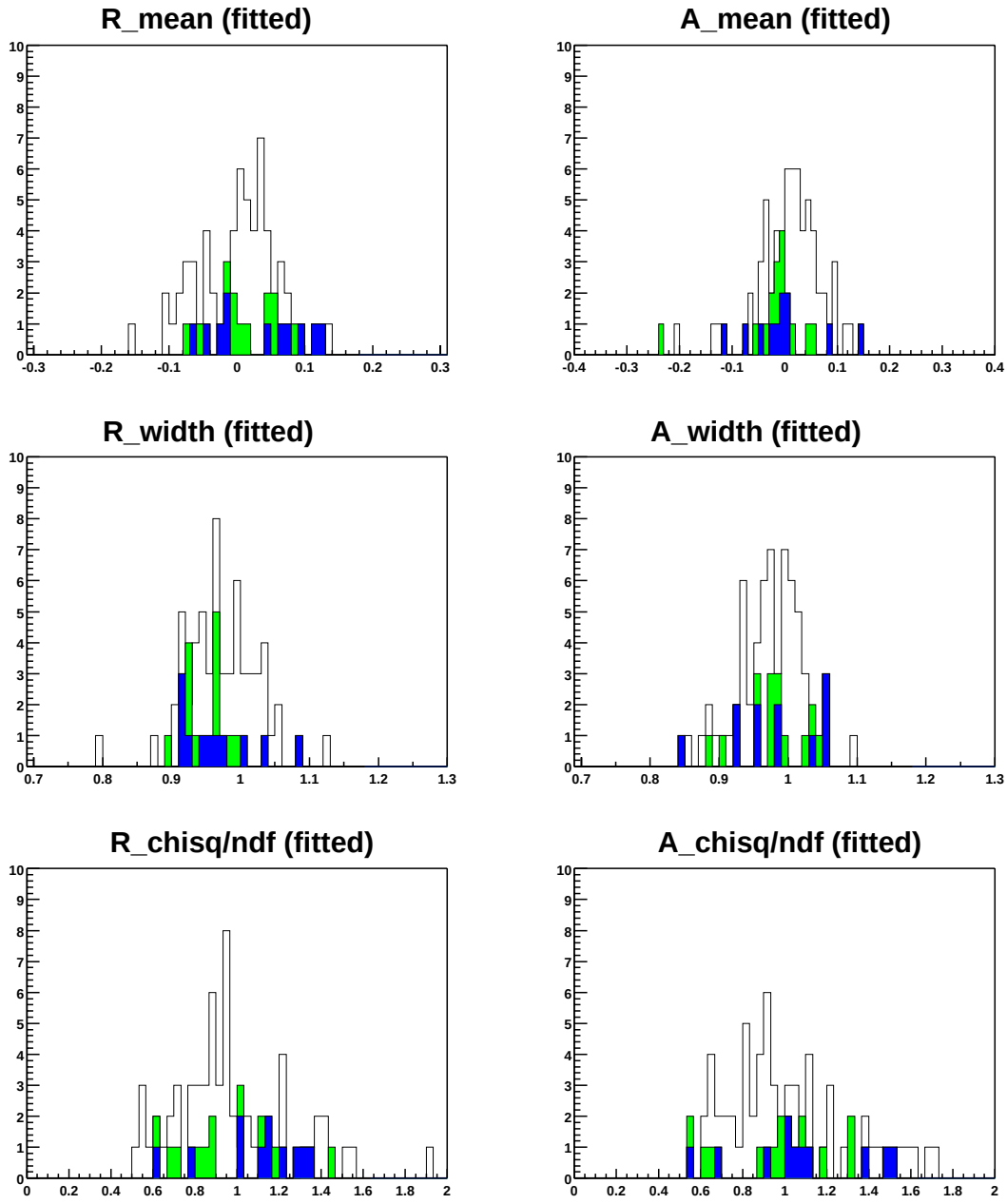

Figure 57: Properties of the correlated differences distributions $\mathcal{D}_R$ and $\mathcal{D}_A$ for fits to the individual detectors for G2Too data, one random sequence. The green entries are for detectors $1-12$ and the blue entries are for detectors $13-24$. The black lines are the properties of the 60 sets of simulated data.

that fits to the individual detectors are not inconsistent with what's expected when the function is the ratio three-parameter function $R(t)$.

Figures 58 and 59 show the distributions $\mathcal{D}_P$ for $P = (A, R, \phi)$ for g2off data and one random sequence for the two detector groups $1-12$ and $13-24$, respectively. For both detector groups, the distributions $\mathcal{D}_P$ are not inconsistent with gaussian functions. The width of $\mathcal{D}_R$ for group $1-12$ is larger at 1.02 ± 0.01 compared to 1.00 ± 0.01 for group $13-24$. The two means are 0.006 ± 0.015 and 0.009 ± 0.015. In this comparison, no systematic drift up/down of the R values versus start time is seen, and the larger swing of R for group $1-12$ produces a bigger width in $\mathcal{D}_R$, 1.02. However, this is not inconsistent with statistics, especially when considered together with the width distributions in Figure 56.

In summary, the statistical checks using the correlated differences distribution for the individual detectors show that the "contiguous detector effect" is not inconsistent with statistical fluctuations.

6 Summary and Conclusion

In this behemoth of a note, an ω_a analysis of the 1999 data using both the g2off and G2Too WFD pulse reconstructions in conjuction with the methods of fill randomization, pileup subtraction and the ratio method was conducted. All the known systematic uncertainties were considered and the dominant ones listed in Table 1. The fit results versus detectors, start times, energy threshholds, etc. were studied and found to be statistically consistent. The one notable statistically unlikely result which was found was that for the g2off data, the fit χ^2/ndf distribution across the detectors was extremely clusted around 1.006, a 2.3 sigma effect (Section 5.1). In light of all the numerous (I assure you of the order of 100's) other tests which were conducted, however, this is not a major concern. In conclusion then I would quote that the final values of R from the ratio method analysis for g2off is $\mathbf{143.37 \pm 1.28 \pm 0.17\ ppm}$, and for G2Too $\mathbf{143.03 \pm 1.28 \pm 0.19\ ppm}$ (with offset). These values were gotten by fitting the summed histograms of all 22 detectors ($1-24$ w/o 2 and 20) for the time interval $34-500$ μs, averaged over six random sequences. The start time of 34 μs used was simply to maximize statistics. The latest detectors gated on were about 30 μs after injection. Giving about 1 μs for the PMT's to recover from the gating would go to about 31 μs. However, the ratio method requires shifting the data by $\pm$ 2.183 μs, and hence the nice round number of 34 μs was used. This start time is at a zero crossing of the g-2 signal.

References

[1] Long Duong, "The Ratio (Orlov-Kindem) Method", g-2 Note 366, August 23, 2000.

[2] Vanya Logashenko, "Shapes of WFD Pulses and the FIT Pulse Finding Algorithm", g-2 Note 369, September 13, 2000.

[3] Fred Gray and Gerco Onderwater, "Love and Death on Long Islands", a writeup on the G2Too pulse fitting.

[4] Cenap Ozben's ω_a report.

[5] Gerco Onderwater's ω_a report.

[6] Cenap Ozben and Yannis Semertzidis, "Removing the Fast Rotation from the Data", g-2 Note 331, July 31, 2000.

[7] Cenap Ozben and Yannis Semertzidis, "Eliminating Pile-up from the g-2 Data", g-2 Note 365, July 31, 2000.

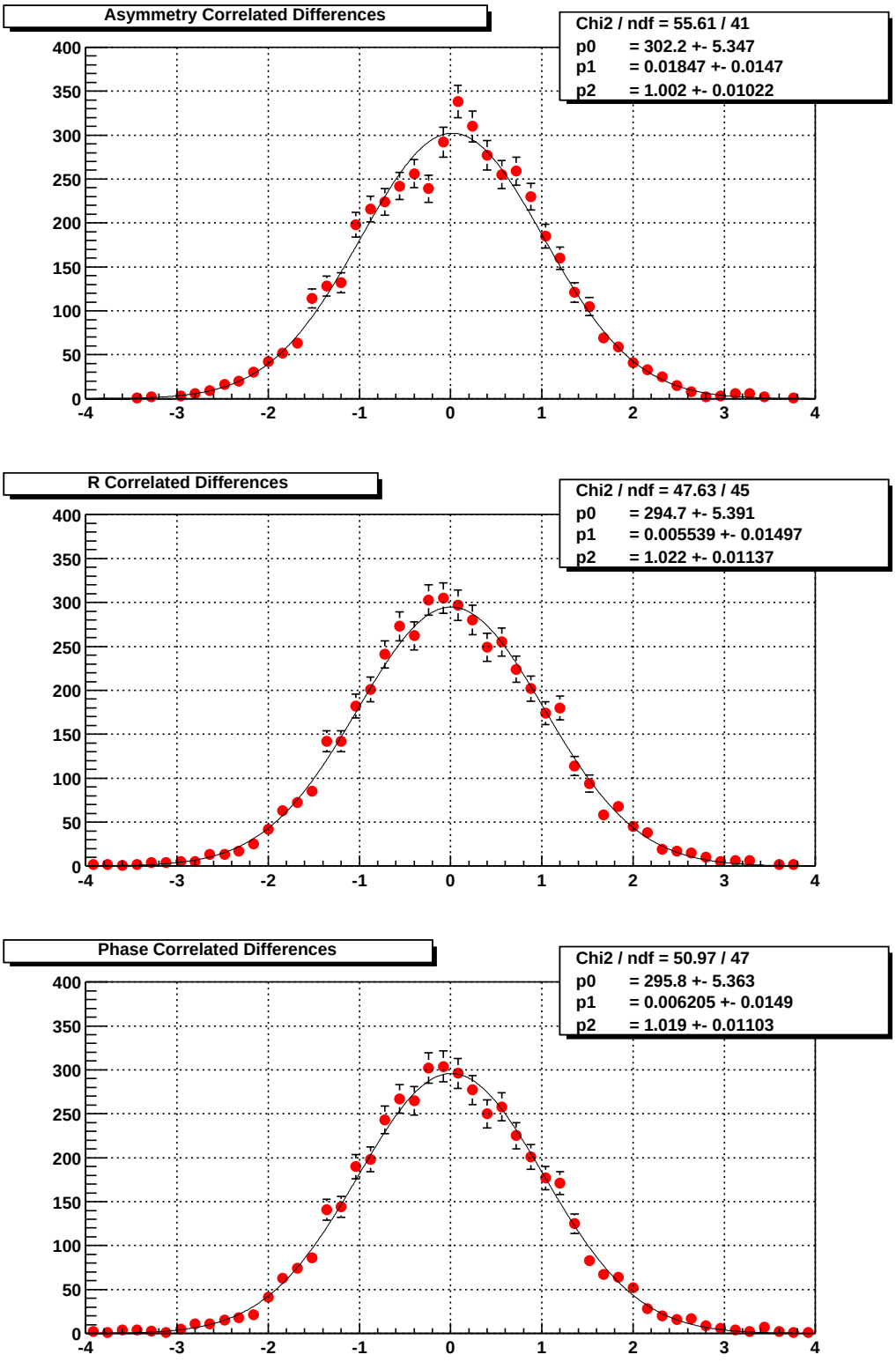

Figure 58: Distribution of values $\mathcal{D}_P = (P(t_2) - P(t_1))/\sqrt{\sigma_P(t_2)^2 - \sigma_P(t_1)^2}$ for the ratio fit parameters (A, R, ϕ) in the case of fitting individual detectors for detectors $1 - 12$. The correlated differences $\mathcal{D}_P$ between start times separated by 2*149.185 ns were calculated for the start time range $34 - 160$ μs. G2off data for one random sequence was used.

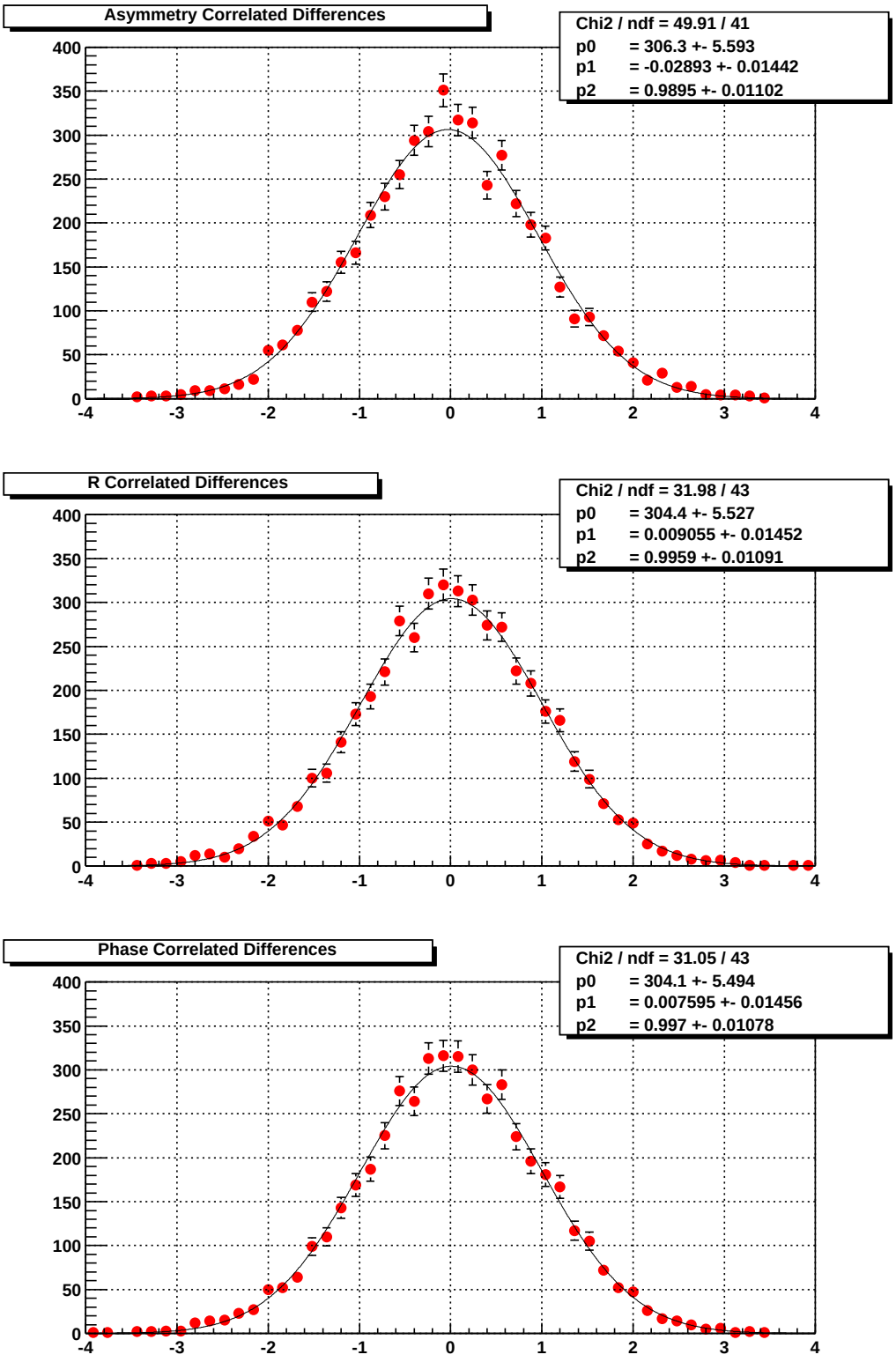

Figure 59: Distribution of values $\mathcal{D}_P = (P(t_2) - P(t_1))/\sqrt{\sigma_P(t_2)^2 - \sigma_P(t_1)^2}$ for the ratio fit parameters (A, R, ϕ) in the case of fitting individual detectors for detectors $13 - 24$. The correlated differences $\mathcal{D}_P$ between start times separated by 2*149.185 ns were calculated for the start time range $34 - 160$ μs. G2off data for one random sequence was used.

[8] Long Duong, "A Study of Gain Changes and Pileup Using the Average Energy Data", g-2 Note 362, May 16, 2000.

[9] Private communication with Ofer Rind: results of Dima's flashlet study to be submitted as a g-2 Note.

[10] Alexei Trofimov's ω_a report.

[11] Sergei Redin, "Set-Subset Problem for g-2", a recent draft which Sergei sent out by email.

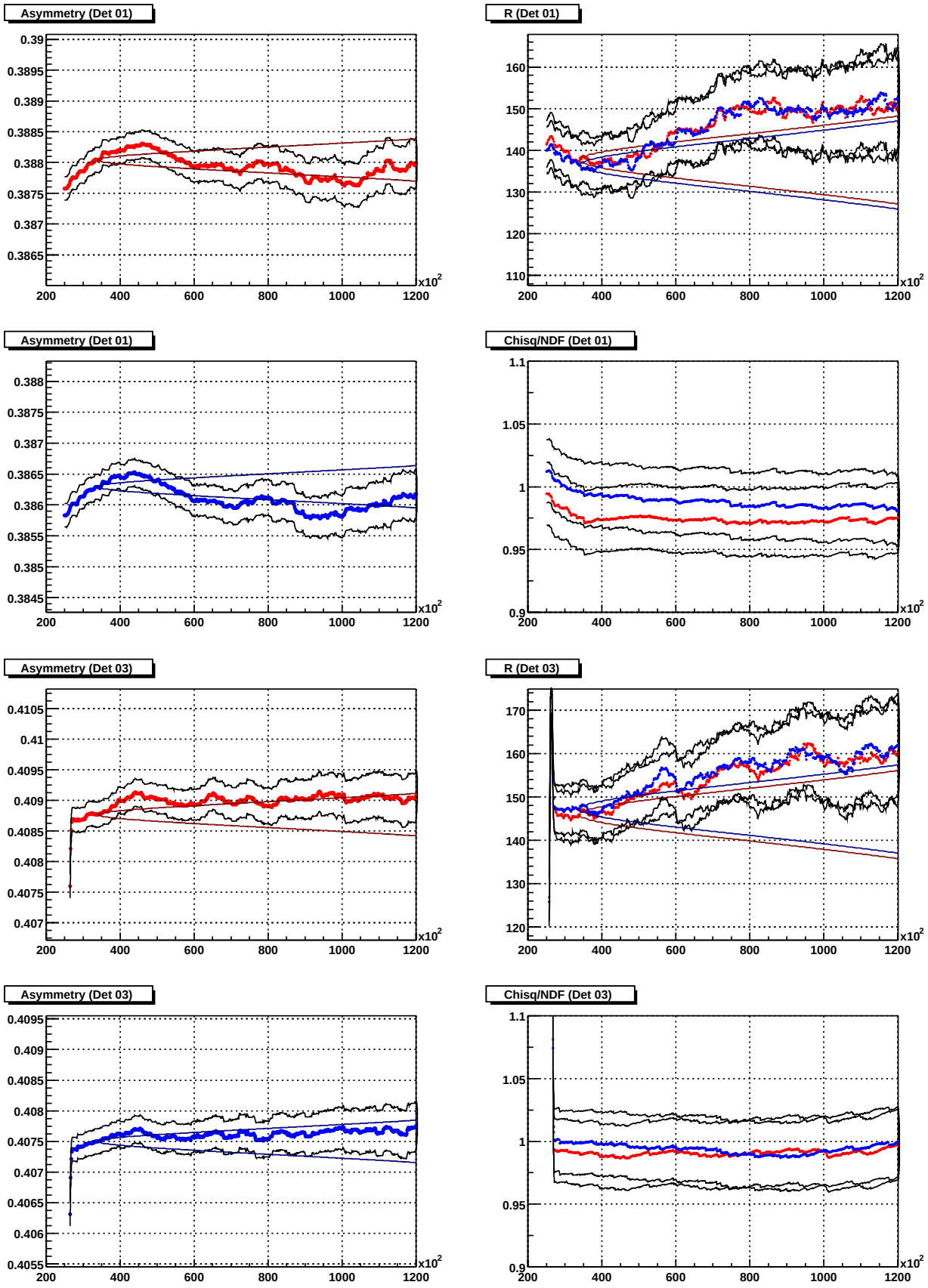

Figure 60: Fit paramters for detector 1 and 3. As usual, R is in ppm and times in ns.

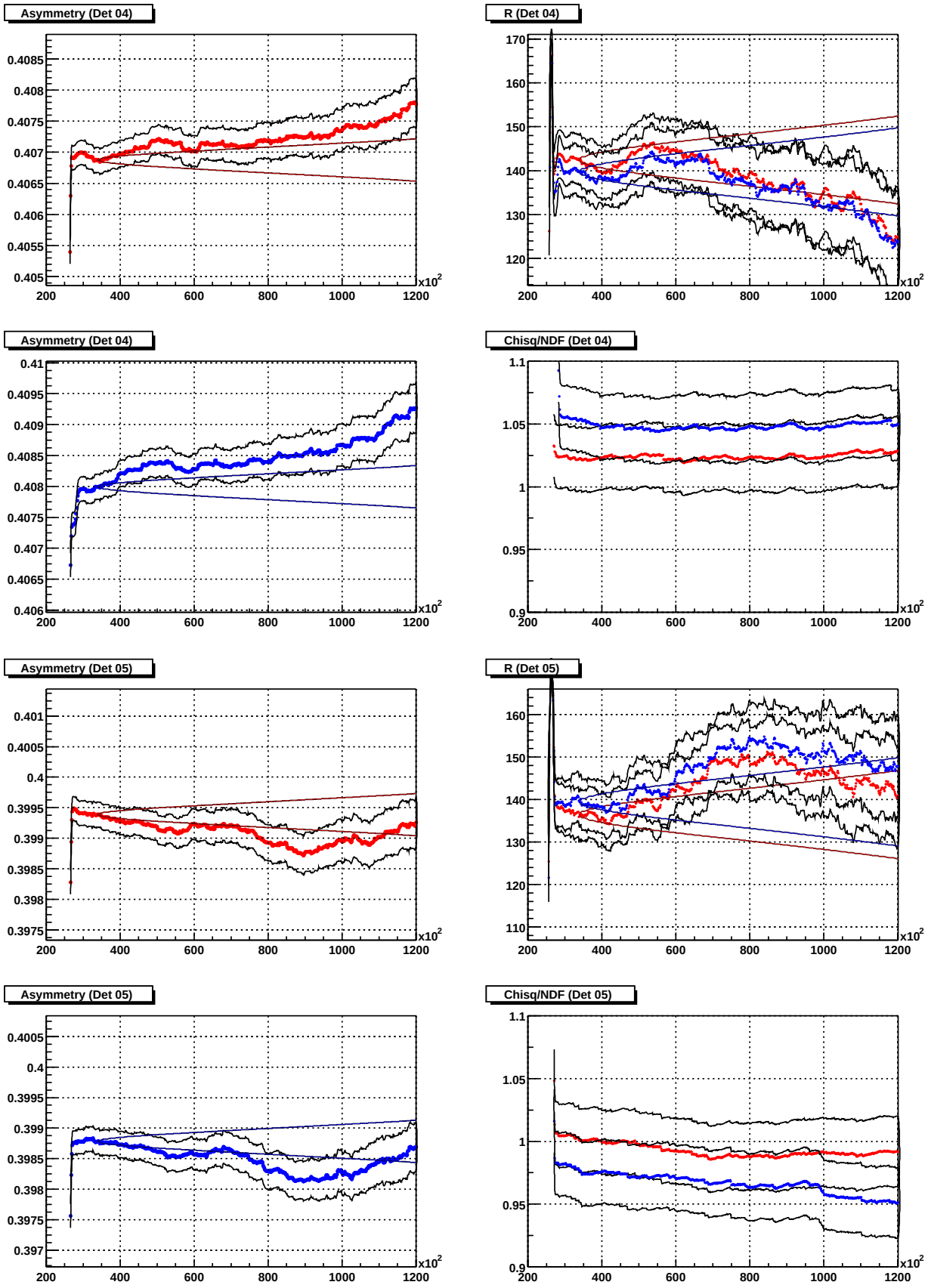

Figure 61: Fit paramters for detector 4 and 5. As usual, R is in ppm and times in ns.

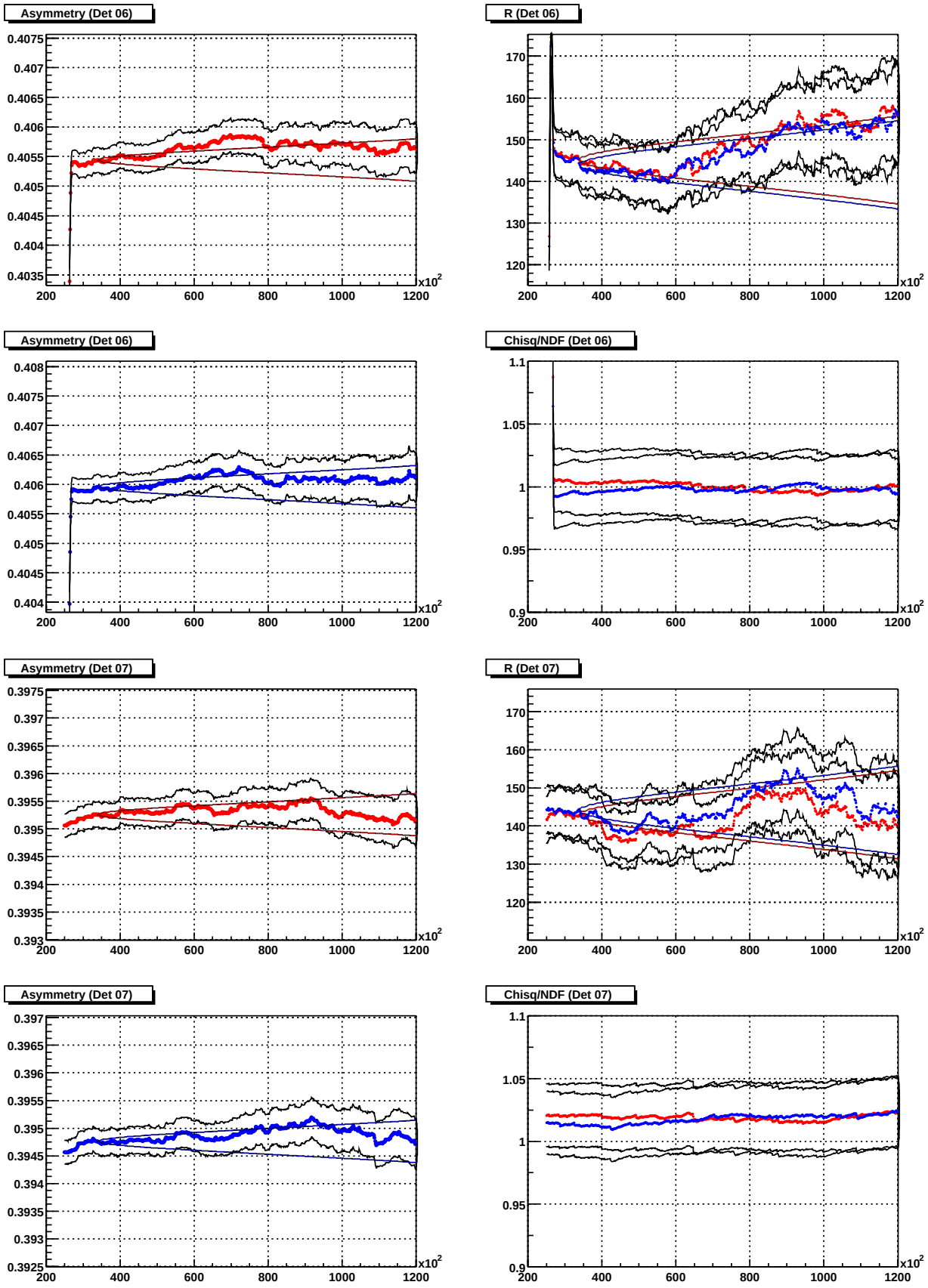

Figure 62: Fit paramters for detector 6 and 7. As usual, R is in ppm and times in ns.

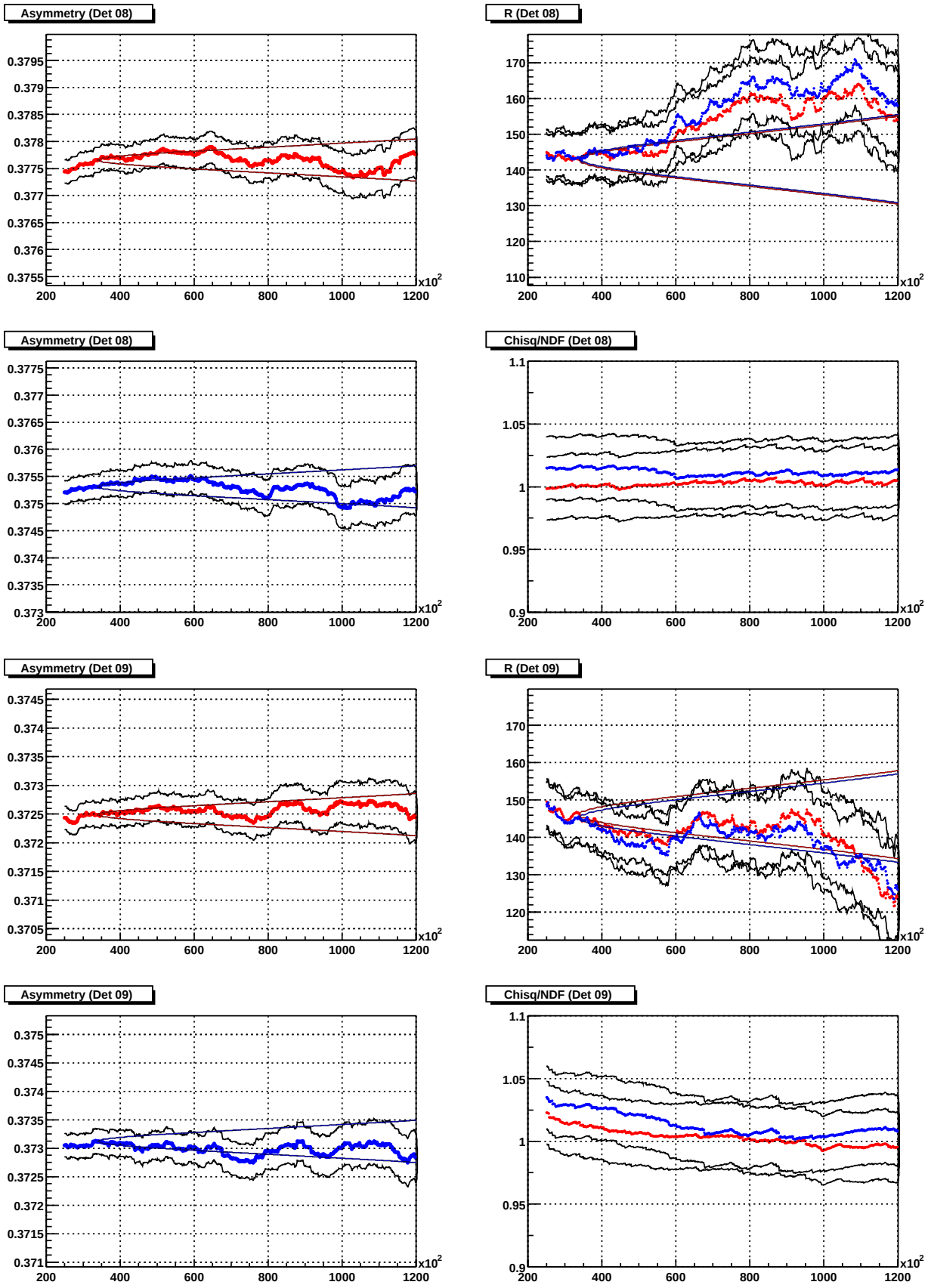

Figure 63: Fit paramters for detector 8 and 9. As usual, R is in ppm and times in ns.

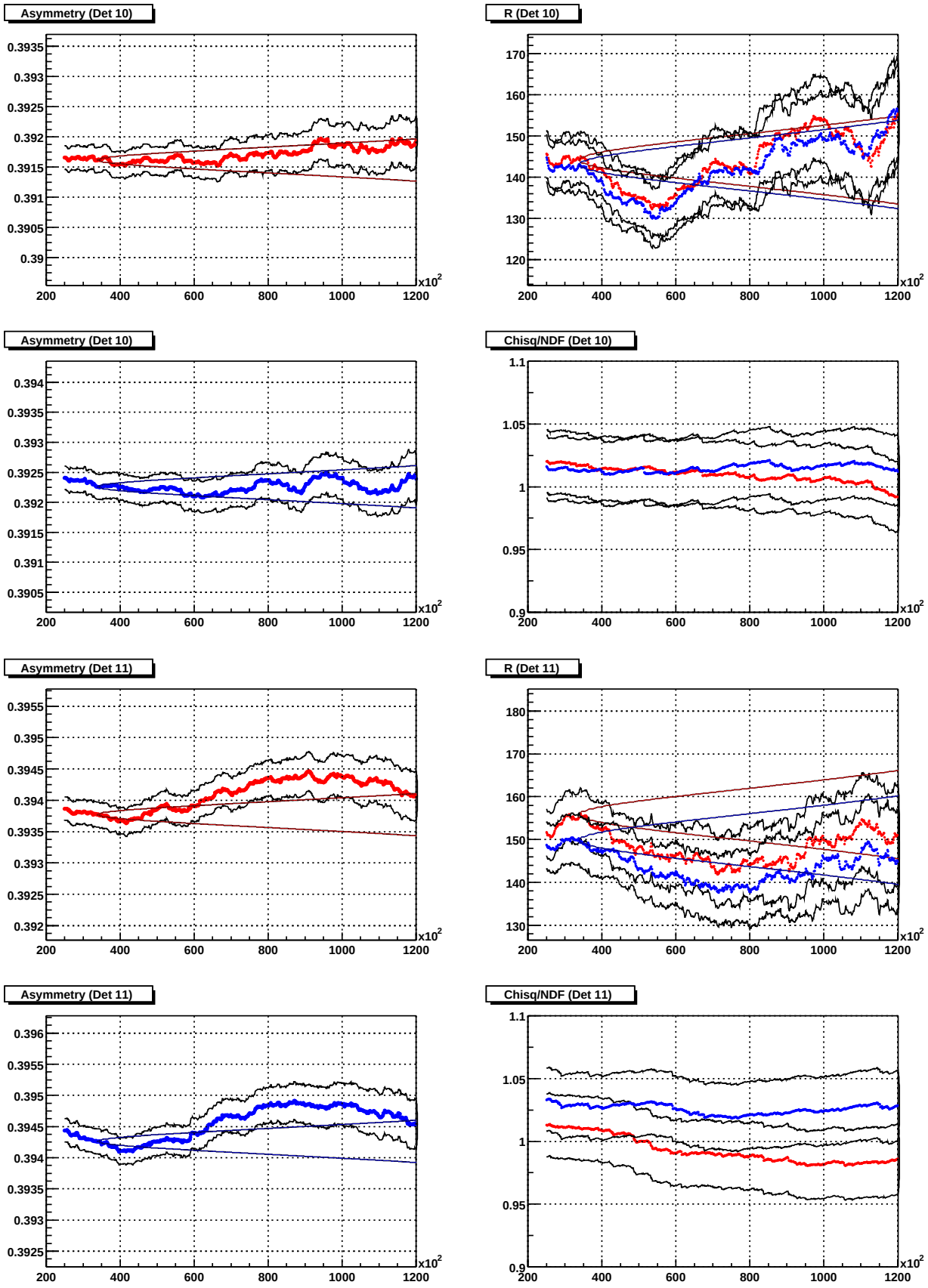

Figure 64: Fit paramters for detector 10 and 11. As usual, R is in ppm and times in ns.

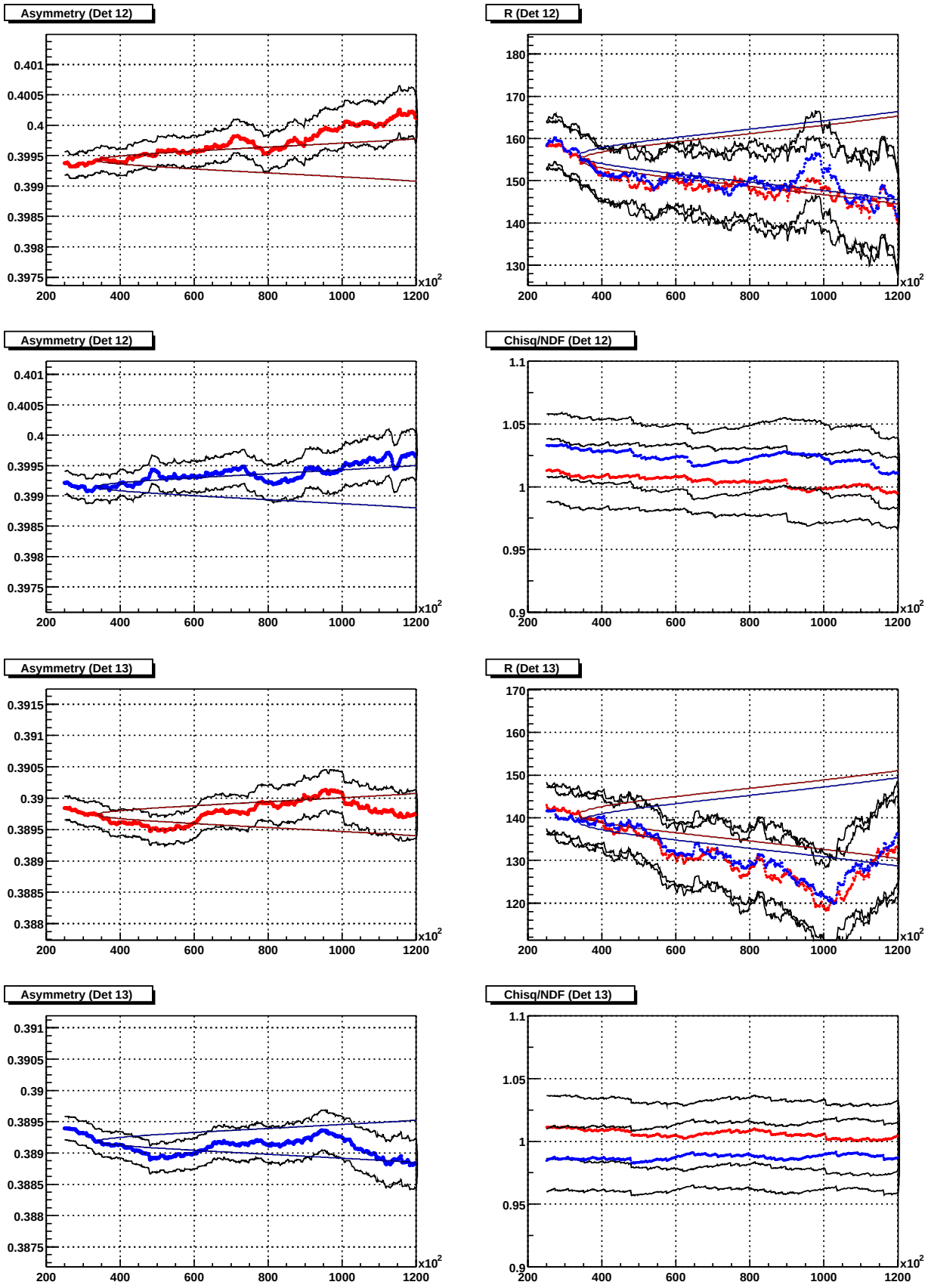

Figure 65: Fit paramters for detector 12 and 13. As usual, R is in ppm and times in ns.

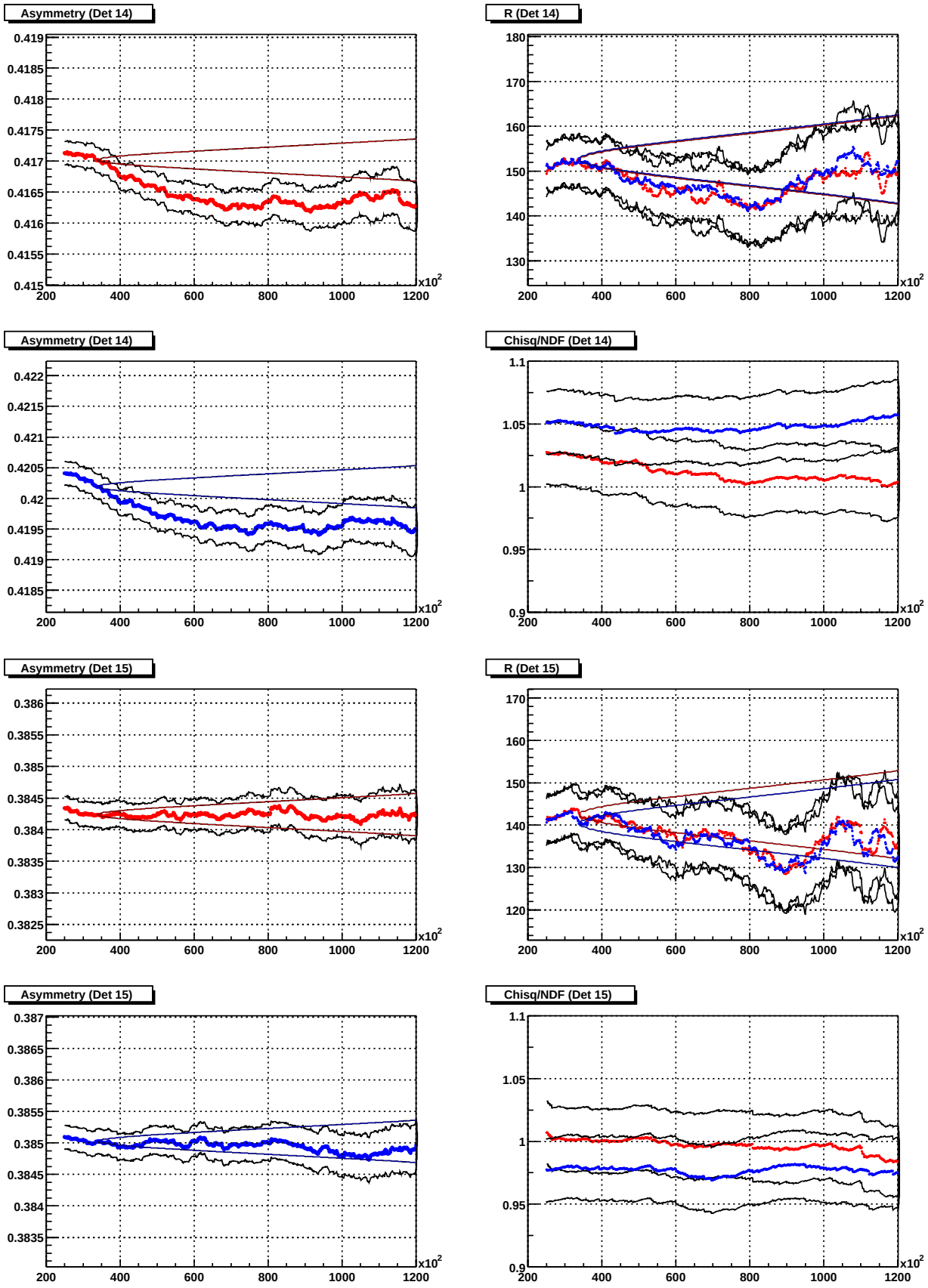

Figure 66: Fit paramters for detector 14 and 15. As usual, R is in ppm and times in ns.

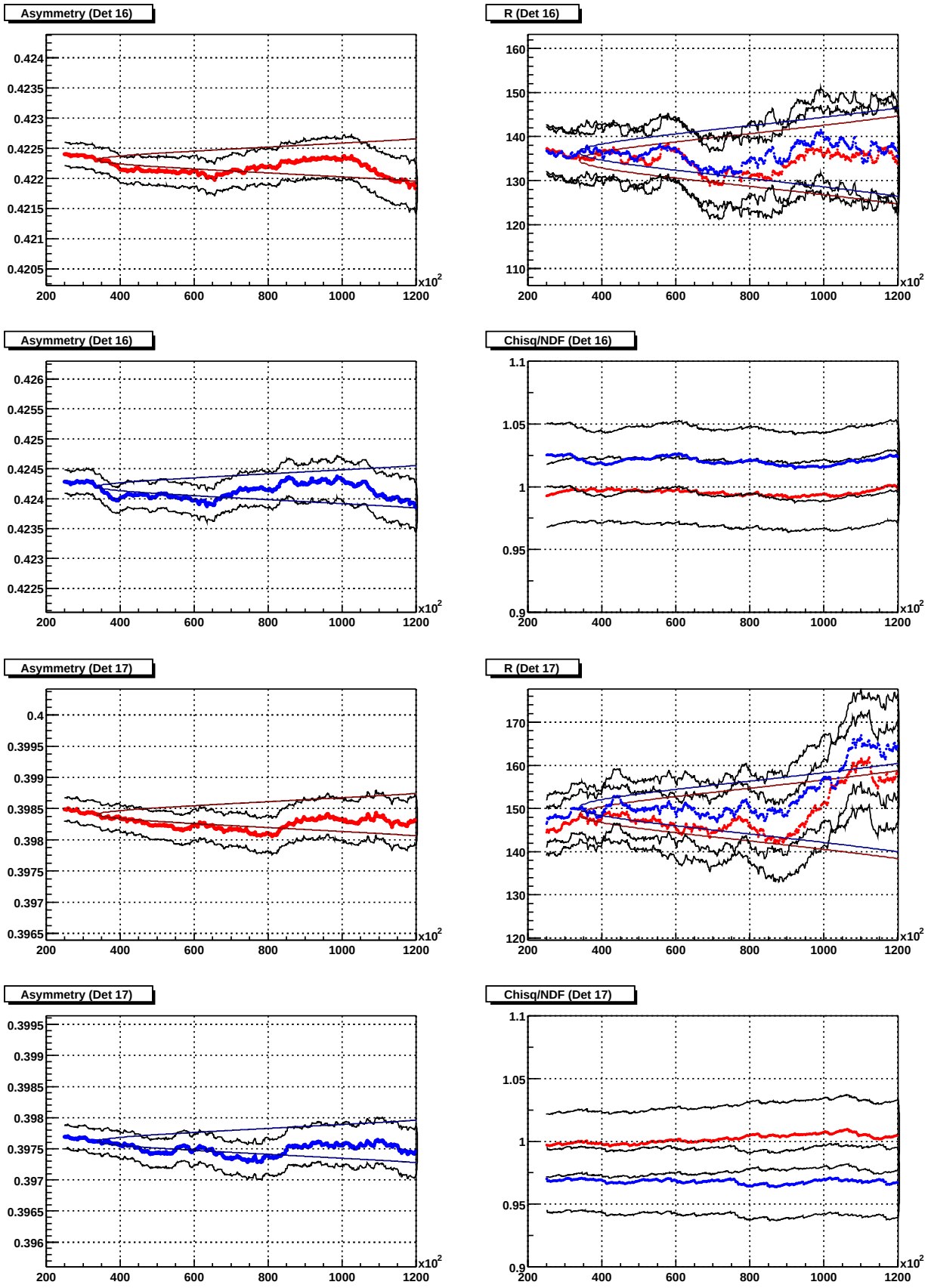

Figure 67: Fit paramters for detector 16 and 17. As usual, R is in ppm and times in ns.

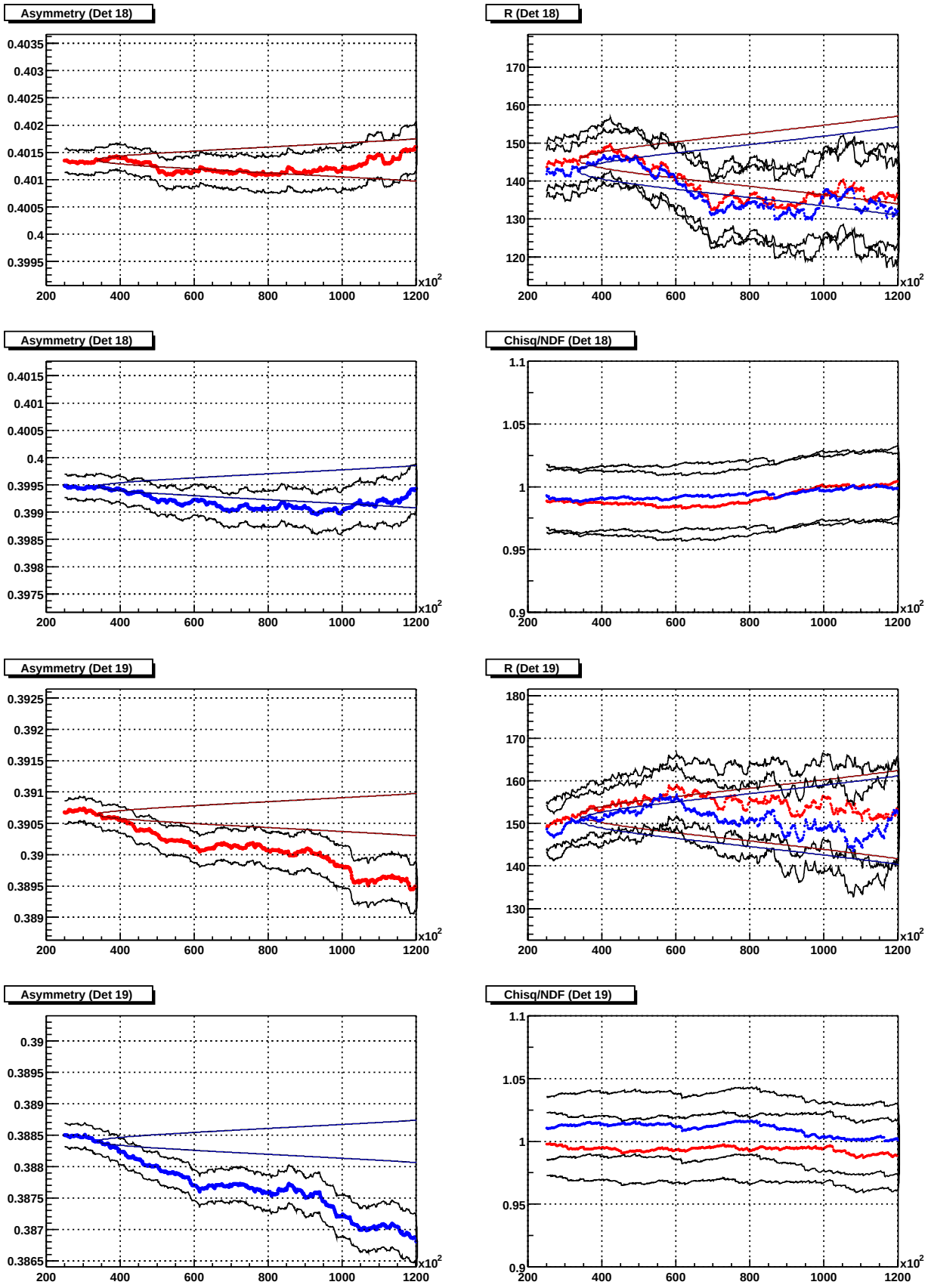

Figure 68: Fit paramters for detector 18 and 19. As usual, R is in ppm and times in ns.

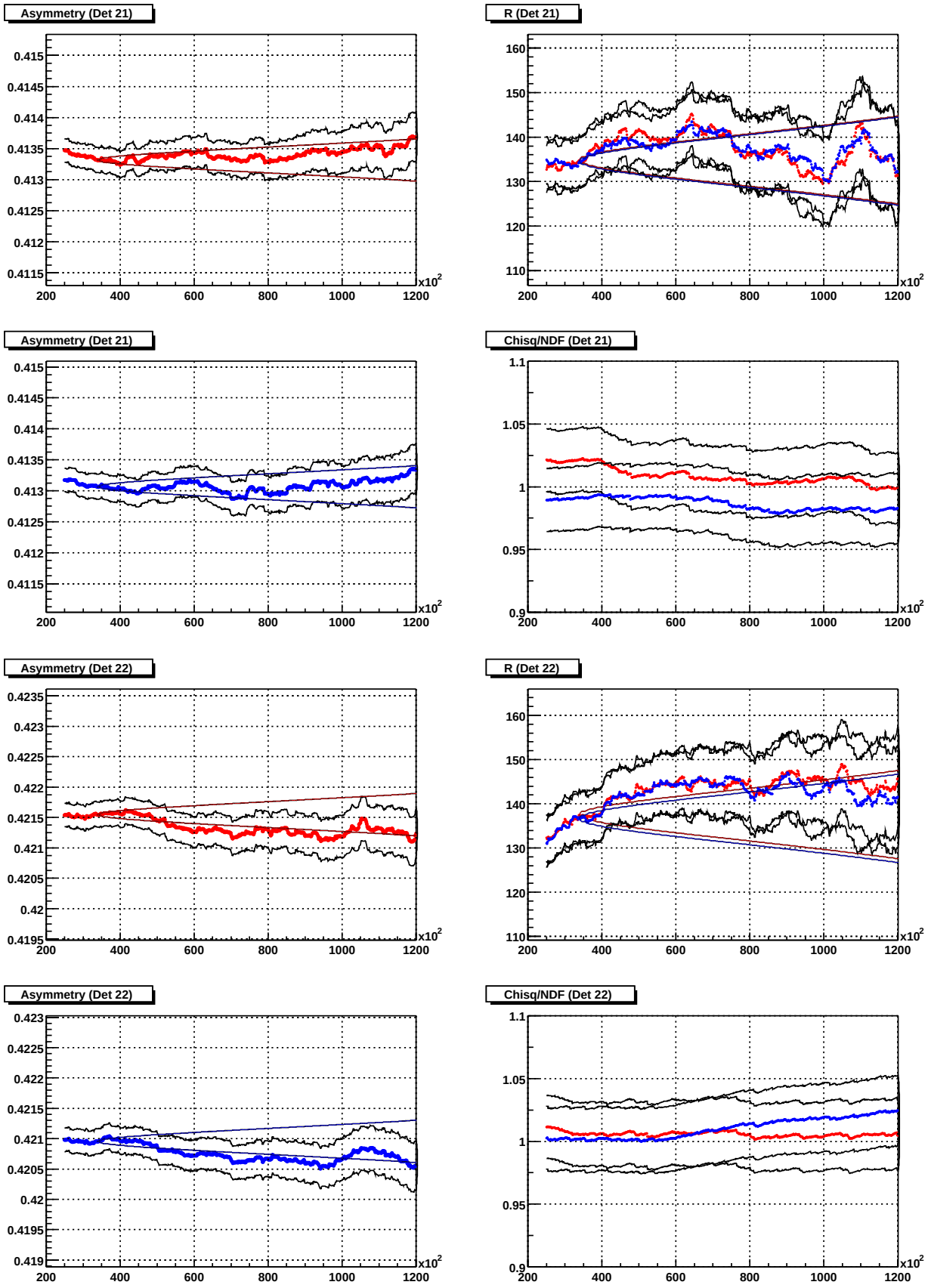

Figure 69: Fit paramters for detector 21 and 22. As usual, R is in ppm and times in ns.

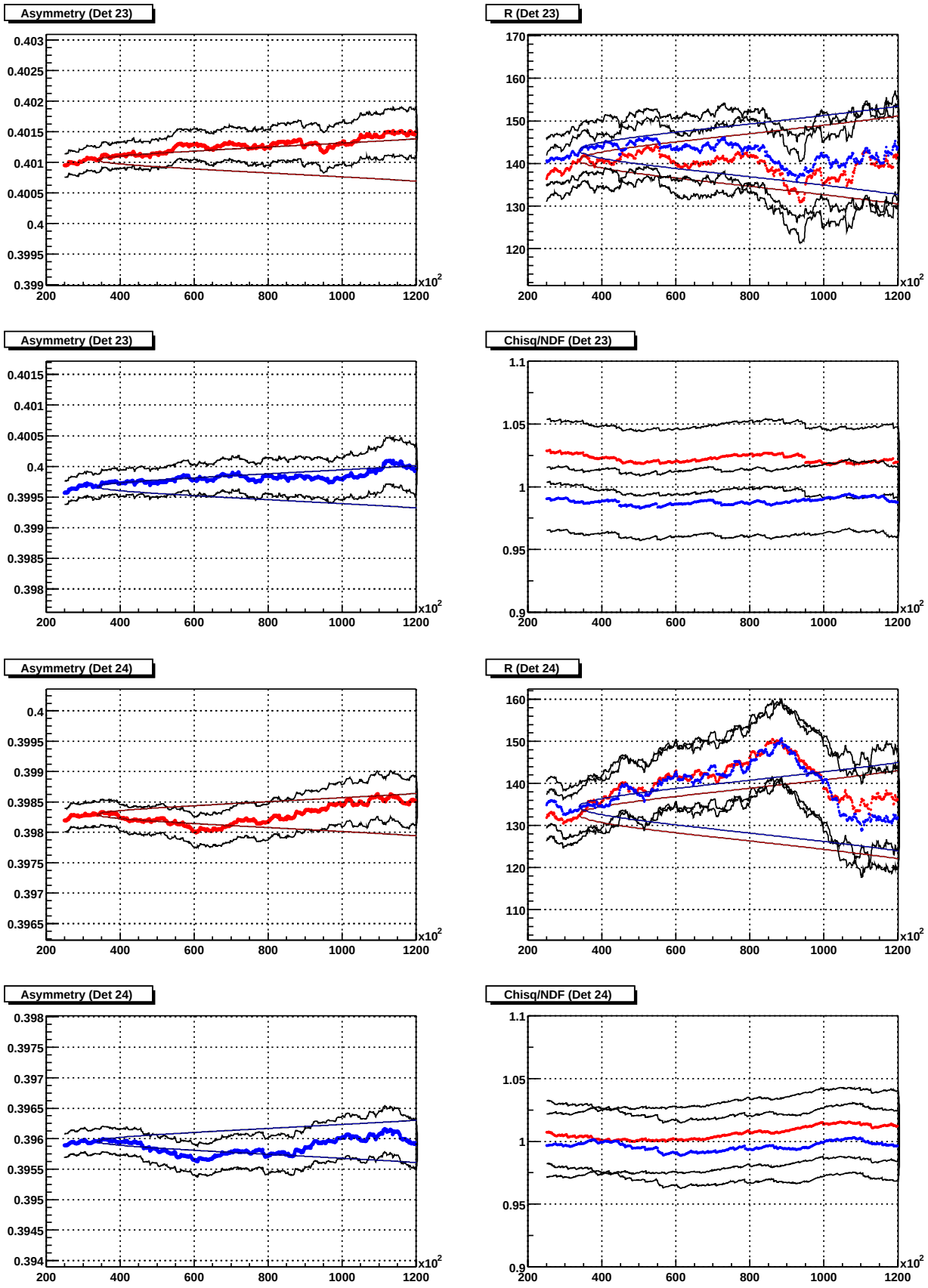

Figure 70: Fit paramters for detector 23 and 24. As usual, R is in ppm and times in ns.